High-Power Operation of Semiconductor Disk Lasers

Dissertation

zur
Erlangung des Doktorgrades
der Naturwissenschaften
(Dr. rer. nat.)

dem

Fachbereich Physik
der Philipps-Universitüt Marburg

Philipps Universität Marburg

vorgelegt von

Dalia Al Nakdali

aus
Homs (Syrien)

Marburg/Lahn, 2015

Vom Fachbereich Physik der Philipps-Universitüt Marburg
als Dissertation angenommen am: 21.09.2015

Erstgutachter: Prof. Dr. Martin Koch
Zweitgutacher: Prof. Dr. Wolfgang Parak

Tag der mündlichen Prüfung: 29.09.2015

Hochschulkennziffer 1180

Table of Contents

Acknowledgments

First and above all, praise be to Allah for guidance and inspiration throughout this work.

It is difficult to put in words my sincere gratitude to my supervisor Prof. Dr. Martin Koch for having given me the great opportunity to learn and work in his group. I thank him for his insight, guidance, support and great deal of patience over the years.

I extend my appreciation to the members of the thesis defense committee, Prof. Dr. Wolfgang Parak and Prof. Dr. Peter Lenz for the time and effort they put into reading this work and for generously offering me valuable feedback and recommendations to improve my thesis.

I would like to thank Dr. habil. Wolfgang Stolz from the *Philipps University of Marburg* and Prof. Dr. Prof. Edik. Rafailov from the *Aston University* for providing me SDL chips.

Many thanks goes to current and past colleagues and PhD-students in our SDL team. I am indebted to Dr. Bernd Heinen who introduced to me the experimental setup as I started my PhD work. I would like to thank Mahmoud Gaafar, Christoph Möller, Fan Zhang, and Dr. Matthias Wichmann for sharing their experimental skill and experience, and for many useful scientific discussions. Thanks in particular to Dr. Arash Rahimi-Iman for wise advice and very constructive and useful comments regarding the text of my thesis.

I would like to thank Marina Gerhard, Sina Lippert, Ronja Woscholski, and Eva Stübling for the great time during the workshop "Women in Optics". I would like to offer my sincerest gratitude to Claudia Goy for being a good friend and perfect colleague. My thanks are due to other PhD-students in our research for the friendly working environment and ever helping attitude.

My acknowledgmens goes to the Marburg University Research Academy (MARA) for the financial support through “Research Assistantship Scholarship" and “PhD Completion Grant".

With all my respect, I am very grateful to my family and would like to especially

thank my parents for everything they have done for me to overcome all of the difficulties throughout my life and for their constant guidance and encouragement to reach this advanced education that they have missed in their own lives. My siblings; you have always been an inspiration to me.

Last but certainly not least, I reserve my deepest gratitude to my beloved husband, Khaled for his sacrifice, patience, unconditional support, and always believing in me.

Marburg in August 2015 Dalia Al Nakdali

Chapter 1

Introduction

1.1 Development of semiconductor disk lasers

In 1961, Basov *et al* for the first time suggested the concept of semiconductor lasers [1]. He reasoned that stimulated emission of radiation could occur in semiconductors by the recombination of carriers injected across a p-n junction. In this context, an important event of optics poses the first demonstration of semiconductor-laser emission in 1962 by three laboratories, from one another [2]. Thereafter heterostructures were explored in 1969. In the heterostructure laser, multiple semiconductor layers of different compositions replaced the simple p-n junction [3].

A few decades later, semiconductor disk lasers (SDLs), known as vertical-external-cavity surface-emitting lasers (VECSELs), were introduced by Kuznetsov et al. in 1997, which can be considered as a combination of the approaches used for the construction diode-pumped solid-state lasers and vertical-cavity surface-emitting semiconductor lasers (VCSELs) [4]. This combination provides SDLs the advantages of both of the aforementioned types of lasers, e.g. high-output-power operation with a near diffraction-limited circular laser-beam profile and wavelength versatility [5, 6].

During the last two decades, SDLs have attracted increasing attention of the semiconductor laser community. So, they have evolved as a key optoelectronic technology that can offer excellent beam quality [7] , high brightness [8], and low-noise performance [9].

SDLs have a number of advantages over other semiconductor or solid-state lasers, which became more and more obvious during their development in the last decade.

- Bandgap engineering allows the design of lasers with special properties, such as a low threshold, high output powers, and a high conversion efficiency.
- (Relatively wide) wavelength tuning (>100 nm) is potentially feasible.
- The structural design and the pool of available materials allows for the coverage of a broad wavelength range, reaching from the ultraviolet to the infrared.
- Without doped semiconductor materials, growth and free carrier absorption, which drastically increases optical losses, is basically no issue.
- No p-n junctions or electrical contacts are necessary (this simplifies chip design and growth, and increases the device reliability): this further eliminates losses due to electrical power (I^2R). In other words, this design results in less heating losses.
- High output powers are achievable via power-scaling techniques with the output beam exhibiting a circular gaussian TEM_{00} profile.
- Efficient intracavity frequency doubling of the laser emission can be achieved using nonlinear crystals, expanding the accessible wavelengths from the infrared into the visible range, or from the visible into the UV, for example.
- External-cavity configurations allow for intracavity techniques such as frequency doubling, wavelength tuning, mode-locking, heat dissipation via intra-cavity heatspreaders, multiple gain elements to be exploited.

The SDL chip itself is basically an active mirror, therefore it achieves two functions within the laser cavity, i. e., it highly reflects light and it amplifies the confined light field. The distributed Bragg mirror (DBR) embedded in the chip features a high frequency-selective reflectivity. On the DBR, quantum dots (QDs) or quantum wells (QWs) are grown, with their gain sufficient enough to compensate for the losses in the structure. The quantum wells or dots are optically excited

to reach a so-called polulation inversion. This corresponds to a high number of charge carriers in the excited states. If the cavity is completed by suitable external mirrors and the gain is sufficiently large, the laser action starts through stimulated emission processes.

In the field of SDL development, primarily QW SDLs were used until recently. Then, quantum dots (QDs) based SDLs were introduced as an alternative to quantum well devices. In 2005, the first report of a realized QD based SDL was presented [10]. QDs are nano-sized semiconductor structures, that are inserted in multiple layers into the chip as an active medium, sandwiched by a semiconductor material with a larger bandgap. The QDs provide a number of advantages over QWs that can be exploited for improved semiconductor lasers. The features offered by QDs in semiconductor lasers are:

- A broad spectral coverage in the region of 1–1.3 μm which can be used in many applications, such as biophotonics.
- Owing to their broad gain bandwidth, a broad wavelength tunability can be exploited in compact and cheap tunable laser sources.
- A reduced lasing threshold and lower thermal sensitivity can improve the performance and efficiency of these devices.
- For mode-locked SDLs, QDs can offer ultrafast charge-carrier dynamics (promissing shorter pulse durations) and have been also employed successfully in saturable absorber structures.

1.2 Aim and concept of this work

This work is devoted to the development of semiconductor disk lasers based on novel quantum dot (QD) structures. QD structures were embedded in this type of laser recently and allowed for a number of advantages over the widely used quantum well (QW) structures. Within the studies of this work, QD-SDLs at new spectral regions with record-high output powers were demonstrated. A systematic optimization of the VECSEL system lead to output powers as high as 8.4 W for emission at 1040 nm and 7.2 W for a device lasing at 1180 nm, respectively. The

broad gain bandwidth of the quantum dot material was explored and wavelength tunability up to 45 nm around 1040 nm and 37 nm around 1180 nm demonstrated, respectively [11, 12].

In another part of this work, an expanded description of power losses in an SDL was used that takes into account optical surface scattering on the SDLs chip. Thereby, it was shown that this approach allowed for an improved extraction of the chip's thermal resistance from experimental data and the role of optical scattering losses in the device is highlighted.

This thesis is written in a cumulative form and is structured as follows: Chapter 2 will present the basic operating principles of QD-SDLs, the improvement of QD-SDLs for the achievement of a high output power in the continuous wave regime, and a brief discussion of the heating and non-heating losses in SDLs with a summary of the experimental results. A summary of this thesis is given in Chapter 3. Chapter 4 gives a summary of this thesis in German languge. The presented research results are discussed in detail in the following publications that were published in the course of the accomplishment of this work and are printed in full length in Chapter 5. For a more complete view, attached to each publication are supplementary materials such as figures.

List of publications:

1. D. Al Nakdali, M. K. Shakfa, M. Gaafar, M. Butkus, K. A. Fedorova, M. Zulonas, M. Wichmann, F. Zhang, B. Heinen, A. Rahimi-Iman, W. Stolz, E. U. Rafailov, and M. Koch, "High-Power Quantum-Dot Vertical-External-Cavity Surface-Emitting Laser Exceeding 8 W," *IEEE Photonics Technol. Lett*, vol. 26, no. 15, 2014.

2. D. Al Nakdali, M. Gaafar, M. K. Shakfa, F. Zhang, M. Vaupel, K. A. Fedorova, A. Rahimi-Iman, E. U. Rafailov, and M. Koch, "High-Power Operation of Quantum-Dot Semiconductor Disk Laser at 1180 nm," *IEEE Photonics Technol. Lett*, vol. 27, no. 10, 2014.

3. D. Al Nakdali, M. K. Shakfa, B. Heinen, B. Kunert, W. Stolz, S. W. Koch, J. Hader, J. V. Moloney, A. Rahimi-Iman, and M. Koch, "Analysis of opti-

cal scattering losses in vertical-external-cavity surface-emitting lasers," *Appl. Phys. B*, 2015.

4. M. Gaafar, D. Al Nakdali, C. Möller, K. A. Fedorova, M. Wichmann, M. K. Shakfa, F. Zhang, A. Rahimi-Iman, E. U. Rafailov, and M. Koch, "Self-mode-locked quantum-dot vertical-external-cavity surface-emitting laser," *Opt. Lett*, vol. 39, no. 15, 2014.

5. A. Rahimi-Iman, M. Gaafar, D. Al Nakdali, C. Möller, F. Zhang, K. A. Fedorova, M. Wichmann, M. K. Shakfa, K. A. Fedorova, W. Stolz, E. U. Rafailov, and M. Koch, "Recent Advances in the Field of Vertical-External-Cavity Surface-Emitting Lasers" *Proc. of SPIE*, vol. 9349, 2015.

Chapter 2

Semiconductor disk lasers

2.1 Basic operation principles of SDLs

Like any other laser, an SDL requires three basic elements in order to operate:

1. An active medium, in which the light amplification occurs.

2. An optical resonator (here an external cavity), which is formed by a number of dielectric mirrors and which provide optical feedback of light for gain and laser beam mode selection.

3. A pump source, which supplies the energy required for the laser process to take place and a population inversion to be generated in the active medium.

Fig. 2.1 shows a schematic structure of an SDL that contains all the aforementioned elements. The semiconductor chip is the key element of the SDL. Here, it consists of a multilayer Bragg mirror, an active region and an antireflection (AR) coated cap layer. Next, we will only consider QD-based SDLs, i. e., QDs arranged in multiple layers form the gain region. However, most of the concepts used are similar the predominantly explored for QW-SDL. In the following, the working principle and composition of these components of the chip structure will be briefly summarized.

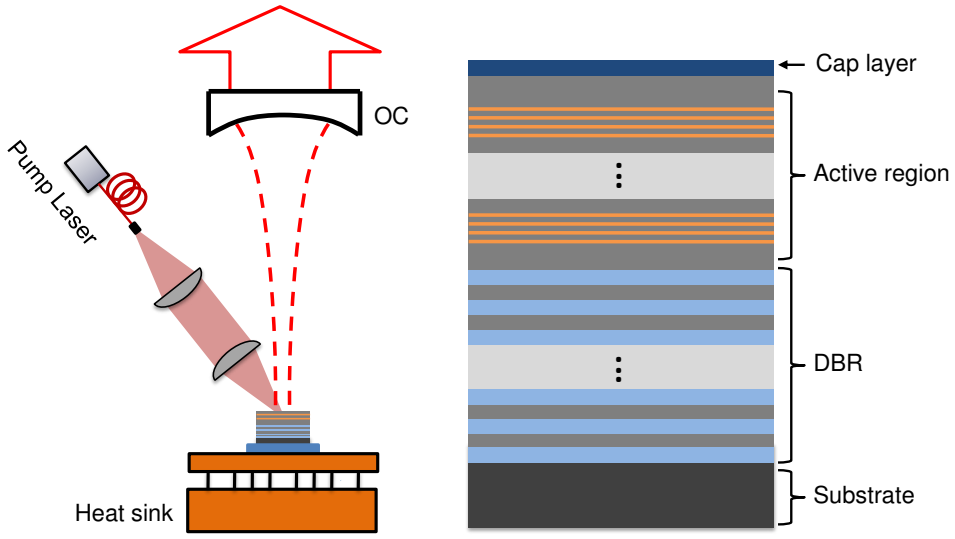

Figure 2.1. Schematic illustrations of SDLs with all components required for lasing(left), and the structure of the SDLs chip (right).

2.1.1 Distributed Bragg mirror

A highly reflective Bragg mirror (distributed Bragg reflector (DBR)) is an essential element of an SDL and completes the laser resonator on the chip side. It is placed between the active region and the heat sink, thus also forming a thermal barrier between both.

The reflectivity of a DBR is typically very high, of the order of 99.9%, which allows for keeping the threshold of the laser low and the output differential efficiency high. To achieve highly reflective DBRs, multiple quarter-wave layer pairs of alternating semiconductor materials with a high refractive index contrast are required. Another key requirement to the DBR structure for good SDL-operation conditions is a suitably low thermal impedance of the mirror structure. To produce particularly good DBRs for the use in high-power SDLs, the quarter-wave layer pairs are chosen to exhibit a particularly high refractive index contrast in order to achieve a high reflectivity with a reduced or minimum number of layer pairs and thus reduced thickness and lower thermal impedance. Moreover, also the thermal conductivity of the DBR materials themselves have to be taken into account. In addition, it is important that the mirror materials are non-absorbing at the wavelength of laser operation and, potentially, the pump wavelength (in order to prevent generation of free carriers in the mirror which contribute to heating

of the device). The DBR, which is composed of alternating quarter-wavelength thick layer pairs with high and low refractive-index material with indexes n_h and n_l [13], leads to a constructive interference of partly reflected light at the interfaces inside the Bragg mirror, if the wavelength is resonant to the Bragg wavelength. How much light is reflected at each interface is determined by the index contrast between the high and low index layers which explains the desire for a high index contrast.

In the case of QD SDLs, GaAs is used as the higher-index material layers and lattice-matched $Al_xGa_{1-x}As$ for the lower-index material layers. We use $Al_xGa_{1-x}As$ instead of AlAs in order to circumvent unwanted pump absorption in these DBRs. The GaAs/$Al_xGa_{1-x}As$ mirrors require around 28 to 35 quarter-wave pairs to achieve the desired reflectivity of $> 99.9\%$. Fortunately, this material combination in DBRs can cover the whole spectral region ranging from 1 to 1.3 μm. The reflectivity value for the Bragg wavelength is calculated by the following equation [14, 15]:

$$R = \left(\frac{n_i n_h^{2N} - n_e n_1^{2N}}{n_i n_h^{2N} + n_e n_1^{2N}} \right)^2 , \tag{2.1}$$

here n_i is the refractive index of the material on the incidence side, n_e is the refractive index of the material on the exit side, n_h and n_l are the refractive indexes of the DBR layers with higher and lower value, respectively, while N is the number of layer pairs used in the DBR.

2.1.2 Active Region

The active region is the key component of the SDL chip, since it provides the necessary optical gain of light to compensate for losses in the cavity. It is a well designed semiconductor-based structure, grown directly on top of the DBR. As mentioned such an active region of SDLs can consist of, for example, quantum wells or even quantum dots. The latter offer wider gain spectra, only a very slight dependence of the emission wavelength on the temperature [16, 17], and can also be operated at relatively low power levels [18, 19]. In the studied QD-SDLs, the active region structure consists of InGaAs QD layers separated by GaAs spacers. The QD-gain layers were grown using the Stranski-Krastanov QD growth formation

mechanism. It is necessary and useful to understand the operating principles of the SDL in order to fabricate chips with an improved structural design. Fig. 2.2 shows the band-gap diagram of an SDL wafer and illustrates the laser operating principles [4, 20]. The pump radiation is mainly absorbed in the GaAs spacers (barriers). This pump absorption will lead to the generation of electron-hole pairs in the spacer material, the latter are the (GaAs) layers that are grown between the QD layers. Generated electrons and holes diffuse and are trapped in QD layers which have a lower potential energy. The gain for the laser radiation is achieved through the recombination of those generated carriers. Optical waves are constantly reflected in the cavity of the laser.

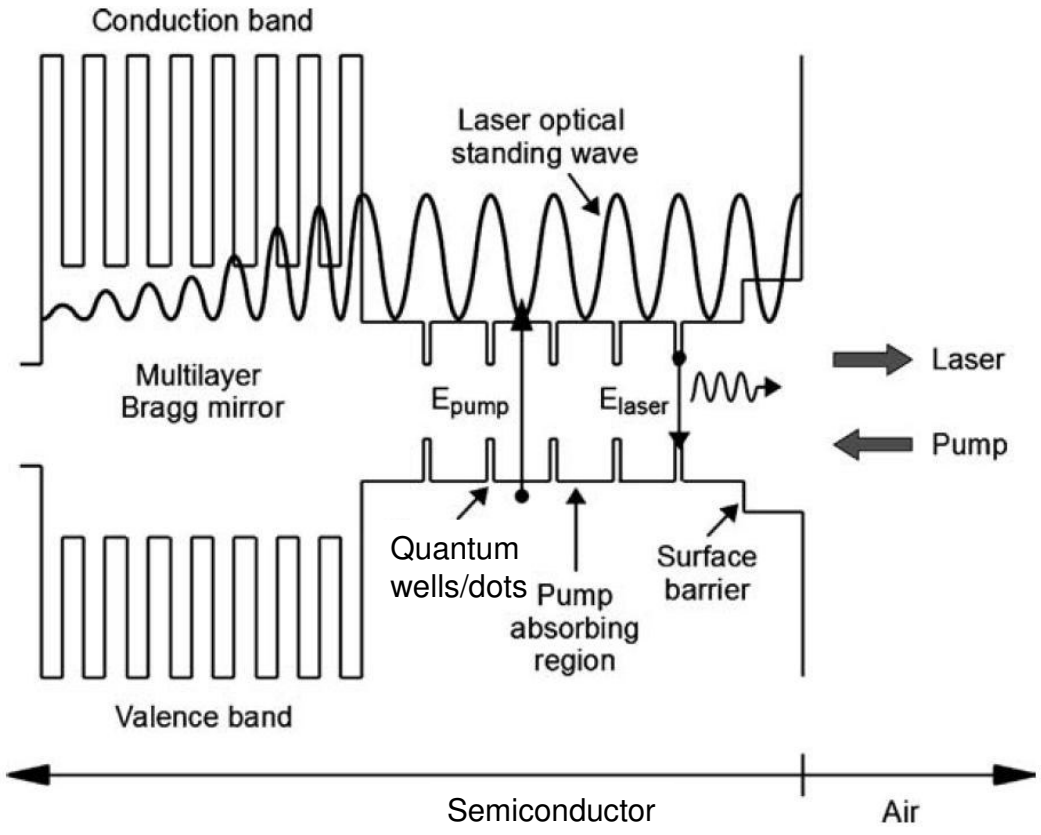

Figure 2.2. Schematic drawing of operating principles of SDLs.

The QD layers are arranged in several identical groups that are distributed within the active region. For maximum gain, QD layer groups are optimally positioned at anti-nodes of the optical standing wave by choosing specific thicknesses of

the pump absorbing regions. This design is called a resonant periodic gain (RPG) structure [21, 22]. Such configuration allows for maximum gain from each active layer as well as it reduces the operational threshold of the device. The effective gain of the device is determined by the number of QW or QD layers [4, 23] that have spectral and spatial overlap with the optical field in the cavity. However, the number of achievable layers is limited by the growth capabilities, i.e. defects can form after a certain number of layers of QDs, owing to strain accumulated during growth. Whereas, these defects have a strong adverse effect on the performance of the device. In addition, the optimum number of layers is related to the preferable length of the sub-cavity. It also must be taken into consideration that the sub-cavity needs to be resonant or antiresonant with the design wavelength. Also the dispersion and pump light absorption need to be taken into consideration, when adjusting the length of the sub-cavity.

The active region at the emission wavelength of 1040 nm is 7.5 times $\lambda/2$ long and consists of 35 layers, which are arranged in 7 identical groups and are deposited each at an antinode position of the optical standing wave in the sub-cavity, taking also into account the sizes of QDs [19, 24]. The active region SDLs designed for emission wavelengths between 1100-1300 nm consists of 6-nm thick QD layers, which are arranged in 13 identical groups with 3 QD layers in each group. The QD layers are separated by 35 nm thick GaAs layers [32, 25].

2.1.3 Cap layer

An $Al_{0.9}Ga_{0.1}As$ layer is grown on top of the active region. It improves pump light transmission into the semiconductor and prevents carriers from diffusion to the surface of the device and non-radiative recombining through surface defects, which would result in a decrease of the device's performance. Finally, a cap layer of GaAs completes the structure to avoid oxidation processes.

2.1.4 Resonator

An external optical cavity of an SDL device is configured by adding, at least, one dielectric mirror. SDL cavities allow for the control of the laser fundamental transverse mode operation as well as for combining multiple gain elements in series

in order to achieve higher-power laser operations [26, 27]. The simplest cavity configuration is the linear cavity. It comprises a gain mirror and an additional external spherical mirror with a radius of curvature R, as shown in Fig. 2.3(a). Such a cavity is usually used for the SDL operation in the CW regime. The TEM_{00} laser mode beam diameters ω_1 on the planar chip and ω_2 on the output spherical mirror can be calculated by [4]:

$$\omega_1 = 2\left(\frac{L\lambda}{\pi}\right)^{1/2}\left(\frac{R-L}{L}\right)^{1/4}, \tag{2.2a}$$

$$\omega_1 = 2\left(\frac{L\lambda}{\pi}\right)^{1/2}\left(\frac{L}{R-L}\right)^{1/4}, \tag{2.2b}$$

here L is the length of the cavity, λ is the laser light wavelength. More complex cavity configurations are used for different applications, various elements can be inserted inside the cavity, such as birefringent filters for the laser wavelength selection and tuning [28], or saturable absorbers for passive mode locking (ML) [29, 30, 31]. This typically requires a three-mirror V-shaped laser cavity to be used, as shown in (Fig. 2.3(c)) with a flat SESAM semiconductor saturable absorber mirror at one end of the cavity. The V-shaped laser cavity of (Fig. 2.3(b)) is also used often together with nonlinear optical crystals for second harmonic generation [25]. In a more complex case, a four-mirror Z-shaped laser cavity configured, such as in (Fig. 2.3(d)), is used for the second harmonic generation and passively mode-locking operation [33, 34]. For higher-power laser operation, more complex multi-mirror cavities are designed using two (Fig. 2.3(e)) [16] or even three active gain chips in the cavity (see Fig. 2.3(f)).

2.1.5 Pump source

The pump source generates the carriers within the semiconductor active region. Typically, the SDL is optically pumped by a fiber-coupled diode laser. The fiber-coupled pump laser requires a combination of collimator lens and a focusing lens which images the pump laser fiber output onto the SDLs chip. Various pump

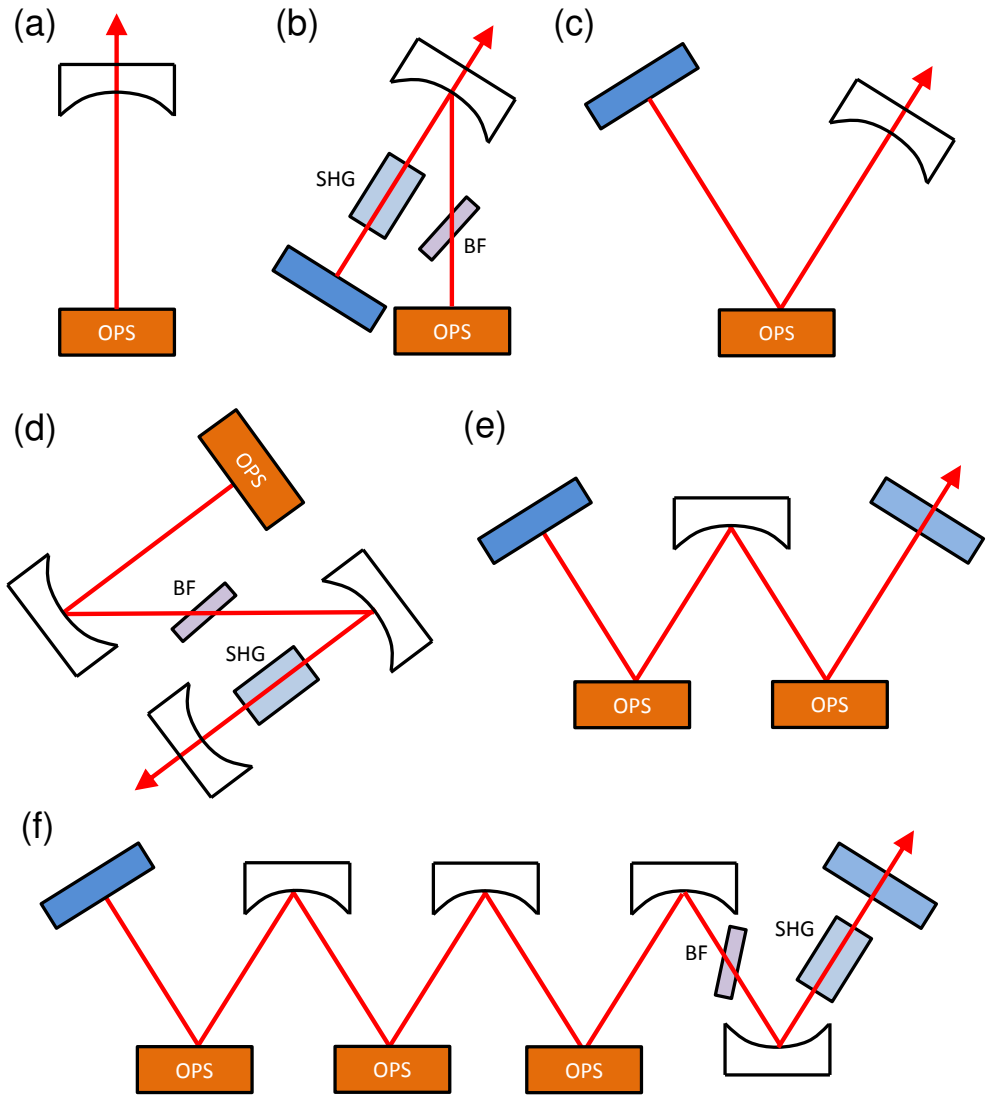

Figure 2.3. SDL laser cavities comprising chip (OPS) and resonator mirrors: (a) linear cavity configuration, (b) V-shaped cavity for SHG, (c) V-shaped cavity for ML, (d) Z-shaped cavity, (e) W-shape cavity with two gain chips, (f) SDL with three gain chips and intracavity elements.

sources are used, namely with powers ranging from a few Watts up to $>$ 100 W. In experiments, the pump laser is often focused onto the SDL's chip under an incidence angle varied between 20 ^{o}C and 40 ^{o}C. Although the spot is slightly elliptical on the chip, a pump spot diameter can be approximated by

$$D_{pump} = D_f \left(\frac{f_{fl}}{f_c} \right) , \tag{2.3}$$

where f_{fl} is the focal length of the focusing lens, f_c is the focal length of the collimator lens, and D_f is the diameter of the fiber core. QD-SDLs with pump spot sizes between 70 and 600 μm are demonstrated. However, the size of the pump spot cannot be extended infinitely [54].

2.2 Wavelength tunability

The wavelength tunability is an important advantage of an SDL device for some applications, especially in spectroscopy, optical fibre communications, biological imaging and other applications. Wavelength tuning in laser resonators containing broadband gain media is achieved by using standard methods, including the use of angle-tuned diffraction gratings, etalons, or birefringent filters (BRFs). The BRF consists of a simple birefringent quartz plate, with its an optical axis parallel to the surface of the plate.

In case of using diffraction gratings, only a narrow-width wavelength part can be reflected back into the resonator chosen via the rotation of the grating. Typically, in SDLs, tunability is commonly accomplished via the use of a birefringent tuning element due to its simplicity, low losses, and easy operation [25, 35]. And, it is placed inside the laser resonator at Brewster's angle to the beam direction. The BRF consists of a simple birefringent quartz plate, which has its optical axis parallel to the surface of the plate. The rotation of the BRF around its surface normal allowed the wavelength of the laser to be tuned.

2.3 High power semiconductor disk lasers

The power scaling ability is one important key property of SDLs. Compact and efficient laser sources with high power and high output beam quality have various important applications, such as optical communication (e.g., fiber-optic and free-space communication), spectroscopy, metrology, biophotonics, material processing, medical surgery [6, 36, 37], and more.

2.3.1 Optimization of cavity parameters

For the power scaling, the size of the area on which pump spot and laser cavity mode overlap, should be increased. Thus, the output power can basically be scaled by adjusting the cavity parameters, which can significantly affect the performance of an SDL device, such as choosing the best spot size, or incidence angle of the pump laser on the SDL chip. Besides, the optimal transmittance of the output coupler (OC) mirror should be carefully determined for the purpose of high-power operation. Furthermore, the mode matching, i. e., the ratio of the pump spot size to cavity-mode size on the SDL's chip significantly affects the SDL device. In the case of a linear cavity, the cavity mode dimensions are typically determined by the cavity length. However, at the conditions of high power SDL operation, the cavity mode size cannot be directly estimated since a transversal multimode emission is expected in this case. Therefore, one can vary the cavity length to achieve the best mode-matching and until heat dissipation becomes the limiting factor.

In this work, the impact of cavity parameters on the performance of QD-SDL devices is studied. Remarkably, a QW-SDL with an output power exceeding 100 W in multimode CW regime with 600 μm pump spot diameters was demonstrated in 2012 [26]. However, in the case of QD-SDLs, power scaling in such devices does not allow for such high powers owing to the gain structure. Nevertheless, with optimized cavity paramters, more than 8 W has been achieved [11], using a 330 μm spot size in the spectral region between 960–1300 nm. Fig. 2.4 shows QD-SDLs with their output powers at different wavelengths, that has been recorded to date. Limitations regarding the output power does not depend only on the heat dissipation. Non-heating losses due to chip-surface roughness and amplified spontaneous emission in the lateral direction have also a significant influence on the performance of SDL devices. The impact of heating and non-heating on SDLs will be discussed in Section 2.4.

2.3.2 Results and discussion

In this thesis, recent achievements and experimental results obtained for optically-pumped QD-SDLs designed for the emission in the infrared spectral region are presented. The results of the studies were published with the titles "High-Power

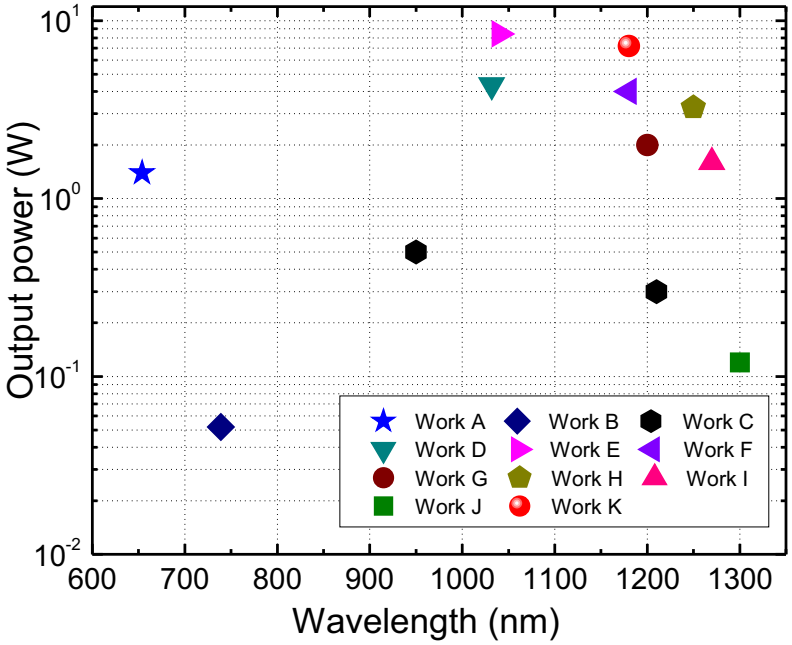

Figure 2.4. Maximum continuous-wave output powers of QD-SDLs to date reported in the literature: A [38], B [39], C [40], D [19], E [11], F [32], G [41], H [27], I [42], J [10], and K [12]

.

Quantum-Dot Vertical-External-CavitySurface-Emitting Laser Exceeding 8 W" (Section 5.1) [11] and "High-Power Operation of Quantum-Dot Semiconductor Disk Laser at 1180 nm" (Section 5.2) [12], respectively.

Two different SDL chips designed for emission at 1040 and 1180 nm, respectively, were studied; both employ an effective medium of Stranski-Krastanov grown (InGa)As QDs. The devices are operated each in a standard linear-cavity configuration. The SDL chip is optically pumped by a continuous-wave (CW) 808 nm fiber-coupled diode laser. The cavity parameters, i.e., the cavity length, the pump-spot width, and the transmittance of the output-coupler (OC) mirror, are systematically varied to achieve an optimization of the operating conditions. After the best optimal parameters were determined, the impact of the heat-sink temperature on the performance of the studied devices is investigated, as it is shown in Fig. 2.5. For QD-SDLs emitting at 1040 nm. The best performance is achieved for a cavity length of 96 mm, a pump-spot width of about 330 μm, and an OC mirror with 0.6% transmission. As a consequence of the optimization of the operation

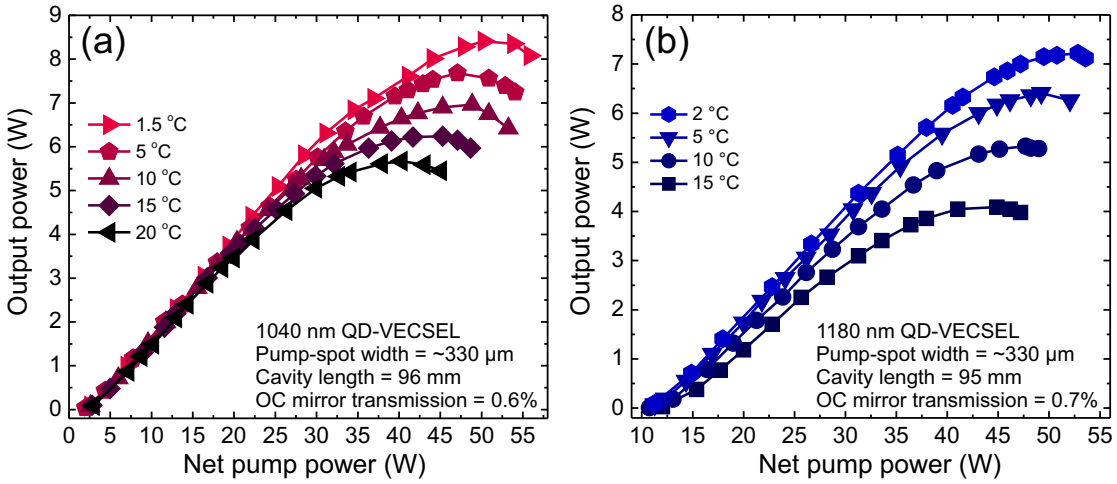

Figure 2.5. Output power characteristics measured at various heat-sink temperaturesfor for (a) 1040 nm and (b) 1180 nm QD-SDLs.

conditions, a maximum continuous-wave output power up to 8.4 W is recorded at a heat-sink temperature of 1.5 ^{o}C. On the other hand, QD-SDLs emitting at 1180 nm with output powers up to 7.2 W are recorded in the regime of transversal multimode operation for an optimized linear cavity of 95 mm length, a pump spot width of 330 μm, and an OC mirror with 0.7% transmission at 2 ^{o}C.

Besides, a wavelength tuning over a range of 45 nm around 1040 nm and of 37 nm around 1180 nm is demonstrated by rotating a 1-mm-thick birefringent filter inside the laser cavity.

The SDL chip designed for emission at 1040 nm was tested also in a V-shape cavity configuration, shown in Fig. 2.6, in order to study the influence of the transmission of the OC mirror on the SDL's performance. The gain chip formed one end of the cavity, while a $R_{oc} = -200$ mm curved mirror with a high reflectivity (HR) of 99.9% served as a folding mirror and a plane output coupler (OC) mirror completed the cavity. The transmittance of the OC mirror is varied between 0.2% and 0.8%. The SDL chip is optically pumped by an 808-nm fiber-coupled diode laser with a spot diameter of approximately 330 μm. The output power as a function of the net pump power was measured for different OC mirrors at a heat-sink temperature of 10 ^{o}C. A maximum output power of 5 W as well as the highest slope efficiency of 13 is obtained for an OC mirror with a transmittance of 0.6%, as it is shown in Fig. 2.7.

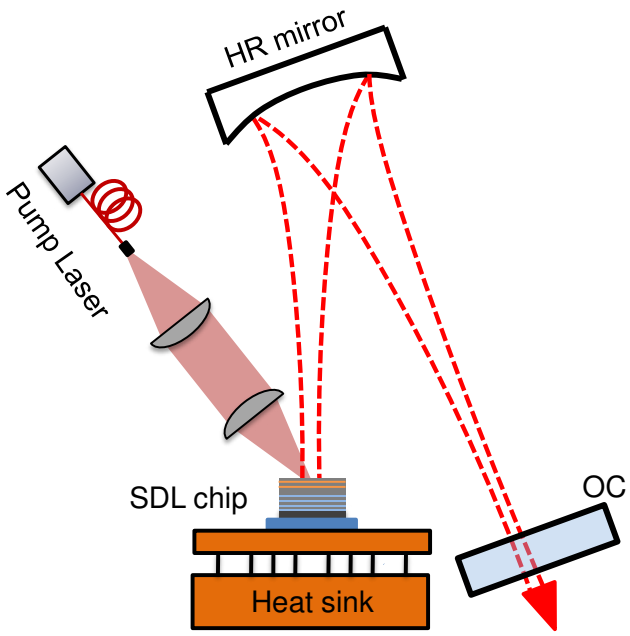

Figure 2.6. Schematic illustrations of the OP-VECSEL cavity setup with a V-shape cavity.

2.4 Heating and non-heating losses in SDLs

The performance of a laser device is influenced not only by the gain but also by the losses in the system. In SDLs, the maximum achievable power is predominantly limited by heating due to non-radiative losses inside the semiconductor gain medium [43]. Several sources for heat can be found in SDLs. Firstly, the pump power is not completely absorbed in the active region, considered power loss P_{NA}, as can be seen schematically in Fig. 2.8. The DBR contains GaAs-layers that absorb photons at the pump wavelength of 808 nm. Hence, a part of the pump power is absorbed in the DBR and converted into heat there. In addition, the heat inside the gain medium is additionally produced by the quantum defect, referred to as power loss P_{QD}, as indicated in the schematic drawing of the band structure in Fig. 2.9. This refers to the fact that by increasing the pump radiation, the difference between pump energy and lasing photons energy is transferred to the heat. While the pump beam passes the chip structure, a part of the pump power is absorbed in the active region of (SDLs). Thus, charge carriers are created by the pump radiation in the pump absorbing regions. Then, the excited carriers relax to

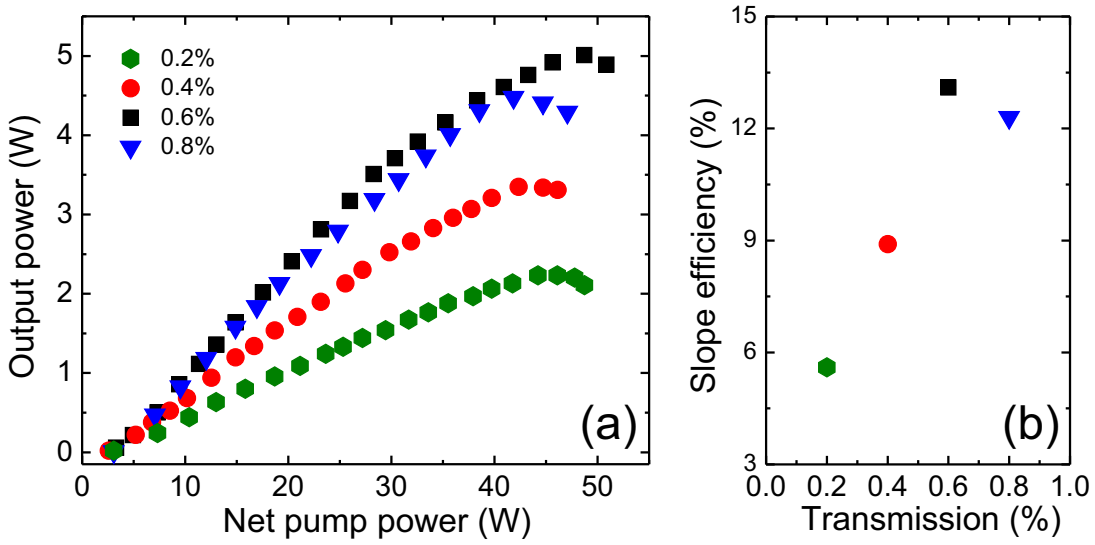

Figure 2.7. (a) Output power characteristics measured for different OC mirrors transmittance, a pump-spot width of about 330 μm and a heat sink temperature of 10^o C (left). The slope efficiency as a function of the OC mirrors transmittance is presented in (b).

the bottom energy level of the corresponding band after initial excitation to higher energy states. By doing this, they transfer the excess energy to the lattice as heat via phonon emission [44].

Another source which contributes to heat in the SDL gain medium is spontaneous emission (SE), which is, on the other hand, a source of noise in the laser oscillator. It occurs over all solid angles. This process takes place when an electron and hole recombine spontaneously, i. e., they release a photon without the presence of a stimulating photon. The emitted photon is not coherent with the laser oscillation, and can be re-absorbed outside the pump spot. The amount of SE is related to the pump spot size and heat extraction efficiency. If the pump spot size is small, a part of the SE is not reabsorbed in the gain material, so this part does not contribute to heating [22, 44, 45]. Besides, there are two basic recombination mechanisms, which contribute to heating, as shown in Fig. 2.10:

- Defect recombination, referred to as power loss P_d (nonradiative recombination): defect recombination in principal does not occur in perfectly pure materials [22, 46]. However, this process occurs in real materials, which naturally feature defects, when an electron falls into an energy level within the

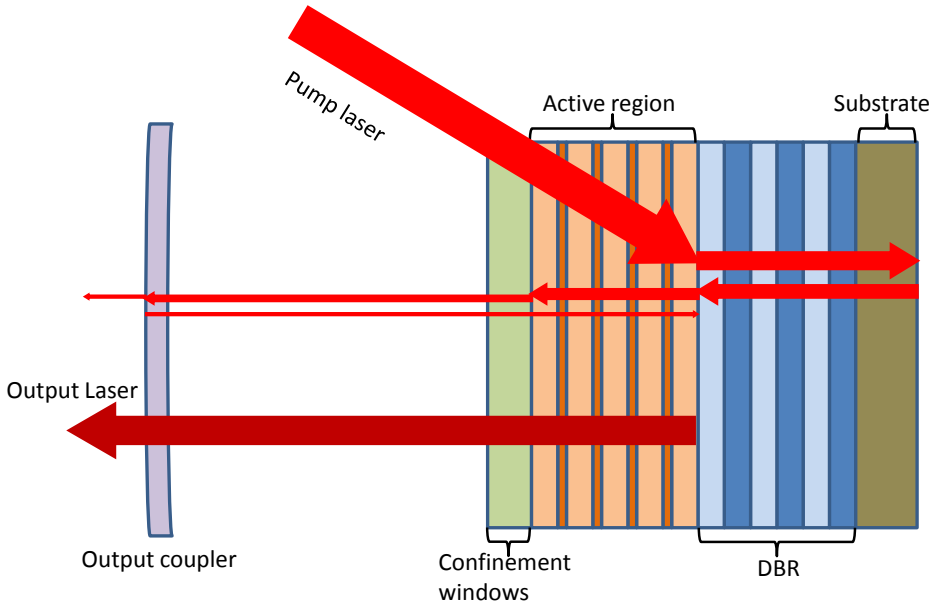

Figure 2.8. Non-absorption process of the pump power in an active region of SDLs.

bandgap caused by a structural defect. Then, in a second step, the electron can recombine with a hole in the valence band, thereby contributing to losses after charge carrier generation. The rate of this process depends linearly on the density of defects and on the carrier density. If high quality growth is achieved, one can reduce the amount of carrier losses in the gain region through this mechanism, however, this growth technique is not practical in terms of industrial-scale chip production.

- Auger recombination [48, 49]: Auger recombination requires three carriers to be present. This process occurs when the excess energy is released during the recombination of an electron and the hole energy is transferred to a third charge carrier. The latter is excited to a higher energy level without transfer to another energy band. After such interaction, the third carrier normally loses its excess energy to thermal vibrations, thus contributing to heat in the gain structure.

Auger recombination depends on the cube of the carrier density, wherefore it becomes a major source of losses in SDLs at high pump powers. The increase of the Auger recombination rate leads to heat being dumped into the chip beyond a certain pump threshold and reducing the gain. In our study, devices with benefi-

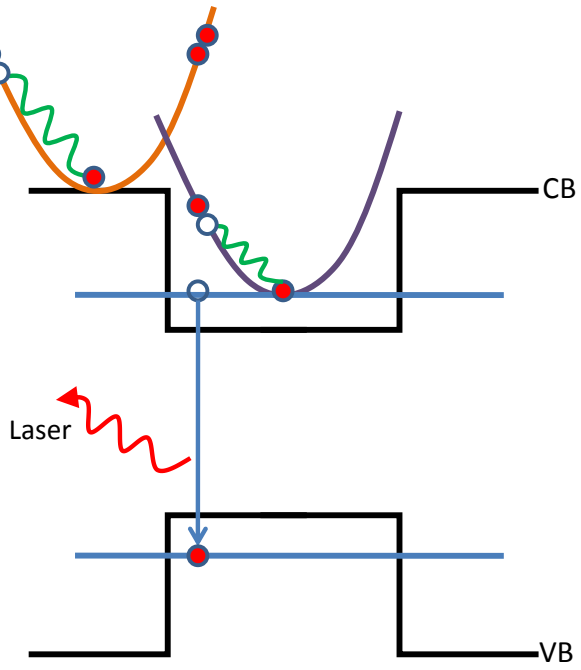

Figure 2.9. mechanism quantum defect in SDLs.

cial properties with respect to a low probability of Auger recombination and other heating losses, such as low threshold carrier densities and good thermal characteristics are desirable. Defect recombination, Auger recombination and spontaneous emission can be described by the following equation [50]:

$$R_{rec} = AN + BN^2 + CN^3 \,, \tag{2.4}$$

where N is the carrier density, A is the defect recombination rate, B is the spontaneous emission rate and C is the Auger recombination rate.

Additional effects limiting the output power include diffraction losses due to the surface roughness. In the case of surface roughness, the intra-cavity surface scattering should be not ignored, a loss channel not contributing to heating. Light scattering is a natural phenomenon that can occur on surfaces which feature height fluctuations and surface artifacts, thus coupling out intracavity power, with the amount of scattering directly corresponding to the surface imperfections [53]. Furthermore, a part of the laser light is diffracted due to thermal lensing. Thermal lensing happens when an excitation laser passing through a chip is absorbed: the chip absorbs the excitation laser and releases part of the light energy as heat due to

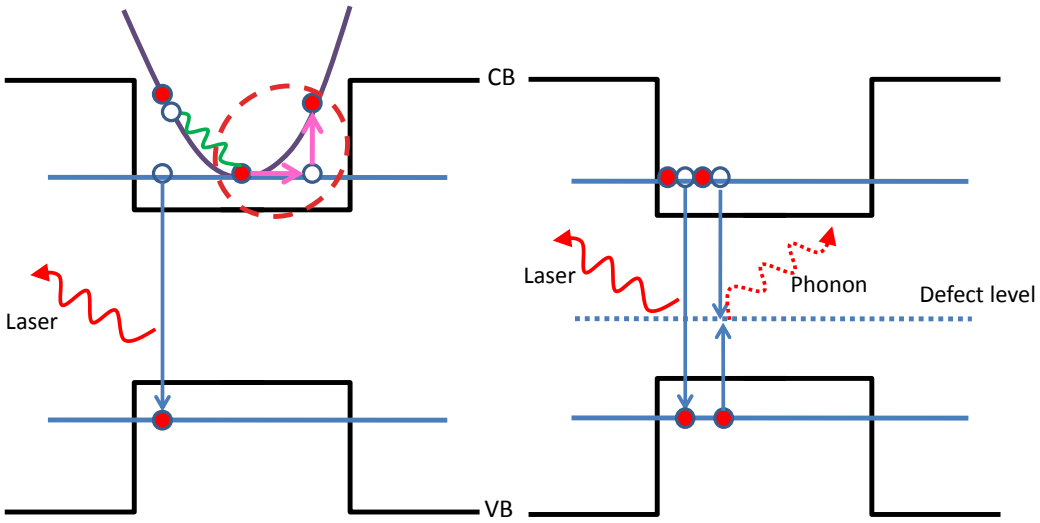

Figure 2.10. Auger recombination (left) and defect recombination mechanisms in semiconductors.

non-radiative recombination. The generated heat leads to an expansion of the chip and the temperature profile features a distribution in the active structure similar to a Gaussian profile. Since the refractive index is dependent on the temperature, thus a refractive index change occurs in the active structure and a concave lens. Thermal lensing has a noticable effect on the SDL's performance, and so prevents power scaling. Therefore, in order to minimize the effect of thermal lensing on the laser's performance, the cavity length should be carefully chosen to be around 50% of the radius of curvature of the output coupler [51, 52]. Both of the above mentioned light-diffracting effects will cause the intracavity light to be attenuated when passing through the SDL chip. When the laser light is attenuated via scattering, the transmitted intensity will exponentially decrease during the transit of a layer with thickness x within the SDL chip, as given by:

$$I = I_0 e^{-\alpha_{ss} x} \,, \tag{2.5}$$

where I_0 is the incident intensity (i.e. before attenuation), and α_{ss} represents the optical surface-scattering-losses coefficient which refers to the roughness and the quality of the SDL chip's surface. Indeed, at each cavity round-trip, a fraction of the intracavity l will be scattered at height fluctuations of interfaces in the

semiconductor gain medium, which leads to a power loss channel.This non-heating loss channel is referred to as the optical surface-scattering power (P_{ss}), which is written [44]

$$P_{ss} = P_{out}\frac{\alpha_{ss}}{\alpha_{out}} , \tag{2.6}$$

the optical surface-scattering losses increase when the pump-laser power increases in SDLs cavity. However, the output power P_{out} depends also on the pump laser power. (P_{ss}) is increased by increasing P_{out} and is inversely proportional with the photon out-coupling losses α_{out}.

2.4.1 Thermal impedance

With increasing temperature, the optical gain for a fixed carrier density decreases. Thus, to maintain the desired gain, a higher carrier density is required which, however, leads to a further increase in the losses due to heating. This self-perpetuating process is accelerated once Auger losses become important since these losses strongly increase with carrier density. Ultimately, the device will shut off due to thermal roll-over. In short-cavity lasers like SDLs, the roll-over effects are accelerated since the heating also shifts the gain away from the wavelength-selecting cavity resonance. Thus, heat management is particularly important in such laser systems [54, 55]. The quality of this management is characterized by the thermal impedance R_{th}, which is a measure of the increase in temperature with heating power. The thermal impedance depends on several factors such as the SDL's chip material, the heat sink geometry, and the pump-spot size. However, it has no correlation with the transmittance of the OC mirror or other resonator components. The determinant of this quantity requires the separation of power losses that contribute to heating from those that do not.

2.4.2 Experimental setup

In this section, the experiment is described with respect to a QD-based device. The structure of the QD-SDL chip employed for this study was grown by molecular beam epitaxy (MBE) on a semi-insulating GaAs substrate, to emit at 1040

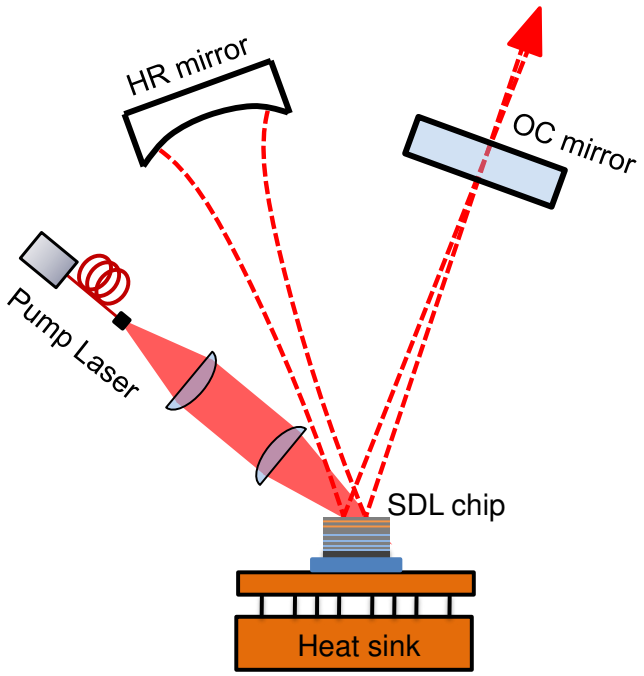

Figure 2.11. Schematic drawing of the experimental setup.

nm. A high reflectivity distributed Bragg reflector (DBR) consisting of 29.5 pairs GaAs/$Al_{0.9}Ga_{0.1}$ was grown on a 500-nm-thick-GaAs buffer. The active medium was grown on the top of the DBR. The latter consists of 35 layers of Stranski-Krastanov grown InGaAs QDs within GaAs spacers, organized as 5 stacks of each 7 QD layers that are placed at the standing-wave electric field maxima inside the cavity. Finally, the structure is capped by an $Al_{0.9}Ga_{0.1}As$ barrier layer followed by a GaAs layer in order to prevent surface recombination of the excited carriers and to avoid oxidation, respectively.

The SDL chip is chemically bonded on a diamond heat-spreader, which is employed for thermal management, and mounted on a Peltier-cooled copper heat-sink. The excess heat, generated during laser operation, is dissipated via closed cycle water cooling. A standard V-cavity configuration is used, shown in Fig. 2.11 schematically, in which the resonator consists of the SDL-chip's DBR, a concave mirror with a high reflectivity (HR) of 99.9% and a curvature radius of - 200 mm, and a plane output coupler (OC) mirror with transmittance of 0.2, 0.4, 0.6 and 0.8%, respectively. The SDL chip is optically pumped by a 808-nm fiber-coupled diode laser with a maximum CW output power of 400 W. The pump laser is fo-

cused onto the SDL chip under an incidence angle of 35 ^{o}C with a spot diameter of approximately 530 μm.

2.4.3 Results and discussion

The output power (P_{out}) of the laser was measured as a function of the pump power P_{pump} for a range of output coupler transmittances between 0.2 and 0.8% at a heat sink temperature of 10 ^{o}C, as shown in Fig. 2.12. Owing to the fact that the roll-over temperature T_{ro} of the SDL chip is independent of the heat sink temperature T_{hs}, the thermal resistance R_{th} can be determined through Eq. 2.7, assuming that the pump power divides between output power and the dissipated heating power, and neglecting any other type of non-heating power loss [44, 55]:

$$T_{\mathrm{hs}} = -R_{\mathrm{th}} P_{\mathrm{heat}}^{\mathrm{ro}} + T_{\mathrm{ro}}, \tag{2.7}$$

where ($P_{\mathrm{heat}}^{\mathrm{ro}}$) is the heating power at thermal roll-over, which can be calculated from:

$$P_{\mathrm{heat}}^{\mathrm{ro}} = P_{\mathrm{pump}}^{\mathrm{ro}} - P_{\mathrm{out}}^{\mathrm{ro}}, \tag{2.8}$$

where ($P_{\mathrm{pump}}^{\mathrm{ro}}$) and ($P_{\mathrm{out}}^{\mathrm{ro}}$) are the pump power and the output power at the outset of thermal roll-over (point of maximum output power). Both powers are recorded at different heat sink temperatures, for different output coupler transmittances. Fig. 2.13 shows the heat sink temperature as a function of the measured $P_{\mathrm{heat}}^{\mathrm{ro}}$. The slope from an experimentally obtained linear dependency represents the thermal impedance R_{th}, according to Eq. 2.7. One can observe that the plotted lines are nearly parallel and the values of the extracted R_{th} for each line are approximately constant at different OC mirror transmittances, as presented in Fig. 2.14(a) by black squares. However, the thermal resistance has to be completely independent of the output coupler transmission or other resonator components. In contrast, it relates only to the SDL chip's materials and structural properties, and hence, the thermal resistance should be absolutely constant. In order to correctly extract this value, the non-heating power loss channel should be

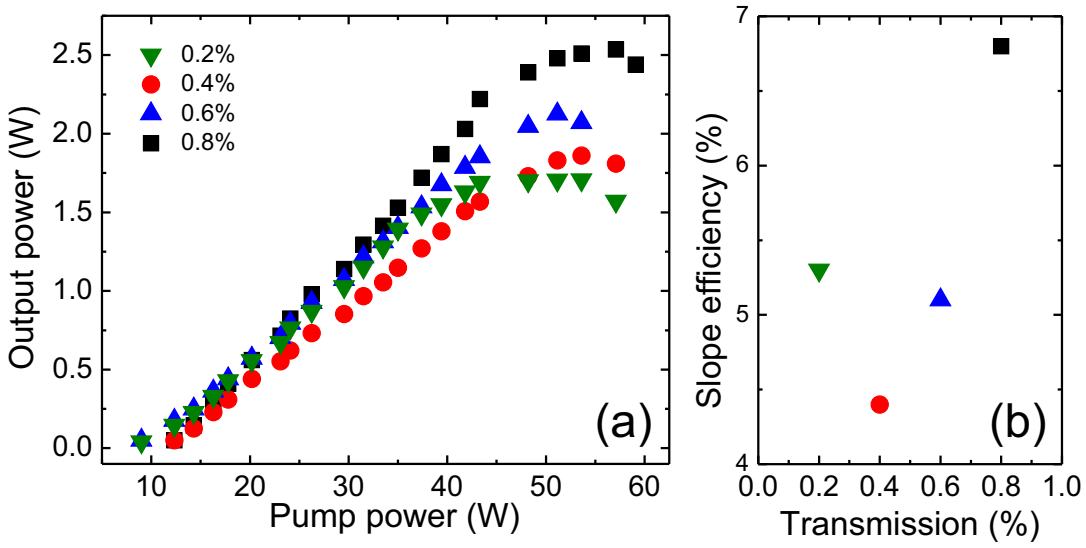

Figure 2.12. Output power characteristics measured for different OC mirror transmittances (a). The slope efficiency as a function of the OC mirrors transmittance (b).

taken into account in Eq. 2.8. The non-heat power consists mainly of spontaneous emission (SE), which does not contribute to heating, and optical scattering of the intra-cavity radiation on the chip's surface. The former one can be neglected due to the large pump spot size, while the latter one, optical surface-scattering power losses P_{ss}, need to be taken into account. Considering P_{ss} at thermal roll-over, given by Eq. 2.6, one can write Eq. 2.8 as follows:

$$P'^{\mathrm{ro}}_{\mathrm{heat}} = P^{\mathrm{ro}}_{\mathrm{pump}} - P^{\mathrm{ro}}_{\mathrm{out}} - P_{\mathrm{out}}\frac{\alpha_{\mathrm{ss}}}{\alpha_{\mathrm{out}}}. \tag{2.9}$$

Inserting Eq. 2.9 in Eq. 2.7:

$$T_{\mathrm{hs}} = -R_{\mathrm{th}}\left[P^{\mathrm{ro}}_{\mathrm{pump}} - P^{\mathrm{ro}}_{\mathrm{out}}\left(1+\frac{\alpha_{\mathrm{ss}}}{\alpha_{\mathrm{out}}}\right)\right] + T_{\mathrm{ro}} \tag{2.10}$$

By analysis of the experimental data according to Eq. 2.10, one obtains the value of the scattering coefficient $\alpha_{ss} = 10^{-21}$ and a constant value of the thermal resistance $R_{th} = 1.78\pm0{,}03$ K/W, which is presented in Fig. 2.14(a) for different values of α_{out} by red dots.

The y-intercept of the fitted line in Fig. 2.13 represents the temperature of the gain medium at the thermal roll-over.

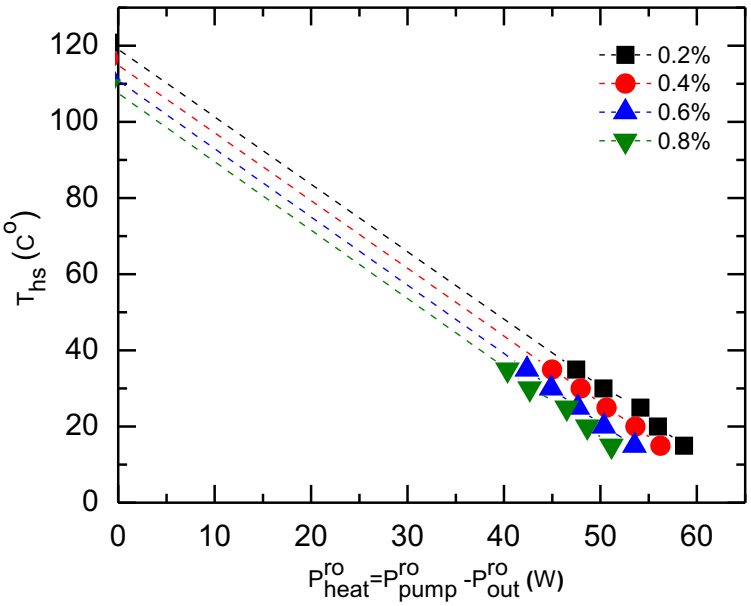

Figure 2.13. Heat sink temperature as a function of dissipated heat power.

The extracted values of T_{ro} from using both models, i. e., without and with taking scattering losses into account, respectively, are presented by black squares (using Eq. 2.7) and red dots (using Eq. 2.10) in Fig. 2.14(b). We observe a very slight deviation of the extracted roll-over temperatures with the expanded model from data yielded from the simple-model analysis which is negligible.

The above performed study is repeated for another position on the QD-SDL chip to understand position dependency and applicability of the expanded thermal-impedance model. The experimental results for this position, e.g. the scattering coefficient of 2×10^{-21} and the thermal resistance of 1.908±0.03 K/W show that the experimental technique is well reproducable and delivers values corresponding to the local chip properties. The slightly worse impedance values for this position is attributed to a local variation in the bonding quality. And at the same time, the obtained values of the scattering coefficient for both positions can be explained by chip's high-quality surface with negligible roughness.

The aforementioned study has also been done for a QW-SDL chip. The results of this study were published entitled "Analysis of optical scattering losses in vertical-external-cavity-surface-emitting lasers" (Section 5.3) [56]. In at study, a QW-SDL chip with enhanced surface roughness was employed to adequately pro-

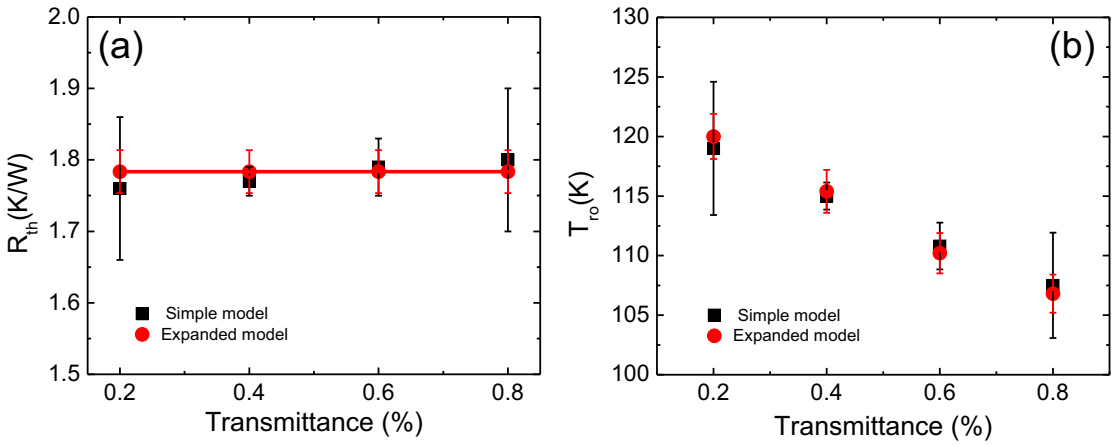

Figure 2.14. (a) Extracted thermal resistance vs. OC transmittance for the simple (Eq. 2.7) and the expanded model (Eq. 2.10), respectively. (b) Thermal roll-over as a function of the OC transmittance for both models.

mote scattering for such an investigation. Also, the study was similarly performed at two positions on the QW-SDL chip. As a consequence of this study, the optical scattering coefficient was found for both positions to amount to α_{ss}=3.7±0.5 and 1.5±0.5, respectively, and a constant thermal resistance amounting to R_{th}= 3.5±0.2 and 3.0±0.1 K/W were yielded for the two different positions on the studied chip, respectively.

2.4.4 Conclusion

The thermal resistance of a reference low-surface-quality SDL chip is determined based on output power measurements for different output-coupler transmittances at thermal roll-over. A significant error is noted in the determination of the thermal resistance by using a theoretical model that neglects non-heating losses. The error can be avoided by taking into account the contribution of non-heating power losses in the laser system. With our systematic study and by using an expanded model for the extraction of the thermal resistance of the chip structure, optical surface scattering is determined to be a non-negligible component of loss channels in an SDL system.

Chapter 3

Summary

The development of semiconductor disk lasers (SDLs), which are also known as vertical-external-cavity surface-emitting lasers (VECSELs), gives rise to semiconductor lasers with high multi-watt output power combined with diffraction-limited output beam-profile.

Owing to a steady progress in the field of SDLs, they feature many advantages over conventional semiconductor (diode) lasers. For instance, high output powers can be achieved with a TEM_{00} beam profile, no p-n junctions are needed in an SDL device which reduces losses due to free-carrier absorption in doped regions, broad wavelength tuning (> 100 nm) is possible due to a broad gain bandwidth in semiconductors, and external-cavity configurations allow for different operation schemes, i. e., intra-cavity frequency conversion, wavelength-tunable single-frequency operation and mode-locking. This versatility is particularly beneficial with respect to applications. Up to now, mainly quantum-well (QW) based SDLs were used due to their strong yield. However, quantum-dots (QDs) based SDLs become increasingly popular, because they offer a number of advantages hardly achievable when using QWs, such as a reduced lasing threshold, a lower thermal sensitivity, and a higher differential gain. In addition, QDs are also applicable for a coverage of different spectral regions such as in the range of 1 to 1.3 μm, they can provide enhanced wavelength tunability and ultrafast carrier dynamics, which potentially will improve mode-locked operation with respect to shorter puls durations.

The work presented in this thesis was focussed on the development and test-

ing of high-power semiconductor disk lasers based on novel quantum-dot structures, and the analysis of optical-scattering losses in SDLs in general. The QDs in the SDL chip structure were formed by molecular-beam-epitaxy growth of InGaAs/GaAs semiconductor materials using the Stranski-Krastanov growth method, and supplied by our cooperation partners for investigations on the performance optimization. The employment of QD materials allowed for the realization of SDLs in the infrared spectral region between 1 and 1.3 μm. Devices with emission wavelengths of 1040 and 1180 nm were subject of this work and QD-based SDLs were tested with respect to high-power operation in a linear cavity configuration.

The experiments were performed in order to achieve a maximum output power in the continuous-wave (CW) regime for the existing chips. Therefore, the cavity parameters, i. e., the cavity length, the pump-spot width, and the transmittance of the output-coupler (OC) mirror, were systematically varied in order to reach the best performance of the studied device. As a consequence of the optimization of the operation conditions, record-high CW output powers up to 8.4 and 7.2 W are obtained at temperatures around 2 ^{o}C for SDLs emitting at 1040 and 1180 nm, respectively. Besides, by rotating an additionally inserted birefringent filter inside the laser cavity, the laser became wavelength tunable over a relatively large range of 45 and 37 nm for SDLs emitting at 1040 and 1180 nm, respectively. Although the results presented in this thesis may have certainly contributed to the development of QD SDLs, more effort is needed to fully explore the advantages of QD based materials. This will include wider research concerning the thermal sensitivity and operational stability of QD based lasers. That would allow for a more accurate design of the devices, which lead to a more efficient operation.

To highlight the influence of optical-scattering losses on the SDL's performance, the thermal resistance of a reference low-surface-quality SDLs chip was analyzed. From experimental input-output characteristics based on thermal roll-over for different output-coupler transmittance values, the optical surface-scattering losses were identified when using an expanded model that takes into account non-heating losses in a device. In this study, we've learned that optical surface-scattering is a non-negligible component of loss in an SDL system, thus further contributing to an understanding of limitations to high-power operation. In conclusion, the best-

quality chips –not only with respect to the structural quality inside the chip, but also to the surface quality– are required for the purpose of high-power operation.

Chapter 4

Summary in German (Zusammenfassung)

Die Entwicklung von Halbleiterscheibenlasern (im Englischen SDL), welche auch als vertikalemittierende Scheibenlaser mit externer Kavität (im Englischen VECSEL) bekannt sind, ermöglichte den Aufstieg von Halbleiterlasern in eine zuvor nicht erreichbare Leistungsklasse bei gleichzeitig hoher beugungsbegrenzter Strahlqualität.

Durch den steten Fortschritt im Bereich der SDLs können diese gegenüber herkömmlichen Halbleiterlasern wesentliche Vorteile aufweisen. Darunter fällt die Erzeugung starker Ausgangsleistung bei Erhalt der TEM_{00} Abstrahlcharakteristik, was bei stark gepumpten Diodenlasern kaum vorstellbar ist. Auch der Verzicht auf einen p-n-Übergang im SDL-Chip macht sich positiv bemerkbar, indem weniger Verluste durch die Absorption freier Ladungsträger in dotierten Bereichen stattfinden. Darüber hinaus ist durch eine große Gewinnbandbreite in Halbleitersystemen eine breite Wellenlängenverstimmung (> 100 nm) möglich. Schließlich erlaubt die Konfiguration mit externer Kavität die Umsetzung diverser Betriebsarten, unter anderem eine intrakavitäre Frequenzkonversion, einen wellenlängenverstimmbaren Einzelfrequenzbetrieb und Modenkopplung. Diese Vielseitigkeit ist insbesondere für Anwendungen vorteilhaft.

Bisher wurden vor allem Quantenfilm (engl. QW) basierte SDLs aufgrund ihrer hohen Ausbeute entwickelt. Jedoch werden Quantenpunkt (engl. QD) basierte SDLs zunehmend beliebter, da sie eine Anzahl an Vorteilen bieten, die mit QW

Strukturen schwer erzielbar ist, wie eine reduzierte Laserschwelle, eine niedrige thermische Empfindlichkeit, und eine höhere differenzielle Verstärkung. Darüber hinaus eignen sich InGaAs-basierte QD SDLs auch in Hinblick auf eine große Abdeckung verschiedener Wellenlängenbereiche im Bereich 1–1,3 μm, auf eine hohe Wellenlängenverstimmbarkeit und sehr schnelle Ladungsträgerdynamiken, welche potenziell eine Verbesserung des Modenkopplungsbetriebs ermöglicht.

Die in dieser Thesis vorgestellten Forschungsarbeiten behandelten primär die Entwicklung und Demonstration von leistungsstarken SDLs basierend auf QD-Strukturen. Die QDs im Halbleiterchip wurden mittels Molekularstrahlepitaxie des InGaAs/GaAs Materialsystems im Stranski-Krastanov Modus gewachsen und wurden von unseren Kooperationspartnern zur Untersuchung der Leistungsoptimierung zur Verfügung gestellt. Der Einsatz eines InGaAs QD Verstärkungsmedium ermöglichte dabei die Entwicklung von SDLs im infraroten Spektralbereich zwischen 1 bis 1,3 μm. In dieser Arbeit wurden daher zwei SDLs mit Emissionswellenlängen von 1040 und 1080 nm untersucht. Für die Leistungsoptimierung wurden die Experimente mit einer linearen Kavitätskonfiguration durchgeführt.

Die in dieser Arbeit vorgestellten Experimente wurden durchgeführt, um eine maximale Dauerstrich-Ausgangsleistung aus einem einzelnen, jeweils vorhandenen QD-Chip zu erzielen. Hierzu wurden systematisch Kavitätsparameter wie die Kavitätslänge, die Anregungsfleckgröße und die Transmittivität des Auskoppelspiegels variiert, um die beste mögliche Leistung des untersuchten Systems zu erzielen. In Folge der Optimierung der Betriebsbedingungen wurden schließlich rekordhohe Dauerstrich-Ausgangsleistungen von bis zu 8,4 bzw. 7,2 W bei Temperaturen um 2 ^{o}C für die SDLs bei 1040 bzw. 1180 nm demonstriert.

Darüber hinaus zeigten die SDLs unter Einsatz eines in die Kavität eingefügten doppelbrechenden Filters eine Verstimmbarkeit der Laseremission über einen relativ großen Bereich von 45 bzw. 37 nm für die SDLs bei 1040 und 1180 nm. Obwohl die in dieser Arbeit vorgestellten Ergebnisse bereits einen Beitrag zur Entwicklung von QD SDLn geleistet haben mögen, sei angemerkt, dass weitere Bemühungen nötig sind, um die Vorteile von QD SDLs weitläufig zu erforschen. Diese werden zum Beispiel weitere Untersuchungen hinsichtlich thermische Sensibilität und Betriebsstabilität der QD basierten Laser beinhalten. Folglich werden daraus neue

Erkenntnisse über bessere Chipdesigns für einen leistungsstärkeren Betrieb erzielt.

Abschließend wurde in dieser Arbeit die Rolle von optischen Streuverlusten in SDLn bei ihrer Leistungsfähigkeit anhand Untersuchungen des thermischen Widerstands eines SDL Chips mit niedriger Oberflächenqualität hervorgehoben. Hierzu wurde aus der experimentellen Eingangs-Ausgangs-Leistungscharakteristik des SDLs basierend auf dem thermischen Überrolleffekt für verschiedene Auskoppeltransmittivitäten im Vergleich mit einem erweiterten Modell für den thermischen Widerstand ein Verlustanteil im Resonatorsystem aufgrund von optischen Oberflächenstreuverlusten bestimmt. Das Modell vernachlässigt dabei nicht den Anteil von nicht wärmebezogener Verluste im SDL. Dadurch ermöglicht diese Studie ein besseres Verständnis der Leistungsbegrenzungen von SDLn, die für den Betrieb bei hoher Ausgangsleistung bestimmt sind. Zusammenfassend lässt sich somit sagen, dass für eine hohe Emissionsleistung des Lasers nicht nur ein Chip mit optimierter Halbleiterstruktur, sondern auch mit möglichst guter Strukturoberfläche und -Beschaffenheit erforderlich ist, da optische Verluste durch Streuung im System nicht vernachlässigbar sind.

Chapter 5

Publications

5.1 High-Power Quantum-Dot Vertical-External-Cavity Surface-Emitting Laser Exceeding 8 W

D. Al Nakdali, M. K. Shakfa, M. Gaafar, M.Butukus, K. A. Fedorove, M. Zulonas, M. Wichmann, F. Zhang, B. Heinen, A. Rahimi-Iman, W. Stolz, E. U. Rafailov, and M. koch, *IEEE Photonics Technol. Lett*, vol. 26, no. 15, 2014.

5.1.1 Abstract:

In this publication, we report on a record-high output power from an optically-pumped vertical-external-cavity surface-emitting laser based on quantum dots (QDs) grown in the Stranski-Krastanow regime. The active gain medium consists of 5 stacks each containing 7 QD layers and being located at antinodes of the optical standing-wave electric-field maxima inside the cavity, optimized for high-power emission at 1040 nm. Continuous wave output powers in excess of 8 W with a slope efficiency of around 19% have been demonstrated for a systematically optimized linear cavity of 96 mm length, with a pump spot width of 330 μm and an output coupler (OC) mirror with a transmittance of 0.6%, at a heat sink temperature of 1.5 ^{o}C.

Moreover, by inserting a birefringent filter inside the laser cavity, a wavelength tuning from 1015 nm to 1060 nm, corresponding to a total range of 45 nm is achieved. Here, a maximum continuous-wave output power of 0.5 W at 1036 nm is recorded due to additional optical losses introducted by the filter..

5.1.2 The author's contribution:

The experimental part of this publication was conducted by myself. Mohammad Khaled Shakfa and Mahmoud Gaafar helped me in the laboratory, with other coauthors of the group in Marburg also having strongly supported the experimental achievements. The QD-VECSEL chip was designed and provided by the group of Prof. Dr. Edik U. Rafailov, which is currently located at Aston University in the United Kingdom. The manuscript was written by Mohammad Khaled Shakfa, Dr. Arash Rahimi-Iman and me. All co-authors contributed with important ideas, fruitful discussions and corrections to the manuscript.

High-Power Quantum-Dot Vertical-External-Cavity Surface-Emitting Laser Exceeding 8 W

Dalia Al Nakdali, Mohammad Khaled Shakfa, Mahmoud Gaafar, Mantas Butkus, Ksenia A. Fedorova, Modestas Zulonas, Matthias Wichmann, Fan Zhang, Bernd Heinen, Arash Rahimi-Iman, Wolfgang Stolz, Edik U. Rafailov, and Martin Koch

***Abstract*— We report on a record-high output power from an optically pumped quantum-dot vertical-external-cavity surface-emitting laser, optimized for high-power emission at 1040 nm. A maximum continuous-wave output power of 8.41 W is obtained at a heat sink temperature of 1.5 °C. By inserting a birefringent filter inside the laser cavity, a wavelength tuning over a range of 45 nm is achieved.**

***Index Terms*— Quantum-dot (QD) semiconductors, optical pumping, vertical-external-cavity surface-emitting laser (VECSEL), semiconductor disk laser (SDL), wavelength tuning.**

I. Introduction

VERTICAL-EXTERNAL-CAVITY surface-emitting lasers (VECSELs) which are also known as semiconductor disk lasers (SDLs) have attracted much attention in recent years owing to their ability to combine high output-powers with diffraction-limited spatial beam quality and a widely accessible spectral range starting in the ultraviolet [1], [2] and reaching the mid-infrared [3], [4]. Novel structures based on quantum dots (QDs) embedded in this type of lasers [5] offer a number of the unique features such as broad gain bandwidth, ultrafast carrier dynamics, low temperature sensitivity, low threshold current and lower absorption saturation [6]. Moreover, their open architecture allows for numerous advantages such as passive modelocking using saturable absorbers [7]–[9] as well as even self-starting modelocking [10], [11] and intra-cavity frequency conversion [12]–[14]. Thus, these optically pumped systems have been employed for a variety of applications–scientific as well as industrial– such as spectroscopy, metrology, biophotonics, optical telecommunication, etc. [1], [3], [15]. It has been furthermore shown, that careful thermal management enables very high power operation for single-chip VECSELs with output powers exceeding 100 W [16]. Power scaling is also achieved by employment of multiple gain elements which can be exploited for frequency-doubled 532 nm devices with more than 60 W output power [17].

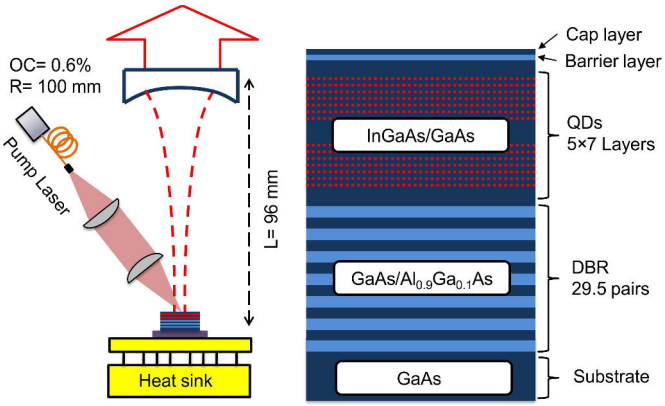

Fig. 1. Schematic illustrations of the OP-VECSEL cavity setup with a linear resonator (left), and the structure of the QD-VECSEL chip (right).

The chips constituting a VECSEL are not limited to periodic gain structures containing numerous quantum wells (QW), but also stacks of QDs layers are used which can be epitaxially grown under self-organization [18]. These QD-VECSELs provide as versatile systems as their similar QW pendants, with an even broader spectral gain and thus better tunability. However, their power output is significantly lower. Nevertheless, QD-VECSELs with up to a few Watts output power were demonstrated for various operation wavelengths in recent years; 1.39 W at 654 nm [19], 2 W at 1200 nm [20], 4.65 W at 1250 nm [21], 5.2 W at 960 nm [22], up to 4 W at 1180 nm [13], and 6 W at 1040 nm [13]. For the last two cases, wavelength tunabilities of 60 and 69 nm are reported, respectively [13].

In this letter, we report on a high performance operation of a QD-VECSEL designed for emission at 1040 nm. The output power is recorded for various pump spot widths and different heat sink temperatures. As a consequence of the optimization of the operation conditions, a maximum continuous-wave

Manuscript received April 29, 2014; revised May 24, 2014; accepted June 2, 2014. Date of publication June 5, 2014; date of current version July 15, 2014. This work was supported in part by the European Union FP7 Programme through the FAST-DOT Project under Contract 224338, and in part by the German Research Foundation through the GRK1782 Project and SFB1083 Project.

D. Al Nakdali, M. K. Shakfa, M. Gaafar, M. Wichmann, F. Zhang, B. Heinen, A. Rahimi-Iman, W. Stolz, and M. Koch are with the Department of Physics and Material Sciences Center, Philipps-University of Marburg, Marburg 35032, Germany (e-mail: dalia.alnakdali@physik.uni-marburg.de; m.k.shakfa@gmx.de; mahmoud.gaafar@physik.uni-marburg.de; matthias.wichmann@physik.unimarburg.de; fan.zhang@physik.uni-marburg.de; bernd.heinen@physik.unimarburg.de; a.r-i@physik.uni-marburg.de; wolfgang.stolz@physik.unimarburg.de; martin.koch@physik.uni-marburg.de).

M. Butkus is with the University of Dundee, Dundee DD1 4HN, U.K. (e-mail: mantas2butkus@gmail.com).

K. A. Fedorova, M. Zulonas, and E. U. Rafailov are with the School of Engineering and Applied Science, Aston University, Birmingham B4 7ET, U.K. (e-mail: k.fedorova@aston.ac.uk; zulonasm@aston.ac.uk; e.rafailov@aston.ac.uk).

Color versions of one or more of the figures in this letter are available online at http://ieeexplore.ieee.org.

Digital Object Identifier 10.1109/LPT.2014.2329269

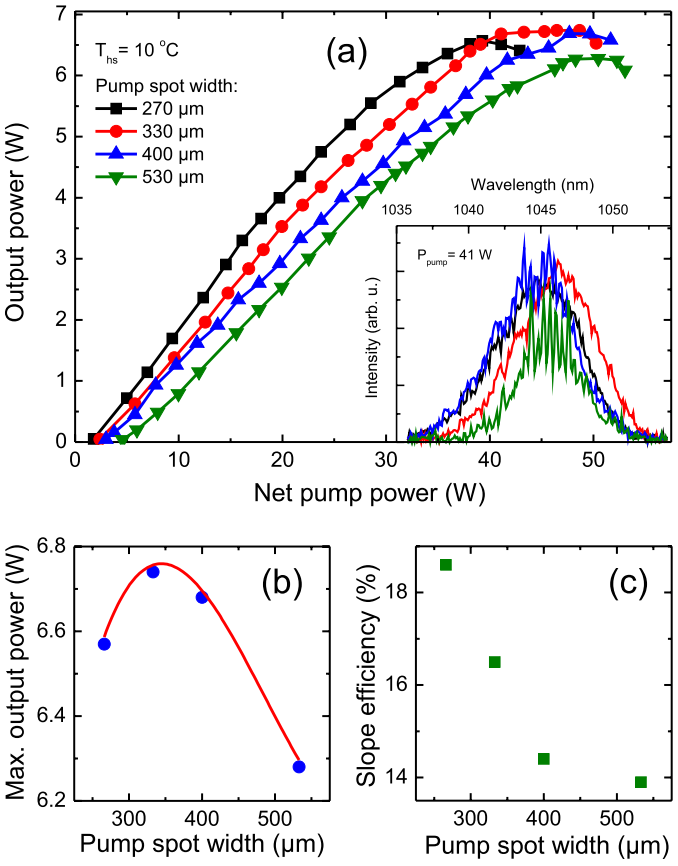

Fig. 2. (a) Input-output power characteristics for different pump spot widths, measured at a heat sink temperature (T_{hs}) of 1.5 °C. The inset in (a) shows the optical spectra of the laser for different pump spot widths, recorded at a net pump power (P_{pump}) of 41 W. (b) and (c) present the maximum (max.) output power and the slope efficiency as a function of the pump spot width, respectively. The red line in (b) serves as a guide to the eye.

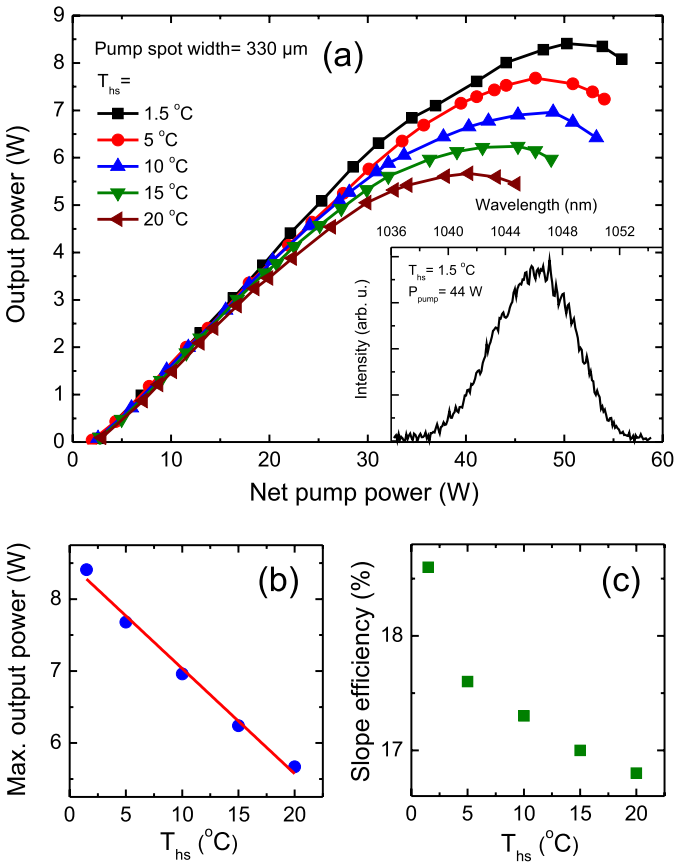

Fig. 3. (a) Input-output power characteristics for different heat sink temperatures, measured for a pump spot width of 330 μm. The inset in (a) shows the optical spectrum of the laser, recorded at a net pump power of 44 W at a heat sink temperature of 1.5 °C. (b) and (c) show the maximum output power and the slope efficiency as a function of the heat sink temperature, respectively. The red line in (b) denotes to a linear fit of the experimental data.

(CW) output power of 8.41 W is obtained for a pump spot width of 330 μm at a heat sink temperature of 1.5 °C. To our knowledge, this record output power is to date the highest reported for QD-VECSELs. Besides, a broad wavelength tunability up to 45 nm is achieved using a birefringent filter (BRF) which is inserted inside the laser cavity at Brewster's angle.

II. Experimental Setup

The VECSEL chip structure exhibits an antiresonant design and was grown on a GaAs substrate by molecular beam epitaxy (MBE) and designed to emit at 1040 nm. After a 500-nm-GaAs buffer, a high reflectivity distributed Bragg reflector (DBR) consisting of 29.5 pairs GaAs/$Al_{0.9}Ga_{0.1}As$ is followed by the active gain medium. The latter consists of 35 layers of Stranski-Krastanow grown InGaAs QDs within GaAs spacer, organized as 5 stacks of each 7 QD layers that are placed at the standing-wave electric field maxima inside the cavity. Finally, the structure is capped by an $Al_{0.9}Ga_{0.1}As$ barrier layer followed by a GaAs layer in order to prevent surface recombination of the excited carriers and to avoid oxidation, respectively. A schematic drawing of the VECSEL chip's structure is shown on the right side of Fig. 1. The VECSEL chip is bonded to an intra-cavity diamond heat-spreader using liquid capillary bonding technique [23], which is employed for thermal management, and mounted on a Peltier-cooled copper heat sink. The excess heat, generated during operation, is dissipated via closed-cycle water cooling.

A linear cavity configuration is used in our study, as shown on the left side of Fig. 1, in which the resonator consists of the VECSEL-chip's DBR and a concave output coupler (OC) mirror with a transmittance of 0.6% and a radius of curvature of 100 mm. The choice of this OC mirror is based on previous investigations, which indicated that by varying the overall output coupling an optimum performance can be obtained. In a study of a linear cavity configuration using three different transmittances of 0.15%, 0.3% and 0.6%, respectively, the best performance was revealed using a 0.6% transmittance. In addition, the optimum performance was obtained at a value of 0.6% in a similar investigation using several OC mirrors with transmittance in the range of 0.2% to 1% in steps of 0.2% in a single-pass V-shaped cavity, wherein the chip serves as an end-mirror such as in the linear configuration. We are confident that even finer tuning of the OC transmittance could still result in an increase of performance. The OC mirror opposes the gain mirror at an optimum distance of approximately 96 mm, resulting in a maximum of the laser output power while the system is operating in a transversal multimode regime.

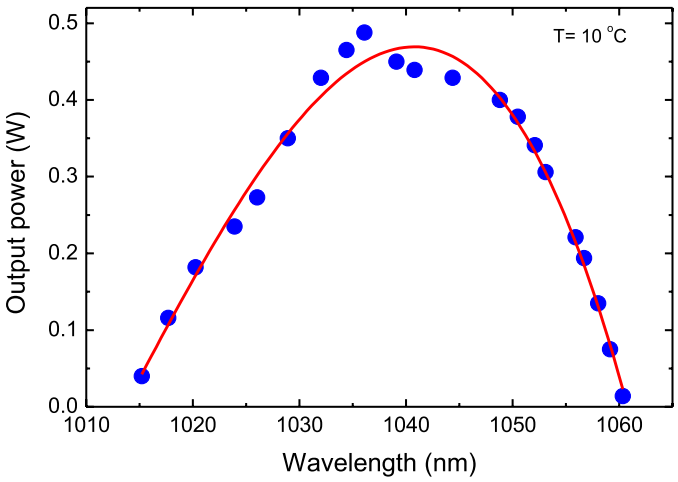

Fig. 4. Wavelength tuning characteristic, measured using a 0.6% output coupler (OC) and a birefringent filter (BRF) at a heat sink temperature of 10 °C. The BRF was inserted inside the cavity at Brewster's angle. The red curve serves as a guide to the eye.

The VECSEL chip is optically pumped (OP) by a 808-nm fiber-coupled diode laser with a maximum continuous-wave (CW) output power of 120 W. The pump laser is focused onto the VECSEL chip under an incidence angle of 35°. While the cavity-mode width at the chip's position and the OC are not changed for all measurements, the pump spot width is varied systematically between 270 μm and 530 μm in order to probe different mode matchings and power scaling effects.

III. Results

In order to optimize the VECSEL's performance we first study the output power of the device for different pump-to-mode matchings which are given by the ratio of the pump spot width to the set cavity-mode width at the chip's position. Fig. 2(a) shows the output power as a function of the net pump power for pump spot widths ranging from 270 μm to 530 μm, measured at a heat sink temperature of 10 °C. While the thermal roll-over together with the threshold occur earlier for reduced pump spot widths, the maximum output power (before the occurrence of the thermal roll-over) exhibits a maximum for a pump spot width of 330 μm, as can be seen in Fig. 2(b). Moreover, the laser's emission wavelength near the thermal roll-over remains independent of the pump spot width (see inset in Fig. 2(a)). However, the slope efficiency, presented in Fig. 2(c), decreases when the pump spot width is increased. For pump spot widths larger than 400 μm its value remains nearly constant.

Subsequently, for a pump spot width of 330 μm, we measured the output power of the VECSEL as a function of the net pump power for different heat sink temperatures corresponding to 1.5, 5, 10, 15 and 20 °C, which are plotted in Fig. 3(a). An obvious increase in the maximum output power as well as the slope efficiency is observed when the heat sink temperature is decreased, as is shown in Figs. 3(b) and (c), respectively. A maximum output power and a slope efficiency of 8.41 W and 18.6%, respectively, are recorded at a heat sink temperature of 1.5 °C. The inset in Fig. 3(a) represents the emission spectrum of the laser, which is recorded before the onset of thermal roll-over at a net pump power of 44 W and a heat sink temperature of 1.5 °C. Furthermore, the heat sink temperature dependence of the VECSEL output power is linear in this temperature range, as can be seen in Fig. 3(b), with an absolute slope of 0.15 W/°C. Hence, an output power of about 10 W could be achieved when the heat sink temperature is decreased to −10 °C.

Finally, we characterize the tunability of the output wavelength of our device. A BRF with a thickness of 1 mm is inserted inside the cavity at Brewster's angle in order to tune the wavelength. Fig. 4 shows the wavelength tuning characteristic, measured for a net pump power of 30 W and a pump spot width of 330 μm at a heat sink temperature of 10 °C. By rotating the BRF in its surface plane, the wavelength can be tuned from 1015 nm to 1060 nm, corresponding to a total range of 45 nm. In this experiment, the highest output power recorded amounts to 0.5 W at 1036 nm due to introduced optical losses.

IV. Conclusion

To summarize, we demonstrate high-power operation of a QD-VECSEL with optical output powers exceeding 8 W at 1040 nm. The input-output characteristics feature a clear dependence on the matching of the laser mode size on the gain mirror to the pump-spot width as well as a dependence on the chips temperature. Eventually, a maximum output power is obtained in the regime of transversal multimode operation for an optimized linear cavity of 96-mm length with a pump spot width of 330 μm at 1.5 °C. Moreover, the laser is tunable over a relatively large range of 45 nm when using a birefringent filter inside the cavity.We are confident that with further optimization of our QD-VECSEL device even higher output powers could be achieved in future studies.

Acknowledgment

The authors would like to thank Innolume GmbH for the fabrication of the VECSEL chip.

References

[1] S. Calvez, J. E. Hastie, M. Guin, O. G. Okhotnikov, and M. D. Dawson, "Semiconductor disk lasers for the generation of visible and ultraviolet radiation," *Laser Photon. Rev.*, vol. 3, no. 5, pp. 407–434, 2009.

[2] Y. Kaneda *et al.*, "Continuous-wave single-frequency 295 nm laser source by a frequency-quadrupled optically pumped semiconductor laser," *Opt. Lett.*, vol. 34, no. 22, pp. 3511–3513, 2009.

[3] A. Garnache *et al.*, "2-2.7 μm single frequency tunable Sb-based lasers operating in CW at RT: Microcavity and external cavity VCSELs, DFB," *Proc. SPIE*, vol. 6184, pp. 61840N-1–61840N-15, Apr. 2006.

[4] N. Schulz, J.-M. Hopkins, M. Rattunde, D. Burns, and J. Wagner, "High-brightness long-wavelength semiconductor disk lasers," *Laser Photon. Rev.*, vol. 2, no. 3, pp. 160–181, 2008.

[5] M. Butkus *et al.*, "High-power quantum-dot-based semiconductor disk laser," *Opt. Lett.*, vol. 34, no. 11, pp. 1672–1674, 2009.

[6] E. U. Rafailov, M. A. Cataluna, and W. Sibbett, "Mode-locked quantum-dot lasers," *Nature Photon.*, vol. 1, no. 7, pp. 395–401, 2007.

[7] U. Keller and A. C. Tropper, "Passively modelocked surface-emitting semiconductor lasers," *Phys. Rep.*, vol. 429, no. 2, pp. 67–120, 2006.

[8] M. Scheller, T.-L. Wang, B. Kunert, W. Stolz, S. W. Koch, and J. V. Moloney, "Passively modelocked VECSEL emitting 682 fs pulses with 5.1 W of average output power," *Electron. Lett.*, vol. 48, no. 10, pp. 588–589, May 2012.

[9] M. Butkus *et al.*, "85.7 MHz repetition rate mode-locked semiconductor disk laser: Fundamental and soliton bound states," *Opt. Exp.*, vol. 21, no. 21, pp. 25526–25531, 2013.

[10] L. Kornaszewski, G. Maker, G. P. A. Malcolm, M. Butkus, E. U. Rafailov, and C. J. Hamilton, "SESAM-free mode-locked semiconductor disk laser," *Laser Photon. Rev.*, vol. 6, no. 6, pp. L20–L23, 2012.

[11] M. Gaafar *et al.*, "Harmonic self-mode-locking of optically pumped semiconductor disc laser" *Electron. Lett.*, vol. 50, no. 7, pp. 542–543, Mar. 2014.

[12] M. Scheller, J. M. Yarborough, J. V. Moloney, M. Fallahi, M. Koch, and S. W. Koch, "Room temperature continuous wave milliwatt terahertz source," *Opt. Exp.*, vol. 18, no. 26, pp. 27112–27117, 2010.

[13] M. Butkus *et al.*, "Quantum dot based semiconductor disk lasers for 1–1.3 μm," *IEEE J. Sel. Topics Quantum Electron.*, vol. 17, no. 6, pp. 1763–1771, Nov./Dec. 2011.

[14] E. Kantola, T. Leinonen, S. Ranta, M. Tavast, and M. Guina, "High-efficiency 20 W yellow VECSEL," *Opt. Exp.*, vol. 22, no. 6, pp. 6372–6380, 2014.

[15] F.-Q. Li *et al.*, "Compact 7.8-W 1-GHz-repetition-rate passively mode-locked TEM_{00} Nd: YVO_4 laser under 880 nm diode direct-in-band pumping," *Opt. Commun.*, vol. 284, no. 19, pp. 4619–4622, 2011.

[16] B. Heinen *et al.*, "106 W continuous-wave output power from vertical-external-cavity surface-emitting laser," *Electron. Lett.*, vol. 48, no. 9, pp. 516–517, Apr. 2012.

[17] J. Chilla, Q.-Z. Shu, H. Zhou, E. Weiss, M. Reed, and L. Spinelli, "Recent advances in optically pumped semiconductor lasers," *Proc. SPIE*, vol. 6451, pp. 645109-1–645109-10, Feb. 2007.

[18] T. Germann *et al.*, "Quantum-dot semiconductor disk lasers," *J. Cryst. Growth*, vol. 310, no. 23, pp. 5182–5186, 2008.

[19] T. Schwarzbäck *et al.*, "High-power InP quantum dot based semiconductor disk laser exceeding 1.3 W," *Appl. Phys. Lett.*, vol. 102, no. 9, pp. 092101-1–092101-4, Mar. 2013.

[20] A. Rantamäki *et al.*, "Flip chip quantum-dot semiconductor disk laser at 1200 nm," *IEEE Photon. Technol. Lett.*, vol. 24, no. 15, pp. 1292–1294, Aug. 1, 2012.

[21] A. R. Albrecht *et al.*, "High-power 1.25 Âμm InAs QD VECSEL based on resonant periodic gain structure," *Proc. SPIE*, vol. 7919, pp. 791904-1–791904-6, Feb. 2011.

[22] M. Hoffmann *et al.*, "All quantum dot based femtosecond VECSEL," *Proc. SPIE*, vol. 7919, pp. 79190X-1–79190X-6, Feb. 2011.

[23] J. E. Hastie *et al.*, "0.5-W single transverse-mode operation of an 850-nm diode-pumped surface-emitting semiconductor laser," *IEEE Photon. Technol. Lett.*, vol. 15, no. 7, pp. 894–896, Jul. 2003.

5.1.3 Supplementary data

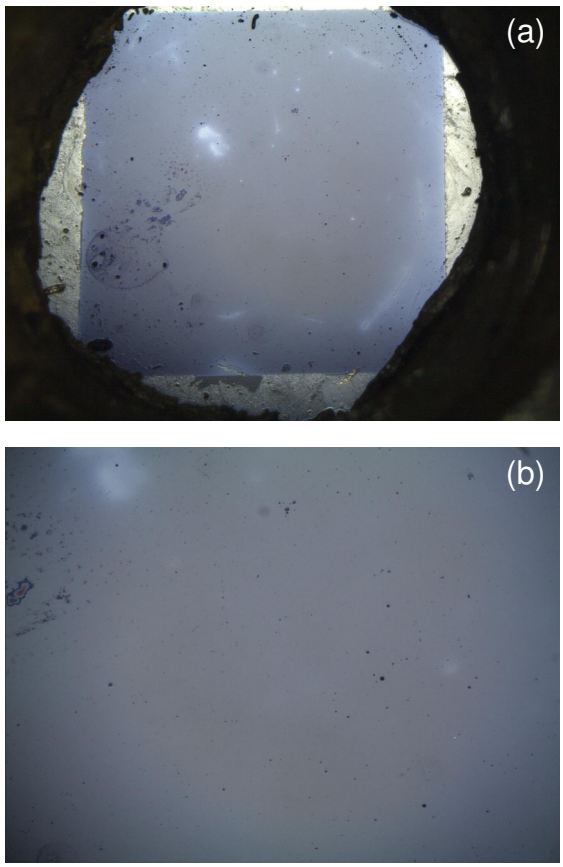

Figure 5.1. Optical microscope image of the studied QD SDLs chip.

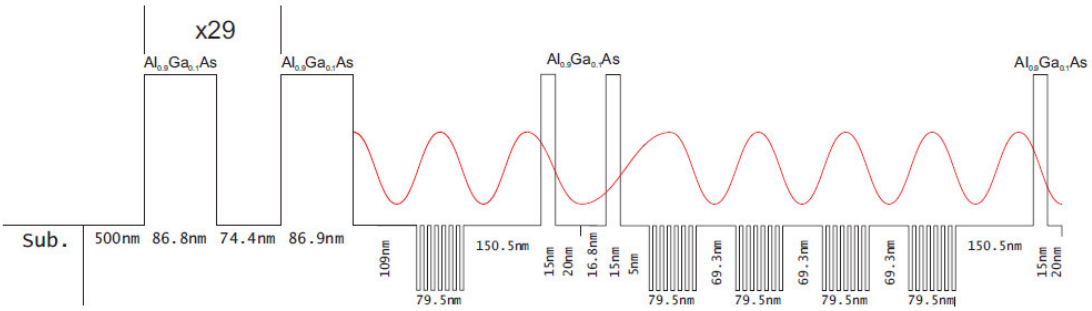

Figure 5.2. The design of the 1040 nm QD chip structure used in this study. In black, the profile of the potential energy in the semiconductor structure is shown. The red line represents the optical standing wave.

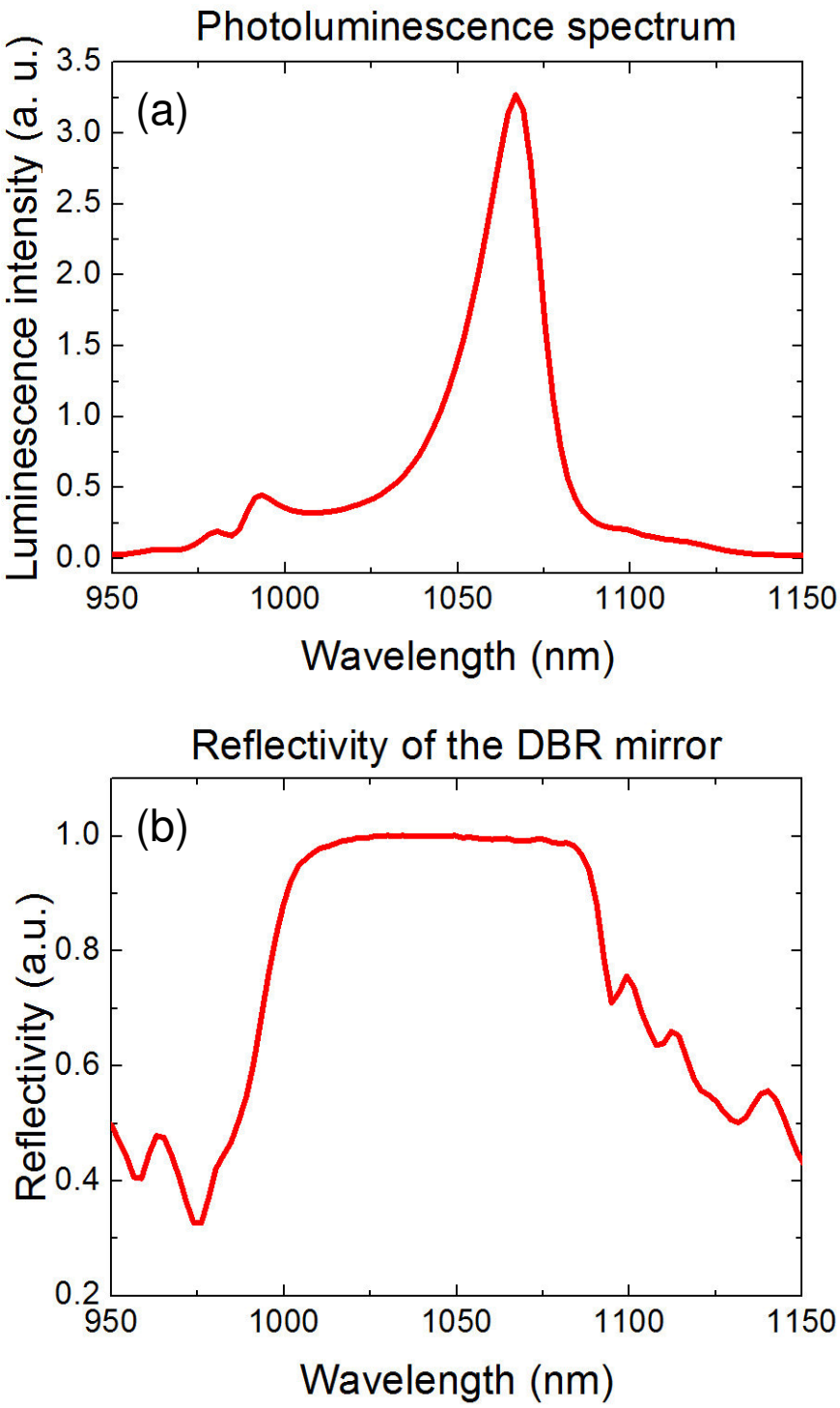

Figure 5.3. (a) Photoluminescence signal from the 1040 nm QD SDL sample. (b) Reflectivity spectrum of the chip's DBR mirror measured after growth.

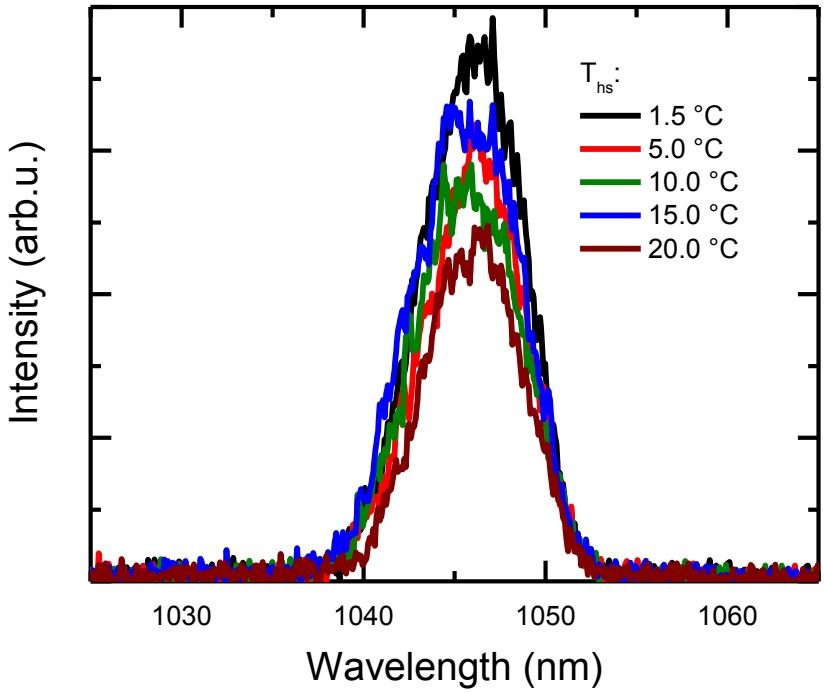

Figure 5.4. Optical spectrum of the laser, recorded at different heat-sink temperatures for a linear-cavity configuration.

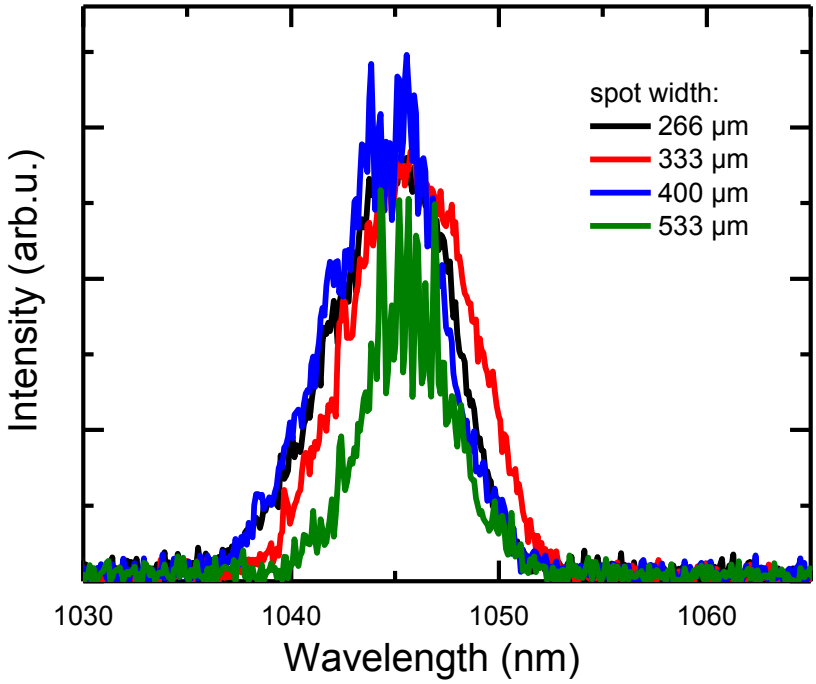

Figure 5.5. Optical spectrum of the laser, recorded at different pump-spot width for a linear-cavity configuration.

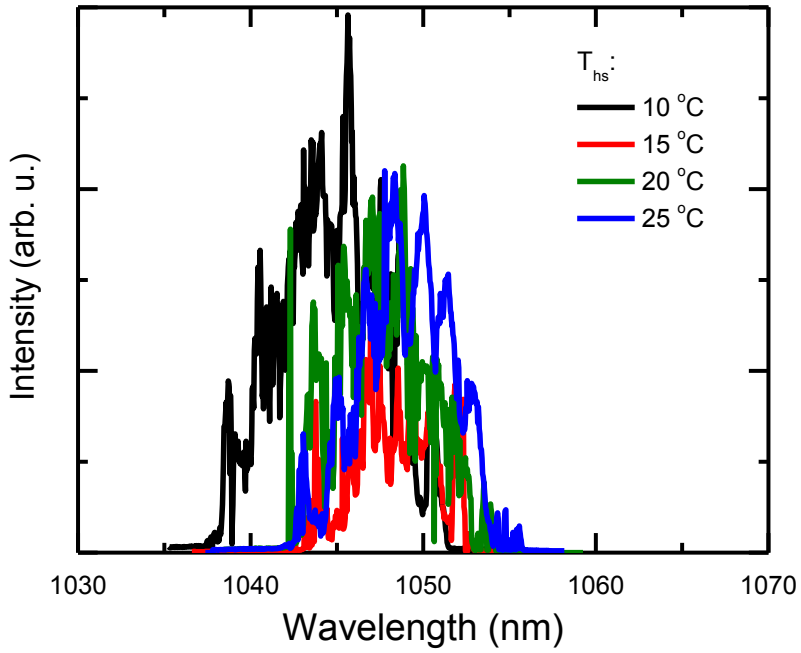

Figure 5.6. Optical spectrum of the laser, recorded at different heat-sink temperatures for a V-cavity configuration.

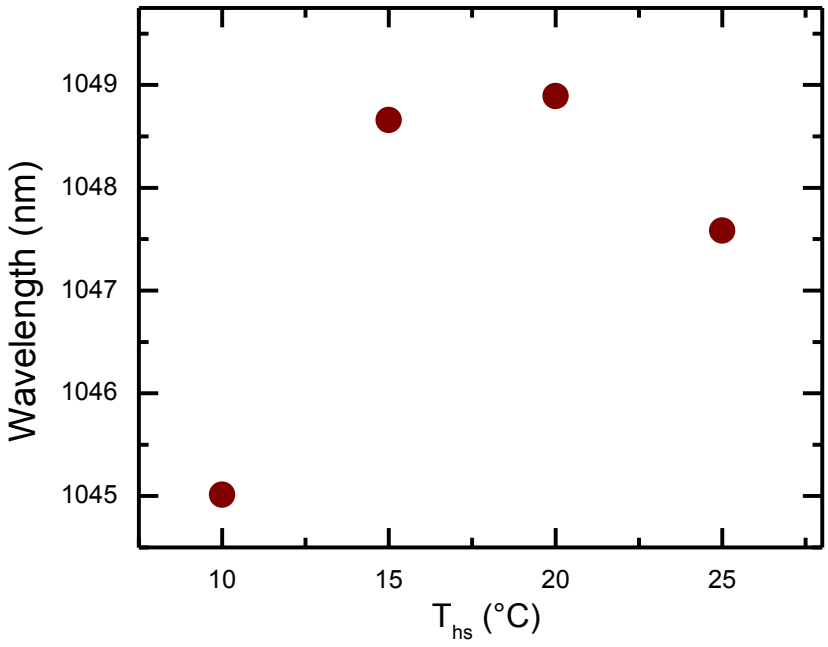

Figure 5.7. Central wavelength of emission extracted from optical spectra as a function of the heat-sink temperature.

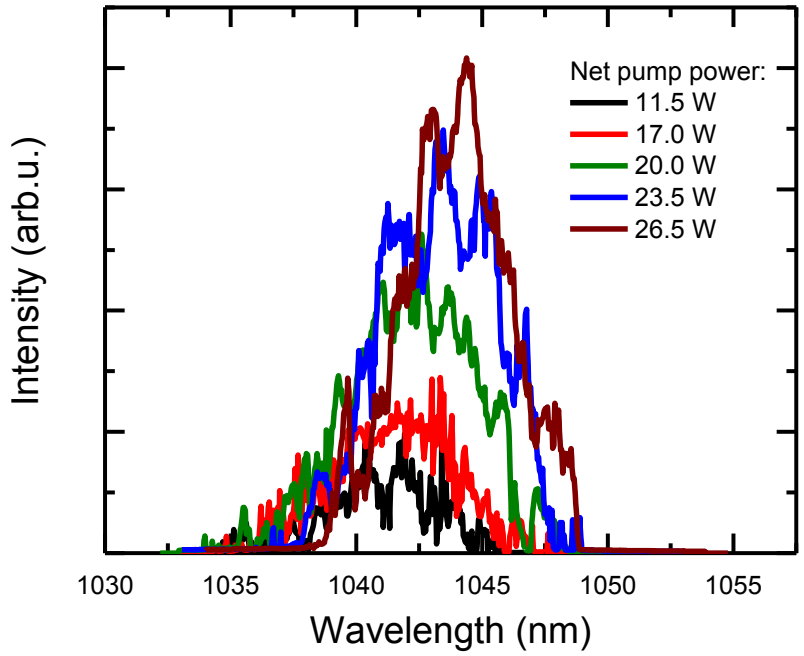

Figure 5.8. Optical spectrum of the laser, recorded at different net pump power for a V-cavity configuration.

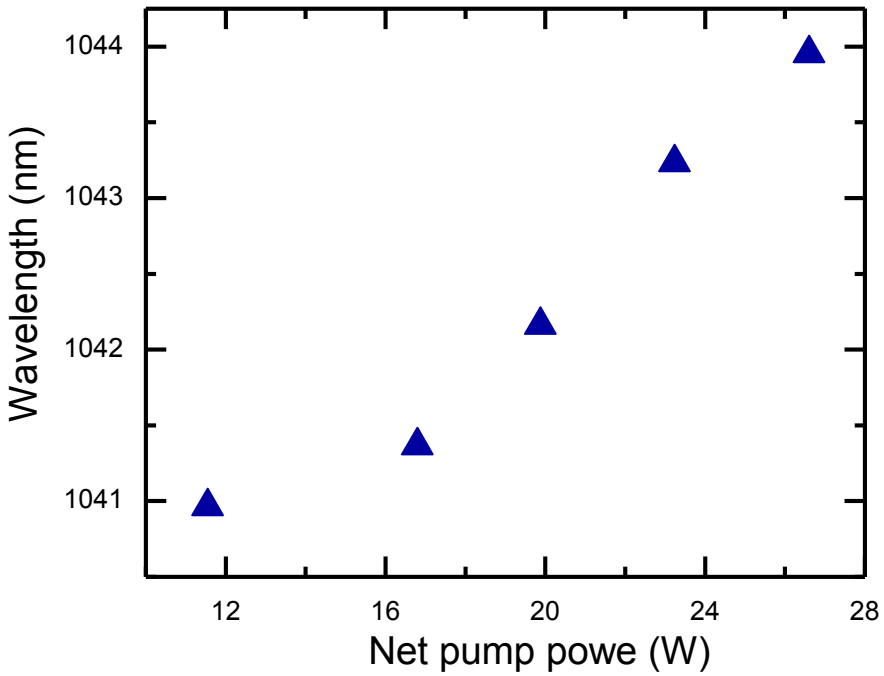

Figure 5.9. Central wavelength of emission extracted from optical spectra as a function of net pump power.

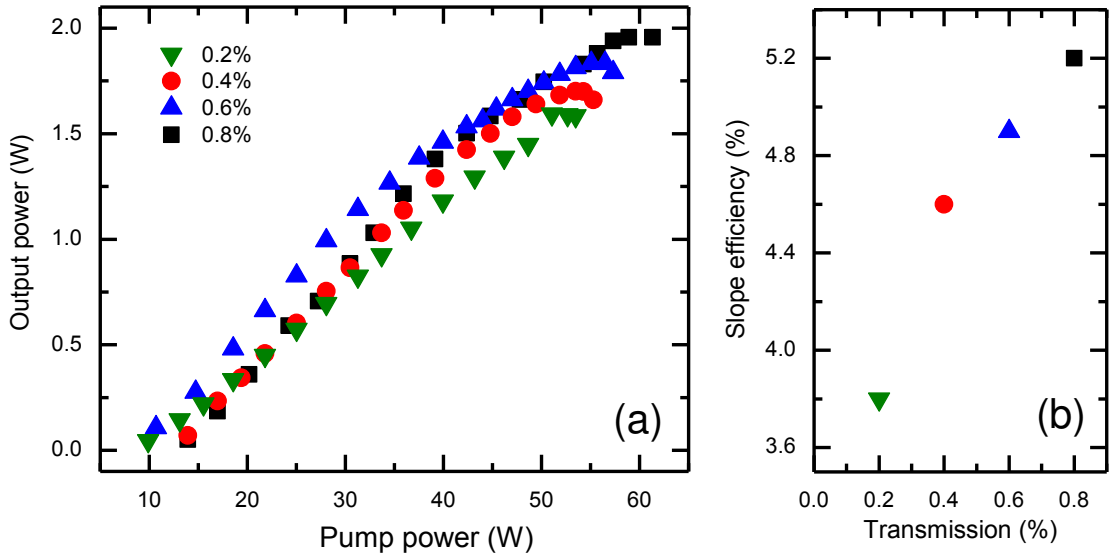

Figure 5.10. (a) Output power characteristics measured for different OC mirror transmittances. The slope efficiency as a function of the OC mirrors transmittance is presented (b) at the second position of the studied chip.

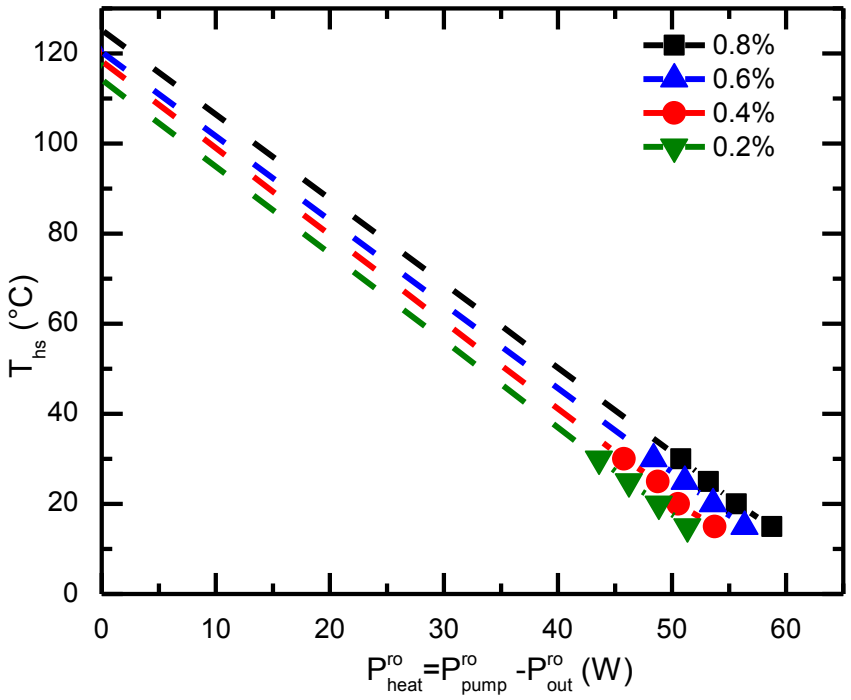

Figure 5.11. Heat sink temperature as a function of dissipated heat power corresponding to a simple model for the extraction of the thermal resistance according to [56].

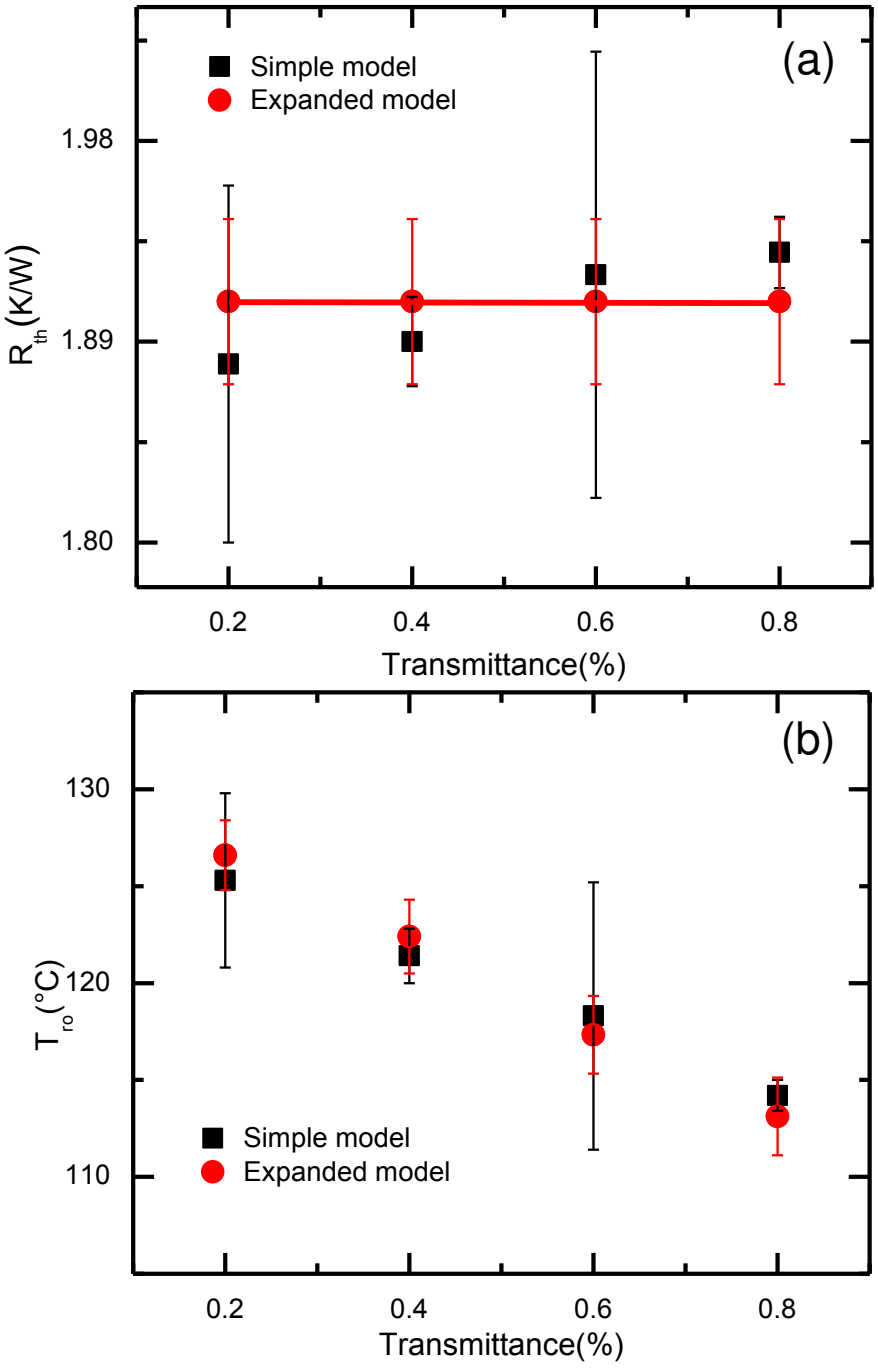

Figure 5.12. (a) Extracted thermal resistance vs. the OC transmittance for the simple- and the expanded model according to [56]. (b) Thermal roll-over as a function of the OC transmittance for both models.

5.2 High-Power Operation of Quantum-Dot Semiconductor Disk Laser at 1180 nm

D. Al Nakdali, M. Gaafar, M. K. Shakfa, F. Zhang, M. Vaupel, K. A. Fedorove, A. Rahimi-Iman, E. U. Rafailov, and M. koch, *IEEE Photonics Technol. Lett*, vol. 27, no. 10, 2015.

5.2.1 Abstract:

In this publication, we report on a record-high output power from a quantum-dot semiconductor disk laser, designed for emission at 1180 nm. The active region with 39 layers of QDs was grown on top of the DBR. The 6-nm thick Stranski-Krastanow-grown QD layers were arranged in 13 identical groups with 3 QD layers in each group and positioned at the antinodes of the standing-wave optical field. The cavity's parameters, i. e., the cavity length, the pump-spot width, and the OC mirror's transmittance were systematically varied in order to reach the optimal performance of the studied device.

For a cavity length of 95 mm, a pump-spot width of about 330 μm, and an OC mirror with transmission of 0.7%, a maximum continuous-wave output power up to 7.2 W with a slope efficiency of 20% at a heat sink temperature of 2 ^{o}C has been demonstrated. For this SDL chip, a broad wavelength tuning range of 37 nm around 1180 nm was experimentally obtained by inserting a birefringent filter inside the laser cavity. Here, a maximum continuous-wave output power of 1.7 W at the central wavelength was recorded.

5.2.2 The author's contribution:

The major experimental part of this publication was carried out by me and Mahmoud Gaafar. The QD-SDL chip designed for emission at 1180 nm was provided by Prof. Dr. Edik U. Rafailov's group at Aston-University in United Kingdom. The manuscript was mainly written by Mohammad Khaled Shakfa, in cooperation with me and Mahmoud Gaafar. All co-authors supported experimental work, data evaluation and contributed with important discussions and corrections to the manuscript.

High-Power Operation of Quantum-Dot Semiconductor Disk Laser at 1180 nm

Dalia Al Nakdali, Mahmoud Gaafar, Mohammad Khaled Shakfa, Fan Zhang, Max Vaupel, Ksenia A. Fedorova, Arash Rahimi-Iman, Edik U. Rafailov, and Martin Koch

***Abstract*— In this letter, we report on a high-power operation of an optically pumped quantum-dot semiconductor disk laser designed for emission at 1180 nm. As a consequence of the optimization of the operation conditions, a record-high continuous-wave output power exceeding 7 W is obtained for this wavelength at a heat-sink temperature of 2 °C. A wavelength tuning over a range of 37 nm is achieved using a birefringent filter inside the cavity.**

***Index Terms*— Quantum-dot (QD) semiconductors, optical pumping, semiconductor disk laser (SDL), vertical-external cavity surface-emitting laser (VECSEL), wavelength tuning.**

I. Introduction

AMONG lasers in general, and semiconductor lasers in particular, semiconductor disk lasers (SDLs), also known as vertical-external-cavity surface-emitting lasers (VECSELs) [1], have attracted increasing attention during the last two decades in the scientific community. Beside their compactness, functionalities, and relatively low costs, SDLs are evolving as a key optoelectronic technology that can offer excellent beam quality [2], high brightness [3], and low-noise performance [4]–[6]. Furthermore, SDLs provide not only high-power multi-mode continuous-wave (CW) operation [7], [8], but also ultra-short pulsed emission [9]–[12] across a wide range of the electromagnetic spectrum, i.e, from the ultraviolet [13], [14] to the mid-infrared [15], [16]. The latter is enriched with successful exploitation of SDLs as a secondary source based on intra-cavity frequency-conversion processes. In particular, benefiting from their unique external-cavity geometry, SDLs are utilized for, e.g., the generation of higher harmonics [17], [18] and the difference frequency generation (room-temperature CW terahertz applications [19]–[21]). However, SDLs operating in the high-power regime are typically required for such non-linear intra-cavity applications.

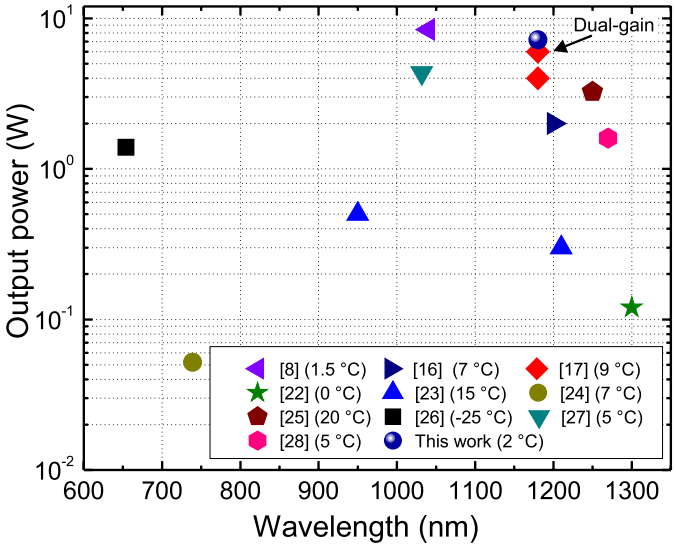

Fig. 1. Fundamental maximum continuous-wave output powers of QD-SDLs to date reported in the literature together with our present work. The corresponding temperatures are presented, each in brackets.

In this context, SDLs with quantum-dots-(QDs)-based active regions have generated an enormous amount of interest due to their potential for long-wavelength applications. In 2005, the first QD-SDL was achieved by Lott et al. [22] emitting near 1300 nm with an average output power of 120 mW. Three years later, QD-SDLs based on InAs/GaAs submonolayer (SML) and InGaAs Stranski-Krastanow (S-K) grown QDs gain material were demonstrated [23]. While for S-K samples, 300 mW output powers at 1040 nm and 1210 nm were reported, output powers of 1.4 W at 1040 nm and 0.5 W at 950 nm were achieved for SML samples. Further work led to an increase in the output power [18] and an extension of spectral coverage by QD-SDLs to red and near-infrared regions with a few tens of milliwatts at 730 nm [24] and multiwatts at 1250 nm [25], respectively. However, the highest output power for QD-SDLs has been recently obtained to be 8.4 W at 1040 nm [8]. A summary of remarkable fundamental maximum CW output powers of QD-SDLs to date is shown in Fig. 1.

In this letter, we report on a high-power operation of an optically pumped SDL based on (InGa)As S-K grown quantum dots and designed for emission at 1180 nm. The impact of the laser-cavity's parameters, i.e., the cavity length, the pump-spot width, and the transmittance of the

Manuscript received December 4, 2014; revised February 17, 2015; accepted February 23, 2015. Date of publication March 3, 2015; date of current version April 29, 2015. This work was supported in part by the European Community's Seventh Framework Programme through the FAST-DOT Project under Contract 224338 and in part by the German Research Foundation under Project GRK1782.

D. Al Nakdali, M. Gaafar, M. K. Shakfa, F. Zhang, M. Vaupel, A. Rahimi-Iman, and M. Koch are with the Material Sciences Center, Department of Physics, Philipps-University of Marburg, Marburg 35037, Germany (e-mail: dalia.alnakdali@physik.unimarburg.de; mahmoud.gaafar@physik.uni-marburg.de; m.k.shakfa@gmx.de; fan.zhang@physik.uni-marburg.de; Vaupelm4@students.uni-marburg.de; a.r-i@physik.uni-marburg.de; martin.koch@physik.uni-marburg.de).

K. A. Fedorova and E. U. Rafailov are with the School of Engineering and Applied Science, Aston University, Aston Triangle, Birmingham B4 7ET, U.K. (e-mail: k.fedorova@aston.ac.uk; e.rafailov@aston.ac.uk).

Color versions of one or more of the figures in this letter are available online at http://ieeexplore.ieee.org.

Digital Object Identifier 10.1109/LPT.2015.2408619

output-coupler (OC) mirror, on the performance of the studied device is systematically investigated to achieve the optimization of the operating conditions. For the optimized aforementioned cavity parameters, the output power is recorded at various heat-sink temperatures. While QD-SDLs at 1180 nm with 4 W and 6 W output powers were previously reported employing a single gain-chip and double gain-chips, respectively [17], [29], we have obtained – using only a single gain chip – a maximum CW output power of 7.22 W at a heat-sink temperature of 2 °C. Moreover, the wavelength tunability is performed using a birefringent filter (BRF). The latter is inserted inside the laser cavity at Brewster's angle.

II. Experimental Setup

The structure of the SDL chip studied in the present work was grown by molecular beam epitaxy (MBE) on a semi-insulating GaAs substrate. Firstly, a highly reflective distributed Bragg (DBR) reflector consisting of 35 pairs of GaAs/AlAs layers was grown on a 500-nm-thick-GaAs buffer. The active medium was grown on the top of the DBR and consists of 39 layers of S-K grown (InGa)As QDs, which are separated by 35-nm-thick-GaAs spacers. Each QDs-layer has a thickness of 6 nm. The QDs-layers are divided into 13 groups and placed at the anti-nodes of the optical standing wave. In addition, 83.4-nm-thick-GaAs spacer layers are placed between the groups of QDs. Then, the active region is capped by an $(Al_{0.9}Ga_{0.1})As$ window confinement layer with a thickness of 50 nm in order to prevent carrier recombination at the structure's surface. Finally, a 42.6-nm-thick-GaAs layer was grown on the top of the whole structure to avoid any oxidation. The above-described structure was designed for operation in the near-infrared spectral range at a wavelength of 1180 nm. More details on the structure's design can be found in the literature [18], [30].

The SDL chip is capillary bonded to an intra-cavity diamond heat-spreader, which is employed for thermal management, and mounted on a Peltier-cooled copper heat-sink. The excess heat, generated during laser operation, is dissipated via closed-cycle water cooling. The device is operated in a standard linear-cavity configuration, in which the resonator consists of the SDL-chip's DBR and a concave OC mirror. The SDL chip is optically pumped (OP) by a 808-nm fiber-coupled diode laser with a maximum CW output power of 120 W. The pump laser is focused onto the SDL chip under an incidence angle of 30°. At the aforementioned pump launch angle, the reflectivity from the diamond top surface and from the semiconductor-diamond interface for the pump wavelength was measured to be almost 10%. In this letter, we used four OC mirrors of an equal radius of curvature of −100 mm and different transmissions of 0.15%, 0.3%, 0.7%, and 1%. Also, the pump spot width is varied systematically in order to find the optimum operation condition for obtaining high output power.

III. Results

In spite of the emission wavelength of an SDL, a critical parameter which can significantly affect the SDL devices performance is the mode-matching, i.e, the ratio, of the pump-spot width to cavity-mode width at the chips position. Besides, the transmittance of the OC mirror should be carefully chosen for the purpose of high-power operation. The cavity-mode width is typically determined from the cavity length in the case of a linear cavity as well as TEM_{00} laser mode for a given radius of curvature of the OC mirror. However, at the conditions of high-power SDL operation, a transversal multimode emission is expected [31] and, hence, the cavity-mode width cannot be directly estimated. Therefore, in the following, we introduce the impact of the variation of the cavity length, instead of the cavity-mode width, on the SDL's performance.

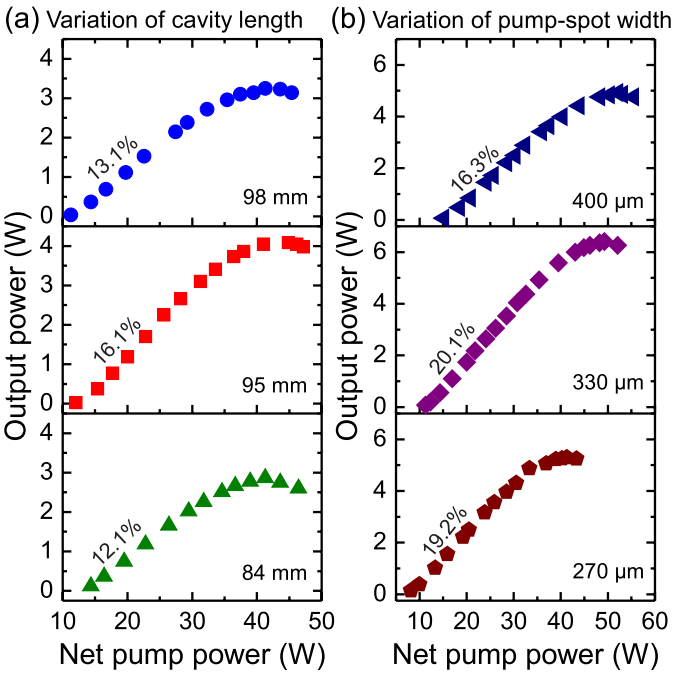

Fig. 2. (a) Output power characteristics measured for different cavity lengths, a pump-spot width of about 330 μm, and a heat-sink temperature of 15 °C. (b) Output power characteristics measured for different pump-spot widths, cavity length of 95 mm, and a heat-sink temperature of 5 °C. An OC mirror with 0.7%-transmission is used for all presented measurements. The inclined number in each subfigure in (a) as well as (b) represents the slope efficiency.

Fig. 2(a) shows the output power as a function of the net pump power for different cavity lengths and an OC mirror with a transmission of 0.7% at a heat-sink temperature of 15 °C. Here, the pump-spot width is set to about 330 μm and the cavity lengths are varied between 84 mm and 98 mm. The maximum output power of about 4.1 W, corresponding to the highest slope efficiency of 16.1%, is obtained for a cavity length of 95 mm. For the latter, on the other hand, the output power against the net pump power is shown in Fig. 2(b) for different pump-spot widths at a heat-sink temperature of 5 °C. In this case, the best performance of the studied device is observed for the pump-spot width of about 330 μm.

Next, we study the influence of the transmission of the OC mirror on the SDL's performance. Considering our above-mentioned findings, the cavity length and the pump-spot width are set to 95 mm and about 330 μm, respectively. However, the transmission of the OC mirror is varied between 0.15% and 1%. The corresponding experimental results are shown in Fig. 3, where the heat-sink temperature is set to 5 °C

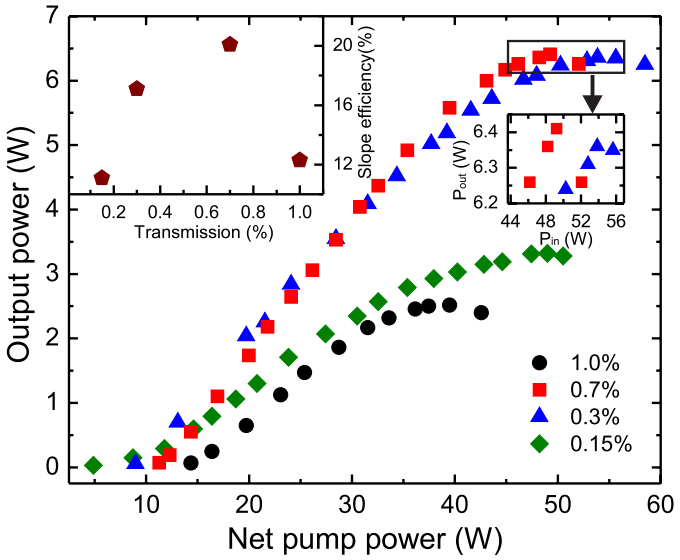

Fig. 3. Output power characteristics measured for for different OC mirrors, a pump-spot width of about 330 μm, a cavity length of 95 mm, and a heat-sink temperature of 5 °C. All OC mirrors have an equal curvature radius of −100 mm, but different transmissions. The left-hand inset shows the slope efficiency as a function of the transmission of the OC mirror. The right-hand inset shows a magnification of the encased area.

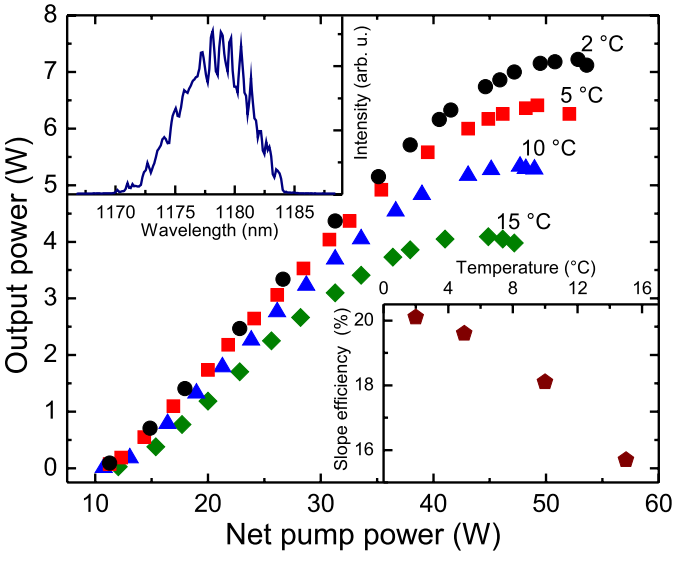

Fig. 4. Output power characteristics measured at various heat-sink temperatures for for a pump-spot width of about 330 μm, a cavity length of 95 mm, and an OC mirror with 0.7%-transmission. The bottom-right inset represents the slope efficiency as a function of the heat-sink temperature. The top-left inset shows the optical spectrum of the laser measured at an output power of 6.5 W at 2 °C.

for all measurements. Although the thermal roll-over of our device in the case of an OC mirror with 0.3%-transmission sets in later than for 0.7%, a maximum output power of 6.41 W as well as the highest slope efficiency of 20.1% is obtained for the second case, cf. the insets of Fig. 3.

Subsequently, the impact of the heat-sink temperature on the performance of our studied device is investigated. Here, the above-determined optimal parameters for our cavity are used, i.e., the cavity length of 95 mm, the pump-spot width of about 330 μm, and the OC mirror with 0.7%-transmission. A clear enhancement in the SDL's performance is observed when the heat-sink temperature is decreased from 15 °C down to 2 °C, as it is shown in Fig. 4. This is represented by the variation of the corresponding slope efficiency which is plotted against the heat-sink temperature in the bottom-right inset of Fig. 4. Remarkably, we obtain a maximum output power of 7.22 W at a heat-sink temperature of 2 °C. To our knowledge, this record output power is to date the highest reported for QD-SDLs emitting in the wavelength region of 1180 nm. However, owing to the different gain medium and chip structure, this result cannot be compared to record output powers in excess of 20 W obtained for quantum-well SDLs emitting at similar wavelengths [32]. The top-left inset of Fig. 4 shows the optical spectrum of the laser, which is centered at 1180 nm, recorded at an output power of 6.5 W and 2 °C heat-sink temperature. The distinct periodically spaced peaks in the output spectrum are caused by an etalon effect introduced by the intracavity diamond heat spreader.

Finally, in order to tune the laser wavelength of our device, an 1-mm-thick BRF is inserted inside the cavity at Brewster's angle. By rotating the BRF, the wavelength is tuned over 37 nm around its central wavelength for an OC mirror with 0.15%-transmission. This is shown in Fig. 5. The output

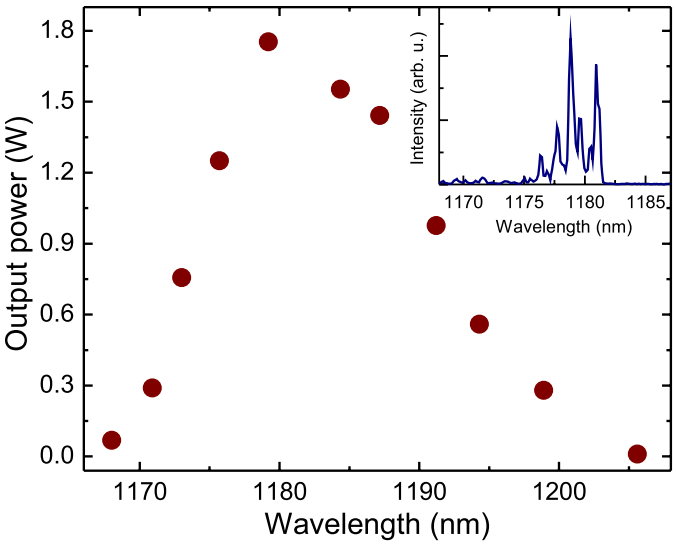

Fig. 5. Wavelength tuning characteristic measured using an 1-mm-thick BRF for an OC mirror with 0.15%-transmission at a heat-sink temperature of 10 °C. The inset shows the optical spectrum of the laser measured after having inserted the BRF inside the cavity.

power at the central wavelength is almost 1.7 W and reduced at the wings of the tuning range. An example of the optical spectrum obtained after having inserted the BRF inside the cavity is presented in the inset of Fig. 5.

IV. Conclusion

High-power operation of an optically pumped QD-SDL emitting at 1180 nm has been demonstrated. The cavity's parameters, i.e., the cavity length, the pump-spot width, and the OC mirror's transmittance, were systematically varied in order to reach the optimal performance of the studied device.

The best performance is achieved for a cavity length of 95 mm, a pump-spot width of about 330 μm, and an OC mirror with 0.7%-transmission. The corresponding maximum continuous-wave output power up to 7.22 W is recorded at a heat-sink temperature of 2 °C. Besides, by rotating a birefringent filter inside the laser cavity, the emission wavelength became tunable over a range of 37 nm.

ACKNOWLEDGMENT

The authors would like to thank Dr. D. A. Livshits from Innolume GmbH for the fabrication of the QD structure and Prof. O. G. Okhotnikov from Tampere University of Technology for the preparation of the VECSEL.

REFERENCES

[1] M. Kuznetsov, F. Hakimi, R. Sprague, and A. Mooradian, "High-power (>0.5-W CW) diode-pumped vertical-external-cavity surface-emitting semiconductor lasers with circular TEM_{00} beams," *IEEE Photon. Technol. Lett.*, vol. 9, no. 8, pp. 1063–1065, Aug. 1997.

[2] L. Fan *et al.*, "Over 3 W high-efficiency vertical-external-cavity surface-emitting lasers and application as efficient fiber laser pump sources," *Appl. Phys. Lett.*, vol. 86, no. 21, p. 211116, 2005.

[3] L. Fan *et al.*, "Tunable high-power high-brightness linearly polarized vertical-external-cavity surface-emitting lasers," *Appl. Phys. Lett.*, vol. 88, no. 2, p. 021105, 2006.

[4] S. Kaspar *et al.*, "Linewidth narrowing and power scaling of single-frequency 2.X μm GaSb-based semiconductor disk lasers," *IEEE J. Quantum Electron.*, vol. 49, no. 3, pp. 314–324, Mar. 2013.

[5] A. Laurain, C. Mart, J. Hader, J. V. Moloney, B. Kunert, and W. Stolz, "15 W single frequency optically pumped semiconductor laser with sub-megahertz linewidth," *IEEE Photon. Technol. Lett.*, vol. 26, no. 2, pp. 131–133, Jan. 15, 2014.

[6] F. Zhang *et al.*, "A 23-watt single-frequency vertical-external-cavity surface-emitting laser," *Opt. Exp.*, vol. 22, no. 11, pp. 12817–12822, Jun. 2014.

[7] B. Heinen *et al.*, "106 W continuous-wave output power from vertical-external-cavity surface-emitting laser," *Electron. Lett.*, vol. 48, no. 9, pp. 516–517, Apr. 2012.

[8] D. Al Nakdali *et al.*, "High-power quantum-dot vertical-external-cavity surface-emitting laser exceeding 8 W," *IEEE Photon. Technol. Lett.*, vol. 26, no. 15, pp. 1561–1564, Aug. 1, 2014.

[9] U. Keller and A. C. Tropper, "Passively modelocked surface-emitting semiconductor lasers," *Phys. Rep.*, vol. 429, no. 2, pp. 67–120, Jun. 2006.

[10] E. U. Rafailov, M. A. Cataluna, and W. Sibbett, "Mode-locked quantum-dot lasers," *Nature Photon.*, vol. 1, no. 7, pp. 395–401, 2007.

[11] M. Gaafar *et al.*, "Self-mode-locked quantum-dot vertical-external-cavity surface-emitting laser," *Opt. Lett.*, vol. 39, no. 15, pp. 4623–4626, 2014.

[12] M. Gaafar *et al.*, "Self-mode-locking semiconductor disk laser," *Opt. Exp.*, vol. 22, no. 23, pp. 28390–28399, Nov. 2014.

[13] S. Calvez, J. E. Hastie, M. Guina, O. G. Okhotnikov, and M. D. Dawson, "Semiconductor disk lasers for the generation of visible and ultraviolet radiation," *Laser Photon. Rev.*, vol. 3, no. 5, pp. 407–434, 2009.

[14] Y. Kaneda *et al.*, "Continuous-wave single-frequency 295 nm laser source by a frequency-quadrupled optically pumped semiconductor laser," *Opt. Lett.*, vol. 34, no. 22, pp. 3511–3513, Nov. 2009.

[15] N. Schulz, J.-M. Hopkins, M. Rattunde, D. Burns, and J. Wagner, "High-brightness long-wavelength semiconductor disk lasers," *Laser Photon. Rev.*, vol. 2, no. 3, pp. 160–181, Jul. 2008.

[16] A. Rantamäki *et al.*, "Flip chip quantum-dot semiconductor disk laser at 1200 nm," *IEEE Photon. Technol. Lett.*, vol. 24, no. 15, pp. 1292–1294, Aug. 1, 2012.

[17] J. Rautiainen, I. Krestnikov, J. Nikkinen, and O. G. Okhotnikov, "2.5 W orange power by frequency conversion from a dual-gain quantum-dot disk laser," *Opt. Lett.*, vol. 35, no. 12, pp. 1935–1937, Jun. 2010.

[18] M. Butkus *et al.*, "Quantum dot based semiconductor disk lasers for 1–1.3 μm," *IEEE J. Sel. Topics Quantum Electron.*, vol. 17, no. 6, pp. 1763–1771, Nov./Dec. 2011.

[19] M. Scheller, J. M. Yarborough, J. V. Moloney, M. Fallahi, M. Koch, and S. W. Koch, "Room temperature continuous wave milliwatt terahertz source," *Opt. Exp.*, vol. 18, no. 26, pp. 27112–27117, Dec. 2010.

[20] M. Scheller *et al.*, "Heterodyne detection of intracavity generated terahertz radiation," *IEEE Trans. Terahertz Sci. Technol.*, vol. 2, no. 3, pp. 271–277, May 2012.

[21] M. Wichmann, M. Stein, A. Rahimi-Iman, S. W. Koch, and M. Koch, "Interferometric characterization of a semiconductor disk laser driven terahertz source," *J. Infr. Millim. Terahertz Waves*, vol. 35, nos. 6–7, pp. 503–508, Jul. 2014.

[22] J. A. Lott, A. R. Kovsh, N. N. Ledentsov, and D. Bimberg, "GaAs-based InAs/InGaAs quantum dot vertical cavity and vertical external cavity surface emitting lasers emitting near 1300 nm," in *Proc. Pacific Rim Conf. Lasers Electro-Opt. (CLEO/Pacific Rim)*, Aug. 2005, pp. 160–161.

[23] T. D. Germann *et al.*, "Quantum-dot semiconductor disk lasers," *J. Cryst. Growth*, vol. 310, no. 23, pp. 5182–5186, Nov. 2008.

[24] P. J. Schlosser, J. E. Hastie, S. Calvez, A. B. Krysa, and M. D. Dawson, "InP/AlGaInP quantum dot semiconductor disk lasers for CW TEM_{00} emission at 716–755 nm," *Opt. Exp.*, vol. 17, no. 24, pp. 21782–21787, Nov. 2009.

[25] A. R. Albrecht *et al.*, "Multi-watt 1.25 μm quantum dot VECSEL," *Electron. Lett.*, vol. 46, no. 12, pp. 856–857, Jun. 2010.

[26] T. Schwarzbäck *et al.*, "High-power InP quantum dot based semiconductor disk laser exceeding 1.3 W," *Appl. Phys. Lett.*, vol. 102, no. 9, p. 092101, 2013.

[27] M. Butkus *et al.*, "High-power quantum-dot-based semiconductor disk laser," *Opt. Lett.*, vol. 34, no. 11, pp. 1672–1674, Jun. 2009.

[28] M. Butkus, J. Rautiainen, O. G. Okhotnikov, S. S. Mikhrin, I. L. Krestnikov, and E. U. Rafailov, "1270 nm quantum dot based semiconductor disk lasers," in *Proc. 22nd IEEE Int. Semiconductor Laser Conf. (ISLC)*, Sep. 2010, pp. 71–72.

[29] J. Rautiainen, I. Krestnikov, M. Butkus, E. U. Rafailov, and O. G. Okhotnikov, "Optically pumped semiconductor quantum dot disk laser operating at 1180 nm," *Opt. Lett.*, vol. 35, no. 5, pp. 694–696, Mar. 2010.

[30] E. U. Rafailov, Ed., *The Physics and Engineering of Compact Quantum Dot-based Lasers for Biophotonics*. Hoboken, NJ, USA: Wiley, 2013.

[31] M. Wichmann *et al.*, "Evolution of multi-mode operation in vertical-external-cavity surface-emitting lasers," *Opt. Exp.*, vol. 21, no. 26, pp. 31940–31950, Dec. 2013.

[32] S. Ranta, M. Tavast, T. Leinonen, N. Van Lieu, G. Fetzer, and M. Guina, "1180 nm VECSEL with output power beyond 20 W," *Electron. Lett.*, vol. 49, no. 1, pp. 59–60, Jan. 2013.

5.2.3 Supplementary data

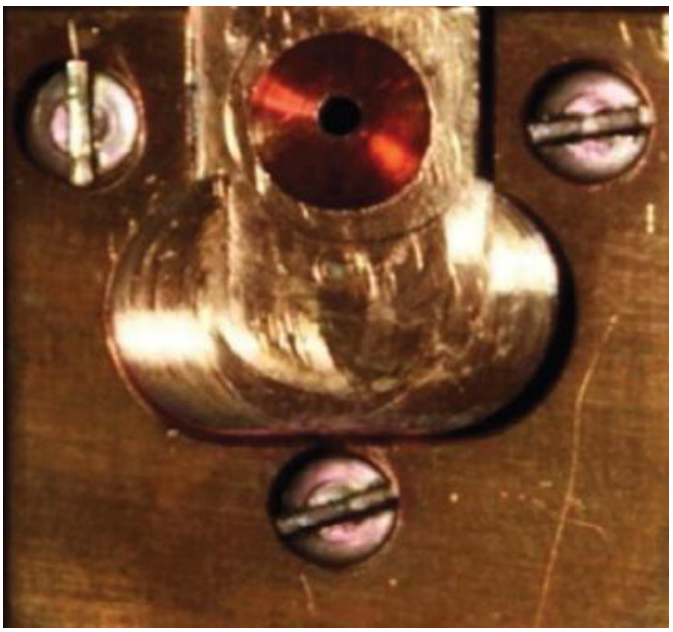

Figure 5.13. A photo of a 1180 nm QD SDL chip bonded to the diamond heat spreader

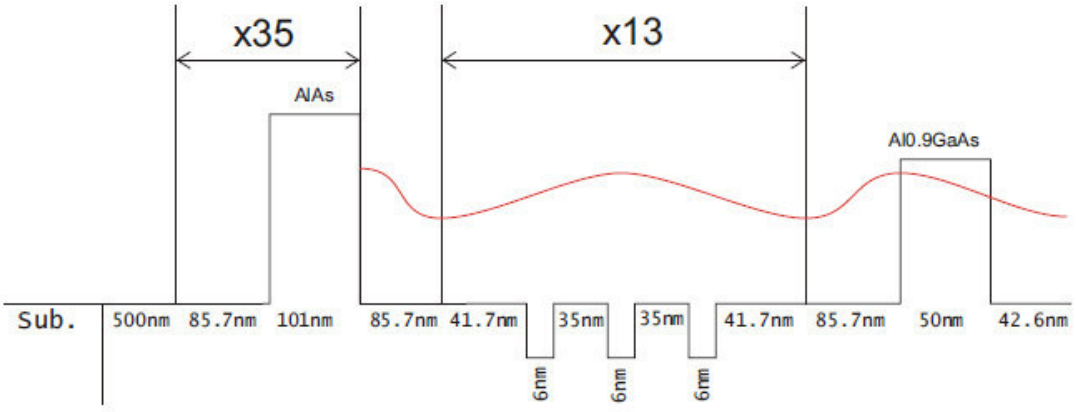

Figure 5.14. The design of the chip structure for a 1180nm QD SDL. In black, the profile of the potential energy in the semiconductor structure is shown. The red line represents the optical standing wave.

5.3 Analysis of optical scattering losses in vertical external-cavity-surface-emitting-lasers

D. Al Nakdali, M. K. Shakfa, B. Heinen, B. Kunert, W. Stolz, S. W. Koch, J. Hader, J. V. Moloney, A. Rahimi-Iman, and M. Koch, *Appl. Phys. B*, 2015.

5.3.1 Abstract:

In this publication, we report on an analysis of optical surface-scattering losses in vertical-external-cavity surface-emitting lasers. In this work, the chip structure is designed for operation at 1010 nm and consists of a GaAsP resonant periodic gain region with ten embedded 8-nm InGaAs quantum wells. Here, a sample chip with enhanced surface roughness has been employed in order to promote the effects of surface scattering for an improved investigation.

The laser chip's thermal resistance was extracted from experimental input-output characterization of powers with respect to the thermal roll-over effect for different output-coupler transmittance values, based on a theoretical model that neglects non-heating losses. Accordingly, a significant underestimation of the thermal resistance is found when using this model.

For an improved extraction of the thermal resistance from experimental data, the simple model is expanded by taking into account a non-thermal component of losses. Thereby, we demonstrate good agreement of experimental data with theoretical modeling when taking into account a power-loss component proportional to an optical surface-scattering-loss coefficient in relation to photon out-coupling rates.

5.3.2 The Authors contribution:

The design of experiments, inspired by previous studies of Dr. Jörg Hader and co-workers, and all the practical steps of this study I carried out myself. The QW-VECSEL chip was designed and fabricated at the Philipps-University of Marburg by Prof. Dr. Wolfgang Stolz's group with the support of the theoretical physicists Prof. Dr. Stephan Koch, Prof. Dr. Jerome Moloney, and Dr. Jörg Hader. The results were interpreted and discussed by me in cooperation with Bernd Heinen, with

constructive ideas and improvements contributed by Prof. Dr. Martin Koch, Mohammad Khaled Shakfa and other coauthors. Dr. Arash Rahimi-Iman wrote the manuscript, with the support of Mohammad Khaled Shakfa and me. All co-authors contributed with valuable discussions, ideas and corrections to the manuscript.

Appl. Phys. B
DOI 10.1007/s00340-015-6094-0

Applied Physics B
Lasers and Optics

Analysis of optical scattering losses in vertical-external-cavity surface-emitting lasers

Dalia Al Nakdali[1] · Mohammad Khaled Shakfa[1] · Bernd Heinen[1] · Bernardette Kunert[2] · Wolfgang Stolz[1] · Stephan W. Koch[1] · Jörg Hader[3,4] · Jerome V. Moloney[3,4] · Arash Rahimi-Iman[1] · Martin Koch[1]

Received: 19 June 2014 / Accepted: 17 March 2015

Abstract We report on an analysis of optical surface-scattering losses in vertical-external-cavity surface-emitting lasers. In this study, a laser chip with enhanced surface roughness compared with a high-quality chip is employed in order to allow for investigation of a scattering loss component described in theoretical considerations. A simple model for the extraction of the laser chip's thermal resistance from experimental input–output characteristics based on thermal roll-over is expanded with respect to a non-thermal component of losses. Thereby, we demonstrate good agreement of experimental data with theoretical modeling when taking into account a power loss component proportional to an optical surface-scattering-loss coefficient in relation to photon out-coupling rates.

1 Introduction

After their first demonstration in 1997, vertical-external-cavity surface-emitting lasers (VECSELs) [1] have received much attention in the last two decades due to their scientific and industrial applications [2, 3]. Owing to their architecture, VECSELs can combine advantages of solid-state and semiconductor lasers, such as high output powers, beam quality and being accessible for a wide spectral range [3–5]. Moreover, recent reports such as the achievement of passive mode-locking operation with 400-fs pulses at 4.35-kW peak powers [6] as well as employment in the field of intra-cavity frequency-mixing applications demonstrate the versatility of such a laser system [7]. It is worth to note that the way to high-power pulsed VECSELs was further paved very recently with the use of self-mode-locking techniques in saturable absorber free systems, which can even run at higher harmonics [8]. Quantum-well (QW)-VECSELs have been even shown to generate a record-high continuous-wave (CW) output power of 106 W at an emission wavelength of 1028 nm [9], while for quantum-dot (QD) VECSELs, a record-high CW output power of 8.4 W was obtained at an emission wavelength of 1040 nm [10]. Furthermore, an optimum output power of nearly 23 W was demonstrated very recently for a single-frequency VECSEL, at 1013 nm [11]. However, for further improvement in such VECSELs' performances, an understanding and quantification of the power loss channels in such devices is essential. Overheating generally limits the VECSEL output efficiency [12]—an effect that reduces gain until complete shutdown of the laser. The onset of this effect is marked by the so-called thermal roll-over power. Thus, heat management is generally very important for such systems [13–17], and methods for a precise determination of a VECSEL's thermal impedance were seeked in recent years [12, 18]. But besides heating losses, also non-heating power losses are expected, in particular optical losses [12, 18, 19], i.e., intra-cavity scattering and spontaneous emission in the chip. In this work, we illuminate optical surface-scattering of intra-cavity light at the semiconductor chip in an

✉ Dalia Al Nakdali
dalia.alnakdali@physik.uni-marburg.de

[1] Department of Physics and Material Sciences Center, Philipps-University of Marburg, Renthof 5, 35032 Marburg, Germany

[2] NAsP-III/V GmbH., Am Knechtacker 19, 35041 Marburg, Germany

[3] College of Optical Sciences, University of Arizona, Tucson, AZ 85721, USA

[4] Nonlinear Control Strategies Inc., 3542 N. Geronimo Ave., Tucson, AZ 85705, USA

Published online: 02 April 2015

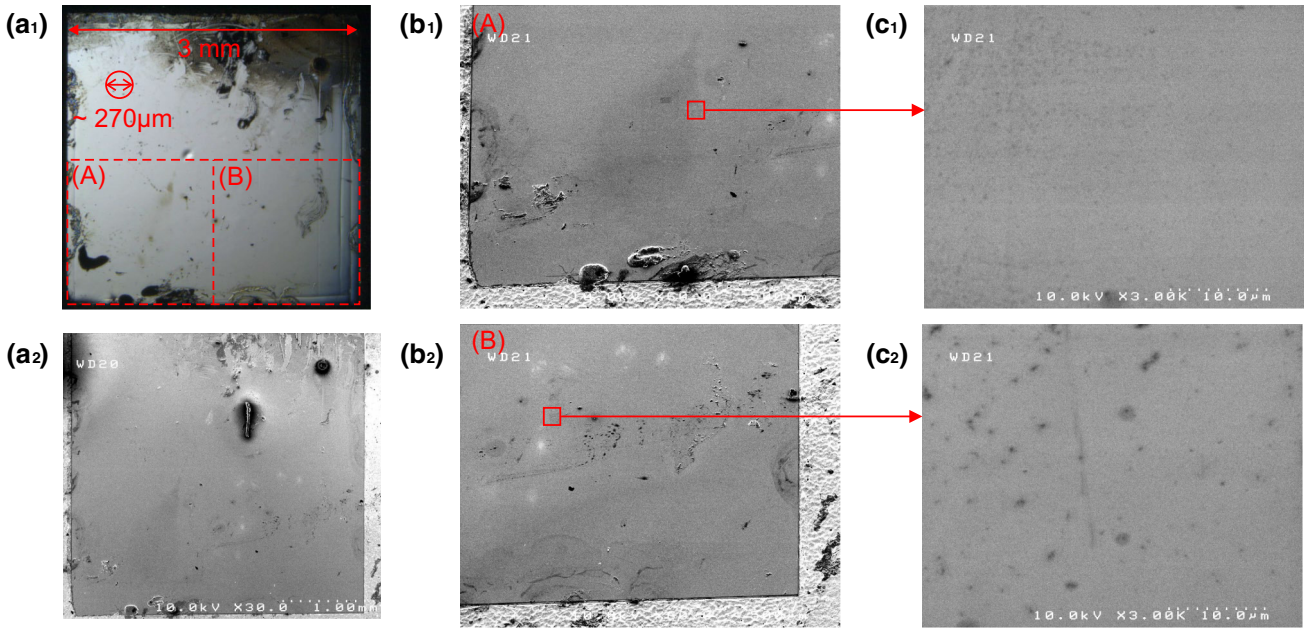

Fig. 1 $\mathbf{a_1}$, $\mathbf{a_2}$ Show the optical and SEM images of the studied VECSEL chip, respectively. The *dashed lines* in $\mathbf{a_1}$ locate the investigated area on the chip. $\mathbf{b_1}$, $\mathbf{b_2}$ are 500-µm-resolution SEM images of the *left-hand* and *right-hand* parts of the studied area, respectively. The areas located by the *red squares* in $\mathbf{b_1}$ and $\mathbf{b_2}$ are magnified in $\mathbf{c_1}$ and $\mathbf{c_2}$, respectively

experimental study, supported by a theoretical description of loss channels. Thereby, we experimentally confirm the validity of a theoretical model reported in Ref. [18] from which a constant value of the chip's thermal resistance can be extracted independent from optical cavity losses by taking into account non-thermal loss channels in the model. The thermal resistance as well as the corresponding scattering coefficient—a measure of power losses via the non-thermal channel—is determined experimentally based on a systematic analysis of the VECSEL's thermal roll-over at different heat sink temperatures for various output coupler mirrors.

2 Experimental setup

The chip structure used in this study is designed for operation at 1010 nm and consists of a GaAsP resonant periodic gain region with ten embedded 8-nm InGaAs quantum-wells and a $\lambda/2$ GaInP cap layer on top. Here, a sample chip was chosen that features an enhanced surface roughness to promote the effects of surface-scattering for an improved investigation. With a high-quality chip suitable for high-power operation, quantification of non-thermal losses is hardly possible. However, a certain amount of optical scattering losses enables us to validate an expanded theoretical model that takes such losses into account. In order to obtain information about the surface roughness and morphology of the studied VECSEL chip, optical microscopy and scanning electron microscopy (SEM) investigations are performed. Fig. 1a_1, a_2 show the optical and SEM images of the whole chip, respectively. The dashed lines in Fig. 1a_1 locate the studied area on the chip, which is divided into two parts; Fig. 1b_1, b_2 show low-resolution SEM images of the left-hand and right-hand parts of the studied area, respectively. Two different positions on the VECSEL chip are investigated: position (A) and position (B) are around the red squares located in Fig. 1b_1, b_2, respectively. In order to evidence an inferior surface quality at positions (A) and (B), we acquired SEM images with a resolution of 10 µm for both positions, which are shown in Figs. 1c_1, 1c_2, respectively. This resolution is relatively high in comparison with the employed pump-spot diameter (about 270 µm). However, these images reveal that both positions (A) and (B) exhibit a certain degree of roughness in addition to some grime. These features are significantly more apparent at position (B).

The temperature of the VECSEL chip is controlled by a thermoelectric cooler. The semiconductor chip is chemically bonded on a diamond heat-spreader and mounted on a Peltier-cooled copper heat sink. The excess heat is dissipated via water cooling.

A standard V-cavity is used, shown in Fig. 2 schematically. The resonator consists of three elements: a curved mirror with a high reflectivity (HR) of 99.9 % and a curvature radius of 200 mm, an AlAs/$Al_{0.20}Ga_{0.80}As$ distributed Bragg reflector (DBR) with 24 mirror pairs within the VECSEL chip, and a plane output coupler (OC) mirror

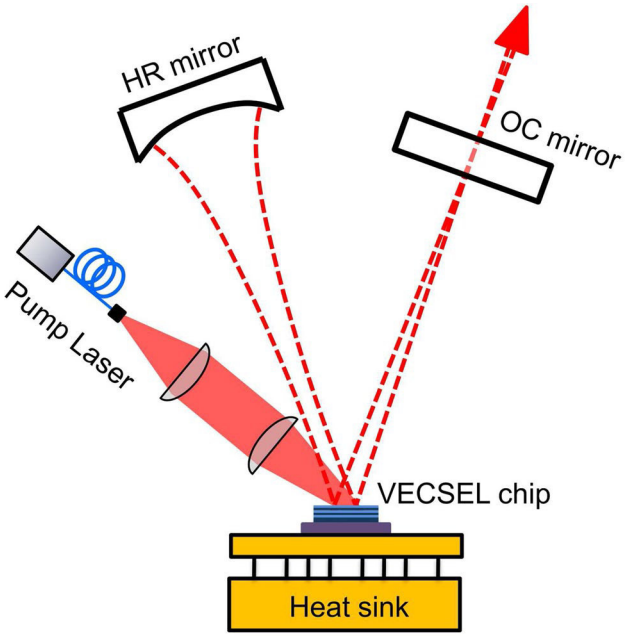

Fig. 2 Schematic drawing of the experimental setup

with transmittance of 1, 3, 5, 7.5, 10, and 15 %, respectively. The distance between the VECSEL chip and the HR curved mirror is about 47 mm, while the OC mirror is located about 150 mm away from the VECSEL chip. The angle between the cavity's arms amounts to approximately 12°. For such a cavity configuration, the calculated TEM_{00} mode radius at the position of the VECSEL chip is about 207 µm. The VECSEL chip is optically pumped by a fiber-coupled diode laser, which has a core diameter of 100 µm and emits at 808 nm in a transversal multimode with a maximum output power of 35 W. The pump laser is focused onto the VECSEL chip under an incidence angle of 45° with a spot diameter of approximately 270 µm.

3 Results and discussion

Firstly, the input–output (IO) characteristic of the device is recorded for the aforementioned range of OC mirror transmittance at a given heat sink temperature. Then, both pump power (P_{pump}) and output power (P_{out}) at the onset of thermal roll-over (point of maximum output power) is captured at different heat sink temperatures, for various output coupler mirrors. In the following analysis, the fact that the roll-over temperature (T_{ro}) of the VECSEL chip is independent of the heat sink temperature (T_{hs}) [18] is used to extract the thermal resistance (R_{th}) from the IO curves via Eq. (1). Here, it is assumed that P_{pump} can be split into two components: P_{out} and the dissipated heating power, while neglecting any other non-heating power losses [12]:

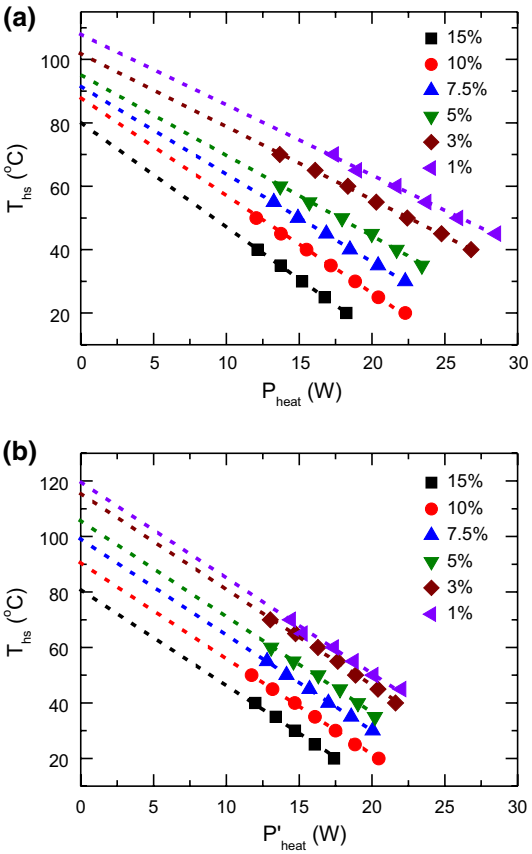

Fig. 3 Heat sink temperature as a function of dissipated heat power, corresponding to **a** the simple model (Eq. 1) and **b** the expanded model (Eq. 5)

$$T_{\mathrm{hs}} = -R_{\mathrm{th}} P^{\mathrm{ro}}_{\mathrm{heat}} + T_{\mathrm{ro}}, \tag{1}$$

where the heating power at thermal roll-over ($P^{\mathrm{ro}}_{\mathrm{heat}}$) is given by

$$P^{\mathrm{ro}}_{\mathrm{heat}} = P^{\mathrm{ro}}_{\mathrm{pump}} - P^{\mathrm{ro}}_{\mathrm{out}}. \tag{2}$$

$P^{\mathrm{ro}}_{\mathrm{pump}}$ and $P^{\mathrm{ro}}_{\mathrm{out}}$ are the pump and output power, respectively, at thermal roll-over. If the heat sink temperature is plotted as a function of the measured $P^{\mathrm{ro}}_{\mathrm{heat}}$ (Eq. 2) as is shown in Fig. 3a for the investigated position (B), the slope from an experimentally obtained linear decrease in T_{hs} can be directly put in relation with the thermal resistance R_{th}, according to Eq. (1). However, lines marking such a linear behavior are not parallel in Fig. 3a and the extracted value of R_{th} based on such an over-simplified model varies for different values of the OC mirror's transmittance, as presented in Fig. 4a by blue dots. The analysis shows that in such a simple model the thermal resistance (Fig. 4a) increases with increasing transmittance. However, no correlation with the transmittance or other resonator components is expected. In contrast, the thermal resistance depends on the VECSEL chip material, the heat sink geometry and the

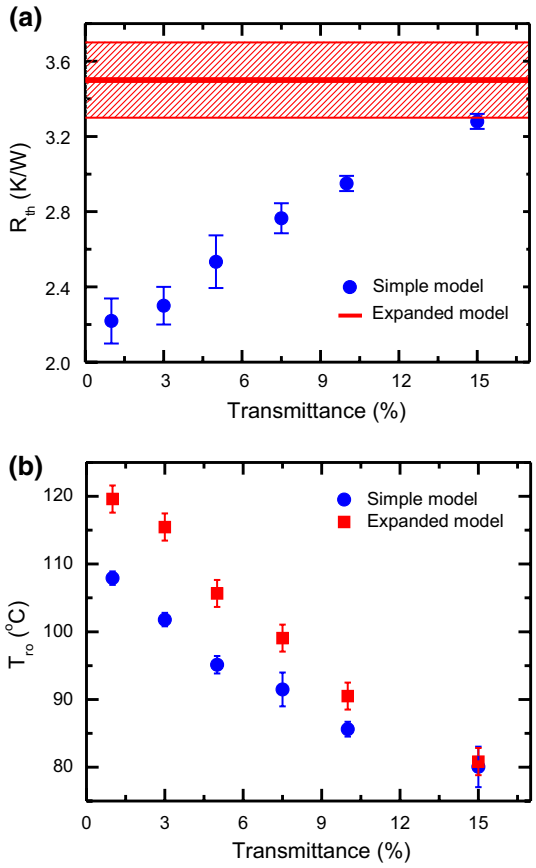

Fig. 4 **a** The thermal resistance as a function of the OC transmittance: the solid circuits are obtained from the simple model (Eq. 1) without taking non-heating losses into account. The *solid line* indicates the constant value of the thermal resistance, which is extracted from the expanded model (Eq. 5) by introducing the optical scattering losses to the aforementioned, simple model. **b** The roll-over temperature as a function of the OC transmittance extracted from both models. Higher values of the roll-over temperature are obtained when optical scattering losses are taken into account. The results presented in **a**, **b** are obtained for the position (B) on the investigated VECSEL chip

pump-spot size, which are all kept constant. From this first result, we thus deduce an incomplete description of losses for our system, i.e., non-heating losses of power must be taken into account to estimate $P_{\text{heat}}^{\text{ro}}$ (Eq. 2) in a correct way.

Non-heating losses for a VECSEL consist mainly of spontaneous emission (SE) originating in the quantum-wells and not being re-absorbed in the gain material as well as optical scattering of intra-cavity radiation on the chip's surface and can consist of scattering at interfaces in the semiconductor chip and diffraction losses due to thermal lensing [18]. The latter two contribute to the power balance just like the surface-scattering losses and are included through one surface-scattering coefficient α_{ss} which is introduced in the following. The SE loss, which describes leakage of photons in the medium out of the pump-spot region, is small and due to its very weak dependency on the pump power [18] neglected here. Moreover, a sample chip was chosen in this study which features an enhanced surface roughness, allowing the implication that optical surface-scattering poses the predominant optical-loss channel. The optical surface-scattering power (P_{ss}) is described by [18]

$$P_{\text{ss}} = P_{\text{out}} \frac{\alpha_{\text{ss}}}{\alpha_{\text{out}}}, \tag{3}$$

where α_{out} is the photon out coupling rate (OC mirror's transmittance) and α_{ss} denotes the optical surface-scattering-losses coefficient. Taking into consideration P_{ss} at thermal roll-over, one can expand Eq. (2) to

$$P_{\text{heat}}^{\prime\text{ro}} = P_{\text{pump}}^{\text{ro}} - P_{\text{out}}^{\text{ro}} - P_{\text{out}} \frac{\alpha_{\text{ss}}}{\alpha_{\text{out}}}. \tag{4}$$

Inserting Eq. (4) in Eq. (1) then provides a more complete expression of the heat sink temperature term:

$$T_{\text{hs}} = -R_{\text{th}} \left[P_{\text{pump}}^{\text{ro}} - P_{\text{out}}^{\text{ro}} \left(1 + \frac{\alpha_{\text{ss}}}{\alpha_{\text{out}}} \right) \right] + T_{\text{ro}} \tag{5}$$

due to which the thermal resistance can be yielded experimentally. Using Eq. (5) for data analysis, one obtains parallel model curves (Fig. 3b) with a scattering coefficient $\alpha_{\text{ss}} = 3.7 \pm 0.5\,\%$ and a constant value of the thermal resistance $R_{\text{th}} = 3.5 \pm 0.2\,\text{K/W}$, which is presented in Fig. 4a for respective values of α_{out} (red line). The given errors (marked by thin red lines for R_{th}) correspond to twice the standard deviation. T_{ro} is a free parameter of the fit function based on Eq. (5), while R_{th} and α_{ss} are shared variables for given sets of power values at different heat sink temperatures. This shows that for a VECSEL with non-thermal losses dominated by optical surface-scattering, the experimental data can indeed be modeled precisely with such a description of loss channels. Here, for very low transmittance values of the OC mirror, the amount of power lost by scattering even becomes comparable to or exceeds the out-coupled power of the device ($\alpha_{\text{out}} < 5\,\%$). Furthermore, the extracted values of T_{ro} from using the discussed modeling techniques are presented by blue circles (using Eq. 1) and red squares (using Eq. 5) in Fig. 4b. T_{ro} which refers to the temperature of the gain medium at the thermal roll-over is determined from the y-intercept of the fitted line concerning both of the models (cf. Fig. 3a, b), with errors smaller than the symbol sizes. For the expanded model, a slight deviation of extracted roll-over temperatures from data yielded from the simple model analysis (Eq. 1) is featured in this graph, representing a more precise estimate of the roll-over temperature. The higher the transmittance, the more has the intrinsic gain to be higher to compensate for out-coupling losses. However, the higher gain can only be provided for a smaller detuning between

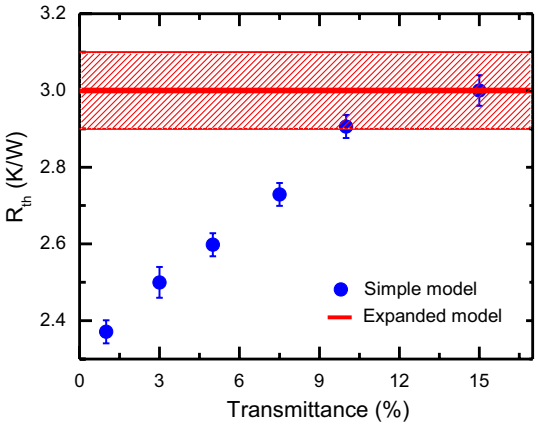

Fig. 5 The thermal resistance as a function of the OC transmittance (for the position (A) on the VECSEL chip): the *solid symbols* are obtained from the simple model, Eq. (1). The *solid line* is extracted from the expanded model, Eq. (5)

cavity and resonance in the gain maximum. Thus, roll-over occurs at lower temperatures.

The above performed study is repeated for the position (A) on the VECSEL chip to understand position dependency and applicability of the model. The experimental results for this position, e.g., the thermal resistance presented in Fig. 5, compare very well to the acquired data presented in this study. Thereby, the optical scattering coefficient amounts to $\alpha_{ss} = 1.5 \pm 0.5\,\%$ and a constant thermal resistance amounting to $R_{th} = 3.0 \pm 0.1\,\mathrm{K/W}$ for different transmittance values of the OC mirror is yielded. This supports the validity of the aforementioned analysis method for the identification of scattering losses and analysis of the thermal resistance. The slightly lower value of R_{th} at this spot compared to the previously investigated position is attributed to a local variation in the bonding quality. Here, a position dependent surface roughness affects α_{ss} for a particularly rough chip owing to a surface homogeneity lower than that of high-quality chips. In particular, while α_{ss} varies between 1.5 and 3.5 % in our case of a low-quality chip, it has been reported to be 0.57 % for a high-quality one [18].

The presented experiment demonstrates good agreement with theoretical expectations [18] and the applied method shows that non-thermal losses can play a crucial role in VECSEL systems which have to be suppressed by means of high-quality chip fabrication in order to enable an efficient high-power laser operation.

4 Conclusion

To summarize, the thermal resistance of a reference low-surface-quality VECSEL chip is analyzed based on input–output characterization of powers with respect to the thermal roll-over effect for different output coupler transmittance values. Accordingly, a significant underestimation of the thermal resistance is found when using a theoretical model that neglects non-heating losses. In this study, an expanded description of power losses in accordance to earlier theoretical considerations is used that takes into account optical surface-scattering on the laser chip. It is shown that this allows for an improved extraction of the thermal resistance from experimental data and confirms the underlying theoretical model. To adequately promote scattering for such an investigation, a chip with enhanced surface roughness has been employed. In the case where surface-scattering losses are the dominant non-heating loss, the error of this method is considered to be vanishing. This is the case here where the only other non-heating loss mechanism is due to spontaneous emission, which had been calculated to be insignificant. Thus, optical surface-scattering is identified to be a non-negligible component of loss channels in a VECSEL system, enriching one's further understanding of boundaries for very high-power operation, while highlighting the requirement of best-quality chips for such purpose.

Acknowledgments Financial support by the German Science Foundation (DFG) through the projects GRK 1782 and SFB 1083 is gratefully acknowledged. The authors would like to thank Christoph Möller for many helpful discussions and for performing scanning electron microscopy measurements.

References

1. M. Kuznetsov, F. Hakimi, R. Sprague, A. Mooradian, IEEE Photon. Technol. Lett. **9**, 1063 (1997)
2. U. Keller, Appl. Phys. B **100**, 15 (2010)
3. S. Calvez, J.E. Hastie, M. Guin, O.G. Okhotnikov, M.D. Dawson, Laser Photon. Rev. **3**, 407 (2009)
4. X. Zeng, D.L. Boiko, G. Cosendey, M. Glauser, J.-F. Carlin, N. Grandjean, Appl. Phys. Lett. **101**, 141120 (2012)
5. S. Ranta, M. Tavast, T. Leinonen, N. Van Lieu, G. Fetzer, M. Guina, Electron. Lett. **49**, 59 (2013)
6. K.G. Wilcox, A.C. Tropper, H.E. Beere, D.A. Ritchie, B. Kunert, B. Heinen, W. Stolz, Opt. Express **21**, 1599 (2013)
7. M. Scheller, J.M. Yarborough, J.V. Moloney, M. Fallahi, M. Koch, S.W. Koch, Opt. Express **18**, 27112 (2010)
8. M. Gaafar, C. Möller, M. Wichmann, B. Heinen, B. Kunert, A. Rahimi-Iman, W. Stolz, M. Koch. Electron. Lett. **50**, 542 (2014)
9. B. Heinen, T.L. Wang, M. Sparenberg, A. Weber, B. Kunert, J. Hader, S.W. Koch, J.V. Moloney, M. Koch, W. Stolz, Electron. Lett. **48**, 516 (2012)
10. D. Al Nakdali, M.K. Shakfa, M. Gaafar, M. Butkus, K.A. Fedorova, M. Zulonas, M. Wichmann, F. Zhang, B. Heinen, A. Rahimi-Iman, W. Stolz, E.U. Rafailov, M. Koch, IEEE Photon. Technol. Lett. **26**, 1561 (2014)
11. F. Zhang, B. Heinen, M. Wichmann, C. Möller, B. Kunert, A. Rahimi-Iman, W. Stolz, M. Koch, Opt. Express **22**, 12817 (2014)
12. B. Heinen, F. Zhang, M. Sparenberg, B. Kunert, M. Koch, W. Stolz, IEEE J. Quantum Electron. **48**, 934 (2012)
13. A.J. Kemp, A.J. Maclean, J.E. Hastie, S.A. Smith, J.-M. Hopkins, S. Calvez, G.J. Valentine, M.D. Dawson, D. Burns, Appl. Phys. B **83**, 189 (2006)

14. A.J. Kemp, J.-M. Hopkins, A.J. Maclean, N. Schulz, M. Rattunde, J. Wagner, D. Burns, IEEE J. Quantum Electron. **44**, 125 (2008)
15. J.-P. Perez, A. Laurain, L. Cerutti, I. Sagnes, A. Garnache, Semicond. Sci. Technol. **25**, 045021 (2010)
16. A. Chernikov, J. Herrmann, M. Koch, B. Kunert, W. Stolz, S. Chatterjee, S.W. Koch, T.-L. Wang, Y. Kaneda, J.M. Yarborough, J. Hader, J.V. Moloney, IEEE J. Sel. Top. Quantum Electron. **99**, 1772 (2011)
17. S.L. Vetter, S. Calvez, IEEE J. Quantum Electron. **48**, 345 (2012)
18. J. Hader, T.-L. Wang, J.V. Moloney, B. Heinen, M. Koch, S.W. Koch, B. Kunert, W. Stolz, J. Appl. Phys. **113**, 153102 (2013)
19. N. Terry, M. Walton, R. Bedford, Proc. SPIE **7597**, 75972B (2010)

5.3.3 Supplementary data

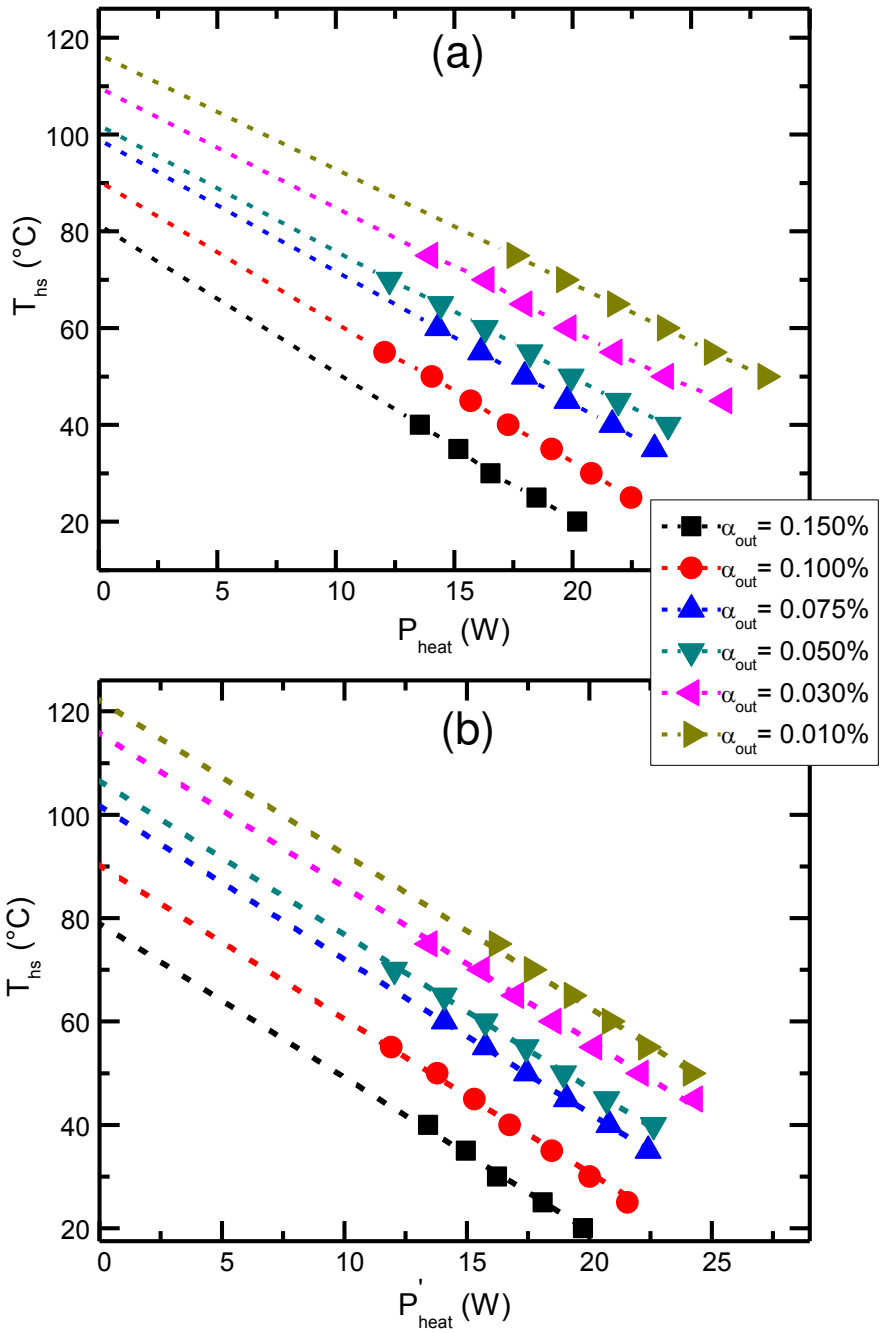

Figure 5.15. Heat sink temperature as a function of dissipated heat power, corresponding to (a) the simple model and (b) the expanded model at the second position of the studied chip.

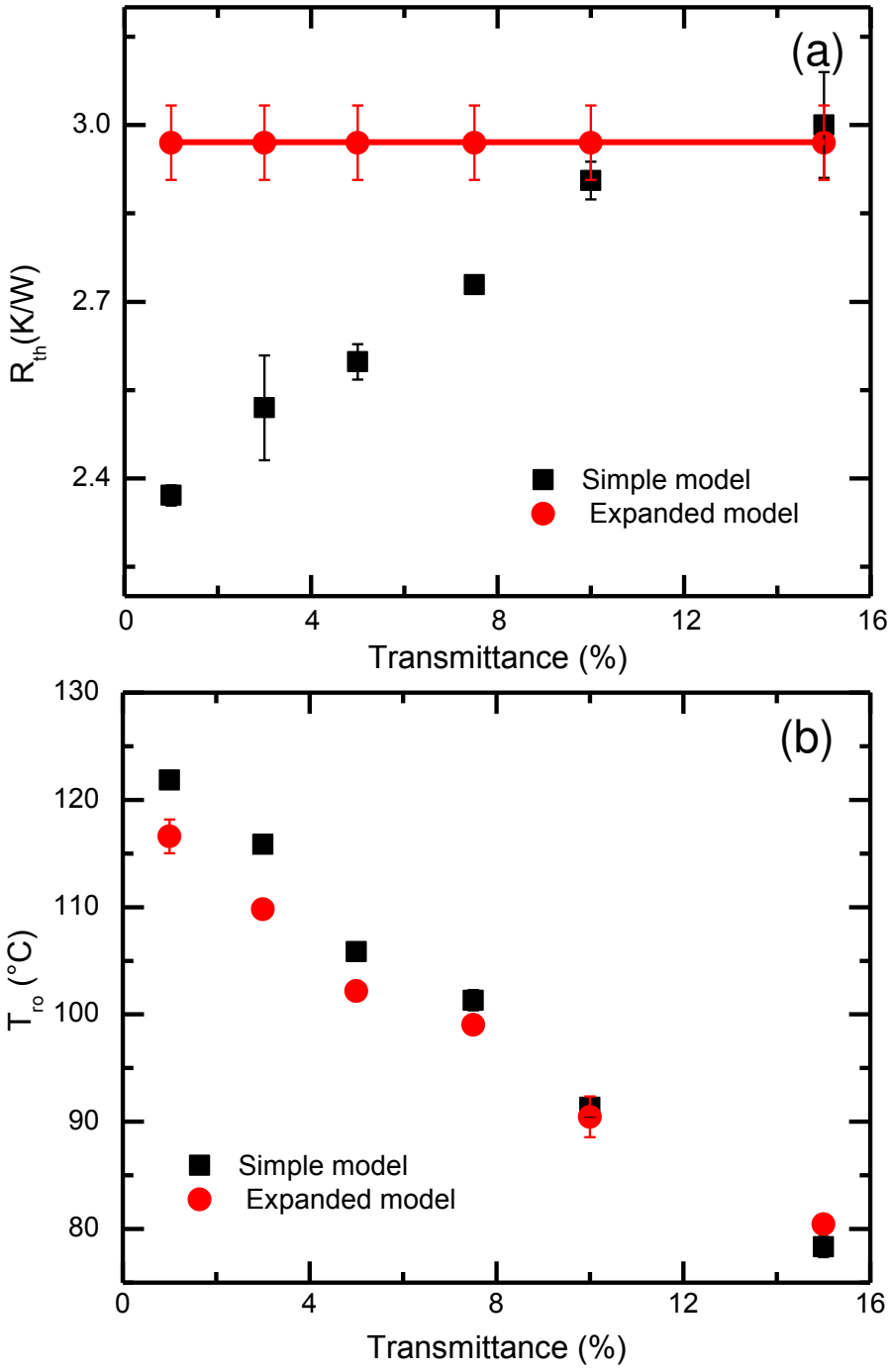

Figure 5.16. (a) Extracted thermal resistance as a function of the OC transmittance for the simple- and the expanded model. (b) Thermal roll-over as a function of the OC transmittance for both models.

5.4 Self-mode-locked quantum-dot vertical-external-cavity surface-emitting laser

M. Gaafar, D. Al Nakdali, C. Möller, K. A. Fedorova, M. Wichmann, M. K. Shakfa, F. Zhang, A. Rahimi-Iman, E. U. Rafailov, and M. Koch, *Opt. Lett*, vol. 39, no. 15, 2014.

5.4.1 Abstract:

In this publication, we present the first successfully self-mode-locked vertical-external-cavity surface-emitting laser (VECSEL) with a quantum-dot (QD) gain region. The active region consists of 35 QD layers with an emission wavelength of about 1040 nm. A standard linear cavity configuration was used in our study. Mode-locking was initiated by introducing a slit acting as an intracavity mode aperture.

Our mode-locked device emits stable pulses of sub-picosecond duration with an average output power up to 750 mW at a repetition rate of 1.5 GHz and a wavelength of 1040 nm. This corresponds to a record-high peak power for mode-locked QD VECSELs of 460 W. In addition to the basic characterization of pulsed emission, we also investigated the temperature dependence of the pulse duration as well as the time-bandwidth product for stable mode locking.

5.4.2 The author's contribution:

The design of experiments and all the practical steps of this study were carried out primarily by Mahmoud Gaafar who performed the work in cooperation with me to achieve these results for a QD-VECSEL chip. After having achieved a record-high continuous-wave output from this device, I could use my experience with this system to reach efficient lasing conditions.The semiconductor laser chip was designed and provided by the group of Prof. Dr. Edik U. Rafailov, currently located at Aston University in the United Kingdom. All co-authors contributed to the experimental achievements, and helped to prepare the manuscript which was mainly written by Mahmoud Gaafar.

Self-mode-locked quantum-dot vertical-external-cavity surface-emitting laser

Mahmoud Gaafar,[1,*] Dalia Al Nakdali,[1] Christoph Möller,[1] Ksenia A. Fedorova,[2] Matthias Wichmann,[1] Mohammad Khaled Shakfa,[1] Fan Zhang,[1] Arash Rahimi-Iman,[1] Edik U. Rafailov,[2] and Martin Koch[1]

[1]*Department of Physics and Material Sciences Center, Philipps University of Marburg, Renthof 5, D-35032 Marburg, Germany*

[2]*School of Engineering and Applied Science, Aston University, Aston Triangle, Birmingham B4 7ET, UK*

**Corresponding author: mahmoud.gaafar@physik.uni-marburg.de*

Received June 5, 2014; revised June 27, 2014; accepted July 4, 2014;
posted July 7, 2014 (Doc. ID 213575); published July 31, 2014

We present the first self-mode-locked optically pumped quantum-dot semiconductor disk laser. Our mode-locked device emits sub-picosecond pulses at a wavelength of 1040 nm and features a record peak power of 460 W at a repetition rate of 1.5 GHz. In this work, we also investigate the temperature dependence of the pulse duration as well as the time-bandwidth product for stable mode locking. © 2014 Optical Society of America

OCIS codes: (140.4050) Mode-locked lasers; (140.5960) Semiconductor lasers; (140.7270) Vertical emitting lasers; (250.5590) Quantum-well, -wire and -dot devices.

http://dx.doi.org/10.1364/OL.39.004623

An optically pumped vertical-external-cavity surface-emitting laser (VECSEL), also named semiconductor disk laser, is a versatile type of laser whose emission wavelength can be tailored according to the demands of a specific application [1]. VECSELs can offer not only high average output powers in continuous-wave (CW) multimode [2] or single-frequency [3] operation, but also in a mode-locked (ML: also "mode locking") regime [4–6]. In addition, VECSELs can provide excellent output beam quality with M^2 values smaller than 1.2 [7,8]. Interestingly, ML VECSELs, which can be employed for a variety of applications ranging from material processing to biophysical imaging, have been demonstrated by exploiting various methods to establish pulsed operation.

Typically, external semiconductor saturable-absorber mirrors (SESAMs) are employed, which exhibit intensity-dependent absorption [9,10] and have to be designed carefully for each wavelength and application—a cost-driving and limiting factor in the development of ML VECSELs. These SESAMs, usually based on quantum-well (QW) or quantum-dot (QD) structures, can even be integrated directly into the chip, resulting in a so-called ML integrated external-cavity surface-emitting laser (MIXSEL) [11]. Since MIXSELs combine both QD and QW technology, this approach is rather complex. A SESAM-free mode-locking technique potentially produces higher output powers because of the absence of nonradiative absorption, which usually is a power-limiting factor in SESAMs. Besides semiconductor materials, graphene [12] as well as carbon nanotube [13] saturable absorbers have been employed for ML operation of VECSELs. However, mode-locking has also been reported to take place even without any additional saturable absorber—an effect called self-mode locking (SML) [14–17]. Different driving mechanisms for the phenomenon of SML were proposed [14–16], but up to now, it is still unclear which mechanism is in force.

Due to the nature of their density of states, QD-based semiconductor lasers have shown their potential for realizing low thresholds and high characteristic temperatures [18]. In addition, the QD gain layers inherently exhibit strong inhomogeneous gain broadening, ultrafast carrier dynamics, and low absorption saturation [19]. Previously, it was demonstrated that the carrier recovery time in such a QD structure is less than 1 ps [20]. VECSELs based on QD gain regions have been reported in CW operation at emission wavelengths between 654 nm [21] and 1300 nm [8,22]. Currently, the highest output power achieved is 8.4 W for 1040 nm [23].

In the year 2008, the first ML QD-VECSEL had been demonstrated to generate 18-ps pulses with an average output power of 27 mW [24], whereas the demonstration of a Watt-level femtosecond QD-VECSEL with 200 W peak power was achieved recently [10]. This elucidates the significant improvements in this field.

In this Letter, we report on the first passively self-mode-locked QD-VECSEL, emitting at 1040 nm. The self-mode-locked VECSEL device was set up in a standard linear cavity geometry in which the VECSEL chip itself and a curved output coupler (OC) formed the laser resonator with a total length of 97 mm [see Fig. 1(a)]. Mode locking was initiated by introducing a slit acting as the intracavity mode aperture. The slit was placed closely in front of the OC mirror, which exhibited a transmittance of 0.6% and a radius of curvature of 100 mm. Stable pulses of sub-picosecond duration with an average output power up to 750 mW have been obtained. This corresponds to a record peak power of 460 W at a repetition rate of 1.5 GHz. Moreover, we investigate the dependence of the time-bandwidth product (TBWP) on the heat sink temperature of the QD-VECSEL device.

The chip structure employed in this study was grown by molecular-beam epitaxy on a GaAs substrate and exhibited an antiresonant design. A ternary distributed Bragg reflector (DBR) is grown, which consists of 29.5 pairs of GaAs-$Al_{0.9}Ga_{0.1}As$. Furthermore, the DBR is transparent to the wavelength of the fiber-coupled 808 nm pump laser. The active gain medium in the structure consists of 35 layers of Stranski–Krastanow grown InGaAs QDs within GaAs spacers, organized as five stacks of seven QD layers each that are placed at the standing-wave electric field antinodes inside the cavity. Both QDs and the DBR are designed for an emission wavelength of 1040 nm. In order to prevent surface

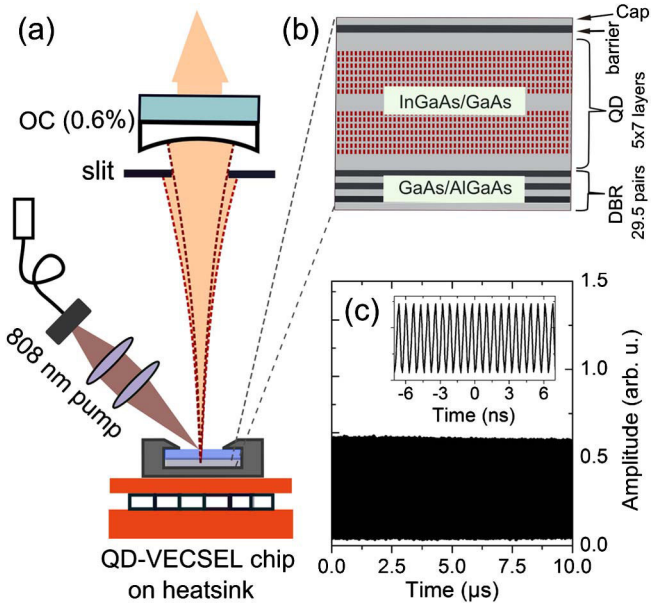

Fig. 1. (a) Schematic drawing of the optically pumped self-mode-locked QD-VECSEL setup. (b) Structure of the QD-VECSEL chip (top right). (c) Oscilloscope time trace of the VECSEL output for a time window of 10 μs and a few nanoseconds (inset), respectively.

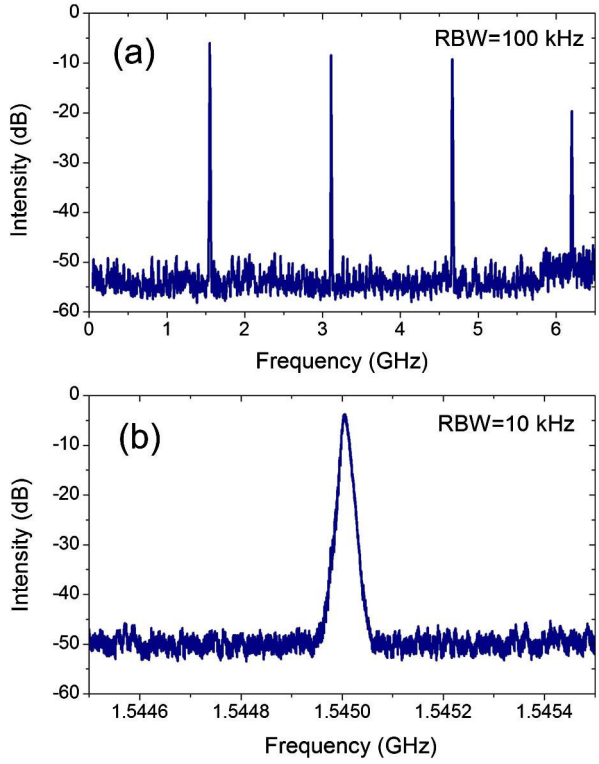

Fig. 2. RF spectra measured over (a) a span of 6.5 GHz and a RBW of 100 kHz, showing the first four harmonics, and (b) a span of 1 MHz and a RBW of 10 kHz. RF signal centered around 1.545 GHz.

recombination of the excited carriers and to avoid oxidation, the structure is capped by an $Al_{0.1}Ga_{0.9}As$ barrier layer followed by a GaAs layer. A schematic drawing of the VECSEL chip's structure is shown in Fig. 1(b).

The VECSEL chip is capillary bonded to an intracavity diamond heat spreader, which is employed for thermal management, and is mounted on a thermoelectrically cooled copper heat sink. The excess heat, generated during operation, is dissipated via closed-cycle water cooling.

Our VECSEL chip is optically pumped by an 808 nm diode laser under an incident angle of 30°. The pump optics is adjusted carefully to ensure good matching between the pump spot and the laser mode on the chip. The latter is estimated to have a radius of ~80 μm. Mode locking is initiated when the slit is moved or its width is varied [17]. Initially, ML operation was not stable and the resonator length was varied carefully by moving the OC in order to stabilize pulsing. Thereby, an improved operation is achieved at a certain cavity length (~97 mm). Stable ML operation was observed at a certain net pump power of about 16 W; otherwise, unstable mode-locking was observed. A representative long-span pulse train of the QD-VECSEL output is shown in Fig. 1(c): the signal was recorded for both a time window of 10 μs and a few nanoseconds (inset), respectively, via an InGaAs photodetector (PD) with a 3 dB bandwidth of 5 GHz and a digital oscilloscope with an analog bandwidth of 2 GHz.

Radiofrequency (RF) spectra measurements are presented in Fig. 2 with a signal-to-noise ratio of 45 dB at 1.5 GHz. For this, the PD is connected to an electrical spectrum analyzer exhibiting a bandwidth of 22 GHz (HP 8566A). Figure 2(a) presents an RF signal measured over a span of 6.5 GHz using a resolution bandwidth (RBW) of 100 kHz. The reduction in the amplitude of the fourth harmonic is attributed to the limited bandwidth of the PD. The corresponding RF spectrum of the fundamental repetition rate measured over a span of 1 MHz using a RBW of 10 kHz is shown in Fig. 2(b). Here, a clear peak at 1.5 GHz is observed corresponding to the total cavity length of 97 mm.

In order to analyze the ML operation further, autocorrelation traces and optical spectra were recorded, which are presented in Figs. 3(a) and 3(b), respectively. Corresponding measurements were performed with an A.P.E. t5050 autocorrelator and an Ando AQ-6315A optical spectrum analyzer. The pulse durations are determined by assuming $sech^2$ shaped pulses in the autocorrelation traces. The optical spectrum of the laser is centered at 1038 nm. The distinct periodically spaced peaks in the spectrum are caused by the spectral filtering induced by the etalon, which is formed by the intracavity diamond heat spreader. The inset in Fig. 3(b) displays a CCD image of the TEM_{00} transverse mode profile of the laser output beam. The laser output is polarized linearly with a horizontal orientation.

As former investigations revealed, ML QD lasers exhibit strong temperature dependence of their mode locking properties [25]. Therefore, as the last part of our study, the performance of the self-mode-locked QD-VECSEL is investigated as a function of operation temperature. Pulse durations are measured in a stable ML regime for several temperatures. Figure 4(a) shows the expected increase of average/peak power (left/right axis) with decreasing temperature, with a peak power of 460 W obtained at 5°C. To our knowledge, this is the highest peak power obtained from a ML QD-VECSEL. Figure 4(b) depicts the decrease of pulse duration with

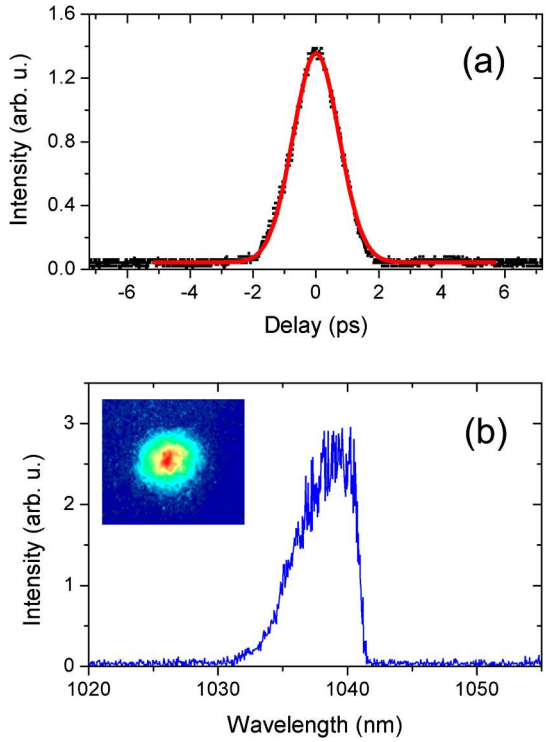

Fig. 3. (a) Autocorrelation trace of the self-mode-locked QD-VECSEL measured at 5°C. Black dots: experimental data. Red line: fit curve assuming a sech^2 pulse. (b) Corresponding optical spectrum. Inset: output beam profile in a false color map.

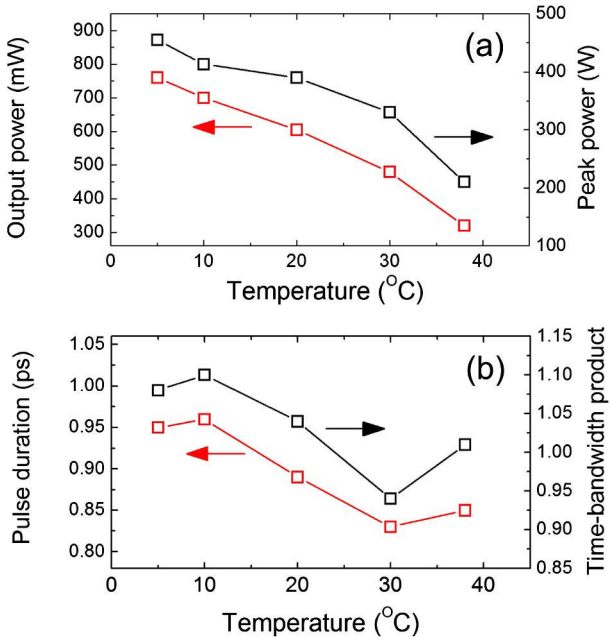

Fig. 4. (a) Average and peak output powers as a function of temperature (left/right axis). (b) Temperature-dependent pulse duration and time-bandwidth product for a sech^2-pulse shape. The optimum TBWP is 0.315.

increasing temperature (left axis). This trend might occur due to a temperature-dependent change of the dispersion inside the gain medium. Here, both output power and pulse duration measurements were performed at a constant net pump power of 16 W. In addition, a slight decrease of the TBWP could be observed as the temperature was increased, as revealed in Fig. 4(b) (right axis). The pulses measured are 3.0 to 3.4 times the transform limit of an ideal sech^2 pulse, confirming that the pulses are still strongly frequency-chirped due to the dispersion within the microcavity. The observed decrease of the TBWP in ML QD lasers has been investigated previously in the literature and several possible reasons have been suggested [25]: on the one hand, this feature implies an increase in the homogeneous linewidth [26], whereas on the other hand, it can be seen as the consequence of a decreased population inversion over the entire gain spectrum due to thermal coupling to the wetting layer, which would reduce the number of modes that reach the threshold [27]. It is worth to note that in our case, the decrease of TBWP is rather small compared with that in the references cited. We should mention that the present average output power and pulse durations are comparable with the results obtained using traditional saturable-absorber mirrors [10].

In conclusion, we have demonstrated the SML of an optically pumped QD-VECSEL. Sub-picosecond pulses with pulse duration as short as 830 fs at 1040 nm and a repetition rate of 1.5 GHz were obtained. Moreover, a record peak power of up to 460 W was demonstrated. A temperature-dependent study of the VECSEL's mode locking properties revealed that the pulse duration as well as the TBWP could be improved if the system is operated at increased temperatures.

The authors acknowledge the financial support by the DFG (GRK1782 and SFB 1083) and the EU FP7 program through the FAST-DOT project (contract no. 224338). M. Gaafar acknowledges the support from the Yousef Jameel scholarship funds. The authors would like to thank Innolume GmbH for the fabrication of the VECSEL chip and G. Bastian for providing the fast oscilloscope.

References

1. M. Kuznetsov, F. Hakimi, R. Sprague, and A. Mooradian, IEEE Photon. Technol. Lett. **9**, 1063 (1997).
2. B. Heinen, T. L. Wang, M. Sparenberg, A. Weber, B. Kunert, J. Hader, S. W. Koch, J. V. Moloney, M. Koch, and W. Stolz, Electron. Lett. **48**, 516 (2012).
3. F. Zhang, B. Heinen, M. Wichmann, C. Möller, B. Kunert, A. Rahimi-Iman, W. Stolz, and M. Koch, Opt. Express **22**, 12817 (2014).
4. S. Husaini and R. G. Bedford, Appl. Phys. Lett. **104**, 161107 (2014).
5. K. G. Wilcox, M. Butkus, I. Farrer, D. A. Ritchie, A. Tropper, and E. U. Rafailov, Appl. Phys. Lett. **94**, 251105 (2009).
6. M. Butkus, E. A. Viktorov, T. Erneux, C. J. Hamilton, G. Maker, G. P. A. Malcolm, and E. U. Rafailov, Opt. Express **21**, 25526 (2013).
7. J. Rautiainen, I. Krestnikov, M. Butkus, E. U. Rafailov, and O. G. Okhotnikov, Opt. Lett. **35**, 694 (2010).
8. M. Butkus, J. Rautiainen, O. G. Okhotnikov, C. J. Hamilton, G. P. A. Malcolm, S. S. Mikhrin, I. L. Krestnikov, D. A. Livshits, and E. U. Rafailov, IEEE J. Sel. Top. Quantum Electron. **17**, 1763 (2011).
9. A. A. Lagatsky, C. G. Leburn, C. T. A. Brown, W. Sibbett, S. A. Zolotovskaya, and E. U. Rafailov, Prog. Quantum Electron. **34**, 1 (2010).
10. M. Hoffmann, O. D. Sieber, V. J. Wittwer, I. L. Krestnikov, D. A. Livshits, Y. Barbarin, T. Südmeyer, and U. Keller, Opt. Express **19**, 8108 (2011).

11. M. Mangold, V. J. Wittwer, C. A. Zaugg, S. M. Link, M. Golling, B. Tilma, and U. Keller, Opt. Express **21**, 24904 (2013).
12. C. A. Zaugg, Z. Sun, V. J. Wittwer, D. Popa, S. Milana, T. S. Kulmala, R. S. Sundaram, M. Mangold, O. D. Sieber, M. Golling, Y. Lee, J. H. Ahn, A. C. Ferrari, and U. Keller, Opt. Express **21**, 31548 (2013).
13. K. Seger, N. Meiser, S. Y. Choi, B. H. Jung, D. I. Yeom, F. Rotermund, O. Okhotnikov, F. Laurell, and V. Pasiskevicius, Opt. Express **21**, 17806 (2013).
14. Y. F. Chen, Y. C. Lee, H. C. Liang, K. Y. Lin, K. W. Su, and K. F. Huang, Opt. Lett. **36**, 4581 (2011).
15. L. Kornaszewski, G. Maker, G. P. A. Malcolm, M. Butkus, E. U. Rafailov, and C. J. Hamilton, Laser Photon. Rev. **6**, L20 (2012).
16. L. Kornaszewski, G. Maker, G. P. A. Malcolm, M. Butkus, E. U. Rafailov, and C. J. Hamilton, Laser Photon. Rev. **7**, 555 (2013).
17. M. Gaafar, C. Möller, M. Wichmann, B. Heinen, B. Kunert, A. Rahimi-Iman, W. Stolz, and M. Koch, Electron. Lett. **50**, 542 (2014).
18. A. R. Kovsh, N. N. Ledentsov, S. S. Mikhrin, A. E. Zhukov, D. A. Livshits, N. A. Maleev, M. V. Maximov, V. M. Ustinov, A. E. Gubenko, I. M. Gadjiev, E. L. Portnoi, J. S. Wang, J. Chi, D. Ouyang, D. Bimberg, and J. A. Lott, Proc. SPIE **5349**, 31 (2004).
19. E. U. Rafailov, M. A. Cataluna, and W. Sibbett, Nat. Photonics **1**, 395 (2007).
20. E. U. Rafailov, S. J. White, A. A. Lagatsky, A. Miller, W. Sibbett, D. A. Livshits, A. E. Zhukov, and V. M. Ustinov, IEEE Photon. Technol. Lett. **16**, 2439 (2004).
21. T. Schwarzbäck, R. Bek, F. Hargart, C. A. Kessler, H. Kahle, E. Koroknay, M. Jetter, and P. Michler, Appl. Phys. Lett. **102**, 092101 (2013).
22. J. A. Lott, A. R. Kovsh, N. N. Ledentsov, and D. Bimberg, in *Proceedings of the CLEO* (2005), pp. 160–161.
23. D. Al Nakdali, M. K. Shakfa, M. Gaafar, M. Butkus, K. A. Fedorova, M. Zulonas, M. Wichmann, F. Zhang, B. Heinen, A. Rahimi-Iman, W. Stolz, E. U. Rafailov, and M. Koch, IEEE Photon. Technol. Lett. **26**, 1561 (2014).
24. M. Hoffmann, Y. Barbarin, D. J. H. C. Maas, M. Golling, I. L. Krestnikov, S. S. Mikhrin, A. R. Kovsh, T. Südmeyer, and U. Keller, Appl. Phys. B **93**, 733 (2008).
25. M. A. Cataluna, E. A. Viktorov, P. Mandel, W. Sibbett, D. A. Livshits, J. Weimert, A. R. Kovsh, and E. U. Rafailov, Appl. Phys. Lett. **90**, 101102 (2007).
26. A. Sakamoto and M. Sugawara, IEEE Photon. Technol. Lett. **12**, 107 (2000).
27. H. Huang and D. G. Deppe, IEEE J. Quantum Electron. **37**, 691 (2001).

5.5 Recent Advances in the Field of Vertical-External-Cavity Surface-Emitting Lasers

A. Rahimi-Iman, M. Gaafar, D. Al Nakdali, C. Möller, F. Zhang, K. A. Fedorova, M. Wichmann, M. K. Shakfa, K. A. Fedorova, W. Stolz, E. U. Rafailov, and M. Koch, *Proc. of SPIE*, vol. 9349, 2015.

5.5.1 Abstract:

In this invited paper, we presented recent developments in the field of vertical-external-cavity surface-emitting lasers (VECSELs). In this work, particular focus was given on self-mode-locking VECSELs as a novel variation of mode-locked VECSELs, which do not require a saturable absorber mirror for pulsed operation, and thus circumvent some limitations set by saturable absorbers. To further motivate work in this direction, a brief overview on intensitve mode-locking studies in the last 15 years was provided. We highlighted the demonstration of self-mode-locking (SML) VECSELs with sub-ps pulses up to the third harmonic at peak powers up to 1 KW in a quantum-well device, supported by thorough experimental characterization of the pulsed laser, and the first demonstration of an SML QD VECSEL. We also briefly reviewed recent advances on high-power single-frequency operation of VECSELs and VECSEL-based two-color emission and frequency conversion.

5.5.2 The author's contribution:

The manuscript primarily written by Dr. Arash Rahimi-Iman is based on recent experimental work which was performed in the research group at the Philipps-University of Marburg, with the help of our cooperation partners. The topics highlighted are mainly related to recent achievements by Mahmoud Gaafar, who contributed significantly to the presented results with the help of the coauthors. In this context, I contributed to the experimental work related to QD-VECSELs and helped writing the corresponding sections in the manuscript. Indeed, all co-authors contributed to this publication and helped to write and improve the manuscript.

Recent Advances in the Field of Vertical-External-Cavity Surface-Emitting Lasers

Arash Rahimi-Iman,*[a] Mahmoud Gaafar,[a] Dalia Al Nakdali,[a] Christoph Möller,[a] Fan Zhang,[a] Matthias Wichmann,[a] Mohammad Khaled Shakfa,[a] Ksenia A. Fedorova,[b] Wolfgang Stolz,[a,c] Edik U. Rafailov,[b] and Martin Koch[a]

[a]Department of Physics and Material Sciences Center, Philipps-Universität Marburg, Renthof 5, D-35032 Marburg, Germany;
[b]Optoelectronics and Biomedical Photonics Group, School of Engineering and Applied Science, Aston University, Aston Triangle, Birmingham B4 7ET, UK;
[c]NAsP III/V GmbH, Am Knechtacker 19, 35041 Marburg, Germany;
*arash.rahimi-iman@physik.uni-marburg.de

ABSTRACT

Vertical-external-cavity surface-emitting lasers (VECSELs) have proved to be versatile lasers which allow for various emission schemes which on the one hand include remarkably high-power multi-mode or single-frequency continuous-wave operation, and on the other hand two-color as well as mode-locked emission. Particularly, the combination of semiconductor gain medium and external cavity provides a unique access to high-brightness output, a high beam quality and wavelength flexibility. Moreover, the exploitation of intra-cavity frequency conversion further extends the achievable radiation wavelength, spanning a spectral range from the UV to the THz. In this work, recent advances in the field of VECSELs are summarized and the demonstration of self-mode-locking (SML) VECSELs with sub-ps pulses is highlighted. Thereby, we present studies which were not only performed for a quantum-well-based VECSEL, but also for a quantum-dot VECSEL.

Keywords: Semiconductor disk lasers, vertical-external-cavity surface-emitting laser, self-mode-locking, mode-locked lasers.

1. INTRODUCTION

Vertical-external-cavity surface-emitting lasers (VECSELs), also known as semiconductor disk lasers (SDLs), are versatile lasers which serve as an excellent platform for the realization of various emission schemes. Following the first demonstration in 1997 by Kuznetsov et al. [1], a wide range of modifications and improvements towards more specific applications were conducted. Optimizations based on microscopic modeling [2] and a detailed analysis of the thermal impedance [3, 4] have pushed the output power of SDLs beyond 100W [5]. Owing to their remarkable design flexibility and features, not only the realization of high-power multi-mode [5, 6] or single-frequency [7] continuous-wave operation schemes have been pushed forward in recent years, but also the accomplishment of dual-color [8] as well as mode-locked [9, 10] operation. Moreover, in order to expand the accessible wavelength range drastically, their external resonator is well exploited for intra-cavity frequency conversion processes via nonlinear elements: while second-harmonic generation pushes the boundaries of the emission wavelength into the UV [11], terahertz frequencies can be reached by difference-frequency generation inside a two-color VECSEL [12, 13]. This is to name a few important achievements in this field.

VECSELs have particularly attracted much attention within the last decade as alternative sources of pulsed laser light, since they can typically provide both a high output power and an outstanding beam quality. The demonstration of the first mode-locked (ML) VECSEL, which was achieved by Hoogland et al. for a central wavelength of 1 μm with 22 ps long pulses [14], dates back to the year 2000 and kicked off a movement towards an entering of the fs-pulse-regime. Additionally, the exploration of pulsed operation for a variety of wavelength has been on the agenda. It did not take long

Vertical External Cavity Surface Emitting Lasers (VECSELs) V, edited by Mircea Guina, Proc. of SPIE
Vol. 9349, 934906 · © 2015 SPIE · CCC code: 0277-786X/15/$18 · doi: 10.1117/12.2079182

that VECSELs—devices which are also compact and robust—were considered becoming cost-efficient alternatives to commercial mode-locked lasers with short pulses, high peak powers and enhanced tenability.

Up-to-date, mode-locking of VECSELs required using resonator-integrated [9, 15] or chip-integrated [16] semiconductor saturable-absorber mirrors (SESAMs). Indeed, besides semiconductor materials, saturable absorbers as graphene [17, 18] and carbon nanotubes [19] have also been employed for ML operation of VECSELs. However, the power-sensitive, complex and costly absorber mirrors, which have to be carefully designed for a certain wavelength range, naturally impose limitations on the device's performance. Fortunately, on the other hand, mode-locking has also been reported to take place without any additional saturable absorber in the system—an effect called self-mode locking (SML) [20–25].

In this context, we highlight recent demonstrations of SESAM-free VECSELs which are operated under SML conditions in this work. Thereby, SML operation is not only presented for a quantum-well VECSEL [22, 25], but also for a quantum-dot device [23]. Furthermore, passively harmonically self-mode-locked devices with sub-ps-pulsed operation are shown which run at discrete power levels up to the third harmonic [22]. However, it is worth to note that the mechanism behind this effect has not been fully understood, yet, and future investigations will provide a broader picture with respect to this feature.

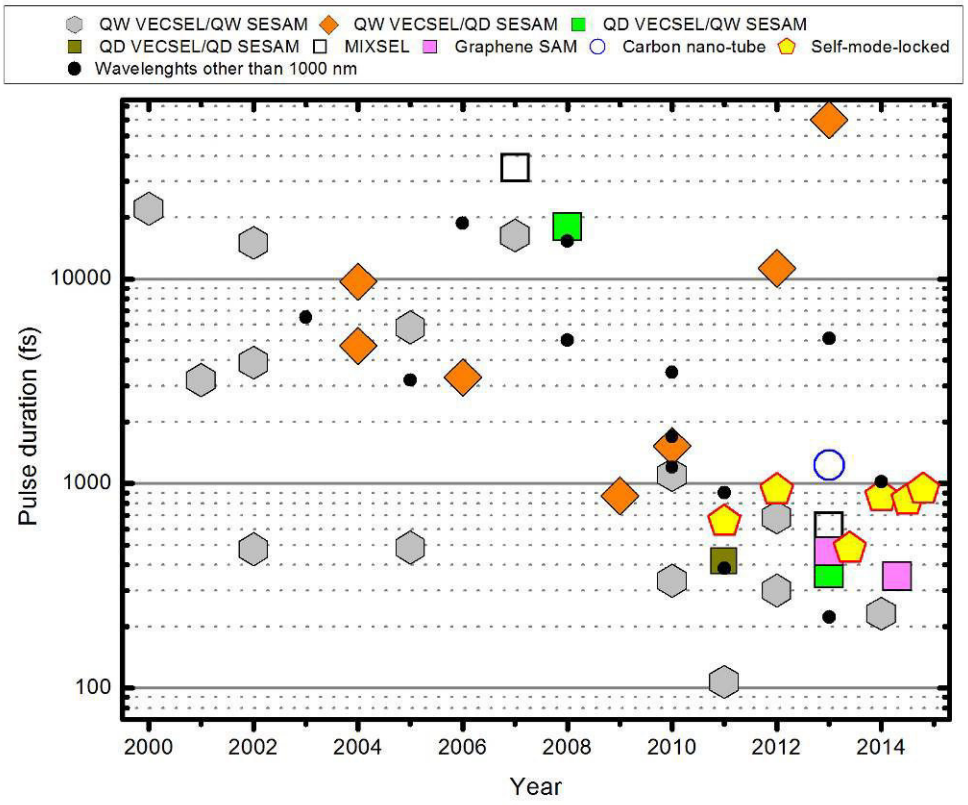

Figure 1. Pulse durations of mode-locked optically pumped VECSELs. Big symbols represent devices emitting around a wavelength of 1µm, while small black dots represent devices with wavelengths other than 1µm.

2. GAIN MIRROR DESIGNS

In the following, a brief overview on the design of the employed chip structures is given. *Structure 1* is a MOVPE grown VECSEL chip with 10 (InGa)As quantum wells (QWs) equally spaced by λ/2 (GaP)As barrier layers. The distributed Bragg reflector (DBR) consists of 24½ pairs of λ/4 GaAs/(AlGa)As layers and is transparent to the wavelength of the fibre-coupled 808 nm diode pump laser. The structure was grown "bottom-

up" and flip-chip bonded with Au–In solid–liquid interdiffusion onto a 350 µm-thick CVD diamond heat spreader. Originally, the chip was designed as a resonant chip and exhibits the micro-cavity resonance at the quantum well gain peak at 1010 nm. For the purpose of mode-locking, the cap layer thickness was reduced from λ/2 to λ/4 via wet etching in order to obtain an anti-resonant micro-cavity with minimized group delay dispersion (GDD) and a spectrally broadened effective gain of the structure. A schematic drawing of the VECSEL chip's structure is shown in Fig. 2(a).

Structure 2 was grown by molecular-beam epitaxy. It consists of 35 layers of Stranski–Krastanow grown InGaAs QDs within GaAs spacers, organized as five stacks of seven QD layers. These stacks are distributed within the cavity to be located at standing-wave electric field antinodes of the optical mode for an optimum gain. As in *structure 1*, a ternary DBR was grown, which consists of 29.5 pairs of GaAs/(AlGa)As and is transparent to the wavelength of the fiber-coupled 808 nm pump laser. Both, the QDs and the DBR, are designed for an emission wavelength of 1040 nm. A schematic drawing of the VECSEL chip's structure is shown in Fig. 2(b). The VECSEL chip is capillary bonded to an intra-cavity diamond heat spreader which exhibits an anti-reflection coating. The anti-reflection coating is also minimizing the GDD at the design wavelength.

Table 1. Overview of the semiconductor disk laser gain mirrors used in this work.

	Structure 1	**Structure 2**
Wavelength (nm)	1010	1040
Gain type	QW	QD
Gain layers	10 single QWs	35 QD layers, in stacks of 7
Mirror pairs per DBR	24.5	29.5
Resonance	Anti-resonant	Anti-resonant
Heat management	Flip-chip bonded onto diamond heat spreader	"Top emitter" with intra-cavity diamond heat spreader

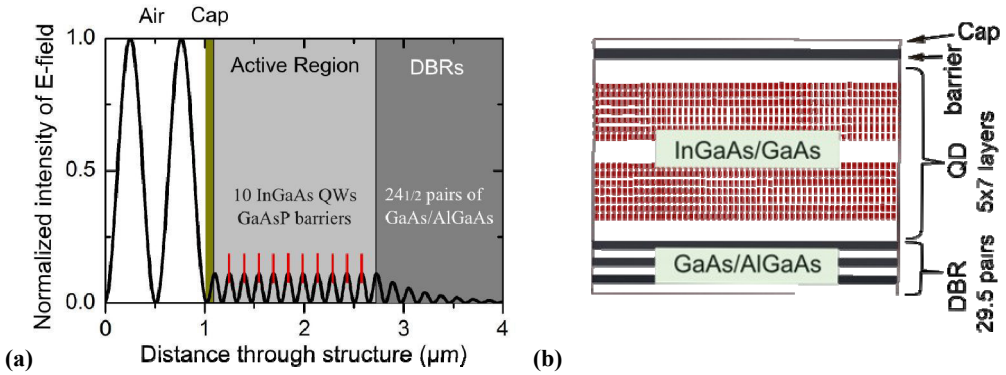

Figure 2. (a) Electric-field distribution of a standing optical wave inside the near-antiresonant gain structures normalized to the input intensity in the case of the QW-gain mirror (*structure 1*). The position of the quantum wells are represented by the vertical red lines. (b) Scheme of the QD-gain mirror structure. 5 Stacks consisting of 7 layers Stransky-Krastanow-grown QDs are incorporated into the active region of the chip (*structure 2*).

3. EXPERIMENTAL SETUPS

Pulsed VECSELs, similar to cw ones, employ the gain mirror in combination with an external cavity, which is defined by at least one mirror. While the cavity geometry of the presented SML VECSELs varies slightly, the principle which

allows for mode-locking remains the same, as mentioned later. Here, the laser setups for a quantum well (QW) and quantum dot (QD) VECSEL are schematically shown in Fig. 3.

As the diamond heat spreader of the QW-VECSEL is attached to the chip's DBR structure, the VECSEL chip is directly mounted on a water-cooled copper heat sink. The laser resonator can be seen as a Z-shaped cavity, which is formed by a flat output coupler (OC) with a transmittance of 1.6%, the gain chip itself, and a highly reflective (HR) curved mirror (CM) with a radius of curvature (RC) of 150 mm as well as a plane HR mirror. With a total cavity length amounting to 30 cm, a free spectral range of approximately 0.5 GHz is determined. The angle of incidence on the curved mirror was kept below 10° in order to avoid excessive astigmatism. The cavity is optimized for mode-locked operation assuming Kerr-lensing inside the VECSEL chip structure. Therefore, a variable slit is placed directly in front of the HR end mirror (cf Fig. 3(a)). An 808 nm fiber-coupled diode laser which can deliver up to 35W output power is used to pump the system.

For the QD-VECSEL setup, the copper heat sink is attached to both the outer region of the intracavity diamond heat spreader on the top of the gain mirror and the DBR structure on the reverse side of the VECSEL chip. A thermoelectric cooler is employed to extract excess heat from the copper heat sink to the closed-cycle cooling water. To complete the laser cavity, a concave (RC=100 mm) OC mirror with a transmittance of 0.6% is placed at a position 97 mm away from the gain chip. Thereby, a linear cavity is formed with a free spectral range of approximately 1 GHz. Similar to the QW-VECSEL setup, a variable slit is inserted close to the external mirror in this linear cavity (cf. Fig. 3(b)). The pump laser system is the same as used in the QW-VECSEL setup.

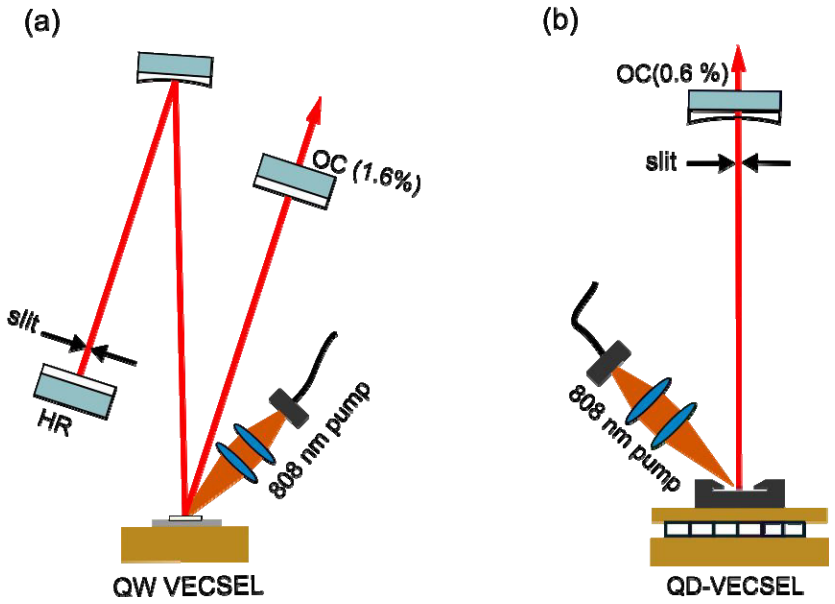

Figure 3. Schematic drawing of the setups used to realize SML (a) for a QW-VECSEL and (b) a QD-VECSEL. These two designs represent the common cavity configurations known as z-cavity and linear cavity, respectively.

4. RESULTS

4.1 Quantum well VECSEL chip

Self-mode-locking, which can be also named saturable-absorber-mirror-free mode-locking, is initiated in the VECSEL system when the slit in front of the HR end mirror is moved or the slit width is narrowed. Moreover, to stabilize SML operation, the cavity length was fine-tuned (see also [21, 22] for more details on the systems). The long-time-span pulse train of the SML QW VECSEL reveals stable operation on the microsecond scale (see Fig. 4(a)), with a repetition rate

faster, while also on the order of Ti:Sapphire oscillators: A 500-MHz repetition rate is demonstrated for the fundamental mode in a close-up of the pulse train, shown in Fig. 4(b). Another indicator of stable pulsed operation can be obtained from RF spectra, of which an example is shown in Fig. 4(c) for the signal of the fundamental repetition rate. Here, the RF linewidth is less than 30 kHz, indicating stable SML operation. The mode-locked pulse duration was measured with a self-made intensity autocorrelator with a scan range of ~130 ps. Figure 4(d) presents a long-delay autocorrelation trace for fundamental mode-locking measured with a self-made intensity autocorrelator with a scan range of ~130 ps, confirming single-pulse operation. This measurement also demonstrates the absence of a pedestal. Typical short-delay autocorrelation traces, from which pulse durations are estimated, are shown in the following section (cf. Fig. 8(a'-c')).

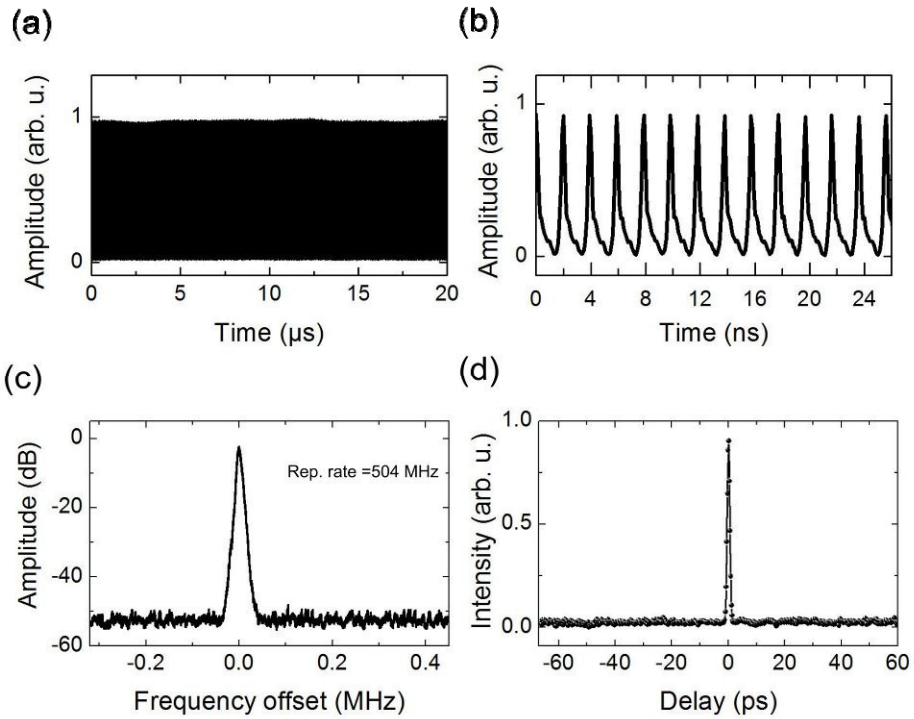

Figure 4. (a) Diagram of the long-time-span pulse train of the SML QW device. (b) A 500-MHz repetition rate is revealed for the fundamental mode in a close-up of the pulse train. (c) RF spectrum of the fundamental repetition rate. The RF linewidth is less than 30 kHz, indicating stable SML operation. (d) Single pulse operation is confirmed by a long-delay autocorrelation trace for fundamental mode-locking.

To provide further evidence of a mode-locked operation, a nonlinear frequency conversion in a BBO crystal is performed using the SML QW VECSEL. By directing the out-coupled laser beam of the VECSEL into the nonlinear crystal, green light is externally produced via second-harmonic generation (SHG) with the infrared pulsed laser light. While a clear spectrum of the SHG signal can be measured if the laser is mode-locked, in the case of continuous-wave operation no SHG signal is observed, owing to the fact that SHG is an intensity-dependent nonlinear effect. Depicted in Fig. 5, the experimental setup of the self-mode-locked QW VECSEL shows how SHG is utilized to produce green light externally. In the top inset of Fig. 5, a spectrum of the frequency-doubled SHG signal together with the spectrum of the original laser output is presented. Finally, a beam quality measurement confirms operation in the fundamental-transverse mode with M^2 values less than 1.1 for both axes, as shown by the bottom insets of Fig. 5 (left: beam profile, right: M^2 measurement). It is worth mentioning, that whenever a new mode-locking technique is demonstrated, the confirmation of mode-locked operation requires different measurements to be carried out, particularly beyond standard characterization methods which typically can't serve as an unambiguous evidence of mode-locking. Indeed, this has motivated part of our experiments and further discussion of the performed investigations and obtained results can be found in Ref. [25].

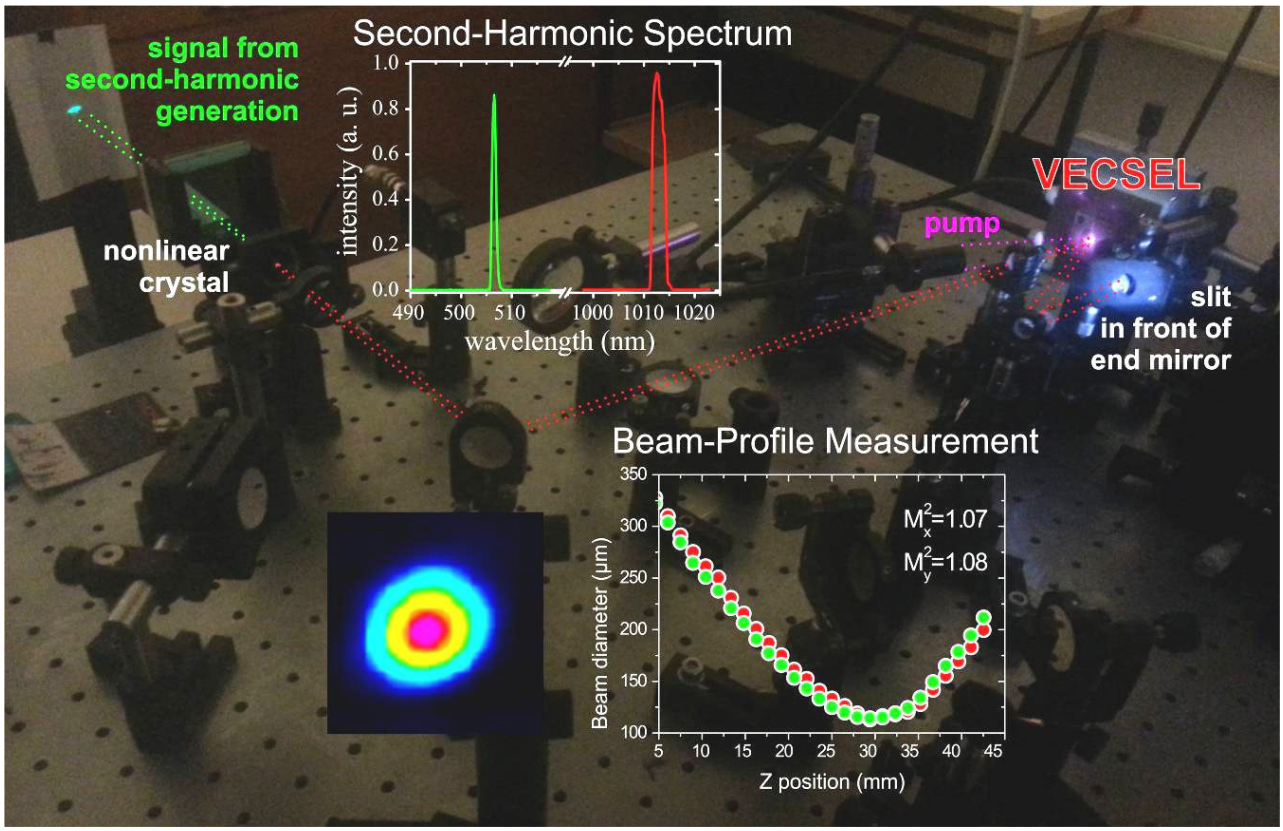

Figure 5. The experimental setup of the self-mode-locked QW VECSEL shows how second-harmonic generation is utilized to produce green light externally via the infrared pulsed laser light. Top inset: Spectrum of the frequency-doubled SHG signal and the original laser light. Bottom inset: Beam quality measurement confirming operation in fundamental-transverse mode with M^2 values less than 1.1 for both axes.

4.2 Harmonic mode-locking

Next, we want to summarize the observation of harmonic self-mode-locking which can be achieved with the presented QW device. Interestingly, mode-locking is only observed for nearly discrete pump levels. The error bars in Fig. 6 represent the pump regions in which a stable ML operation was accomplished in repeated investigations. For the lowest pump level, fundamental mode-locking is observed. For the higher pump levels the repetition rate is doubled and tripled, corresponding to two and three equally spaced pulses in a single cavity roundtrip, respectively. In our observations, ML is not self-starting but can be initiated when the slit width is narrowed or the slit is moved. However, the fundamental mode-locked operation is self-sustaining and the slit can be opened completely without disturbing the ML process. In harmonic operation, a self-sustaining ML is only achieved with the slit partially closed.

In order to confirm stable mode-locking, an RF spectrum (cf. Fig. 7), an optical spectrum and an autocorrelation trace (cf. Fig. 8) was performed. The resulting time bandwidth products of 0.69 (first), 0.73 (second) and 0.72 (third) reveal that the pulses are not transform limited which can be attributed to a remaining GDD caused by the VECSEL chip. Also, we obtain the peak powers 948 W for the first, 752 W for the second and 754 W for the third harmonic ML. The nearly constant peak power for the different power levels indicates that a certain intra-cavity power is needed for the underlying ML mechanism.

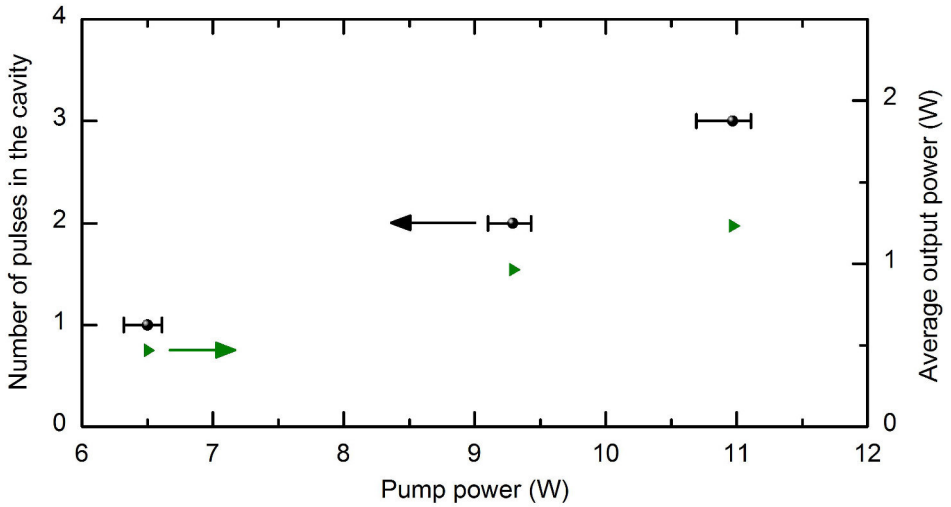

Figure 6. Number of pulses in the cavity as a function of the optical pump power (black squares, left axis). The average output power of the device is plotted with respect to the right axis (green circles).

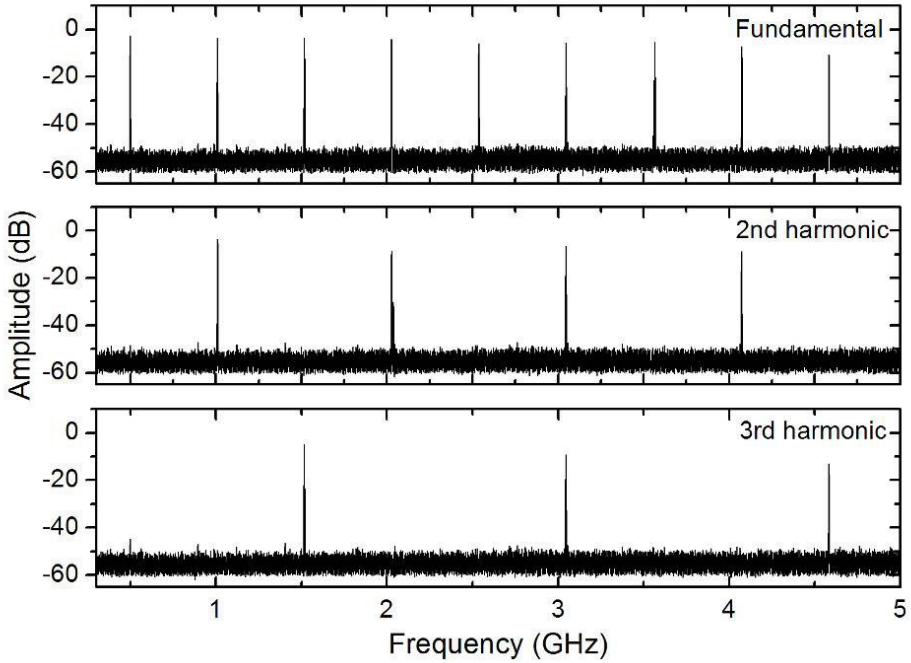

Figure 7. RF spectra reveal fundamental (top row), second harmonic (center) and third harmonic (bottom) mode-locking.

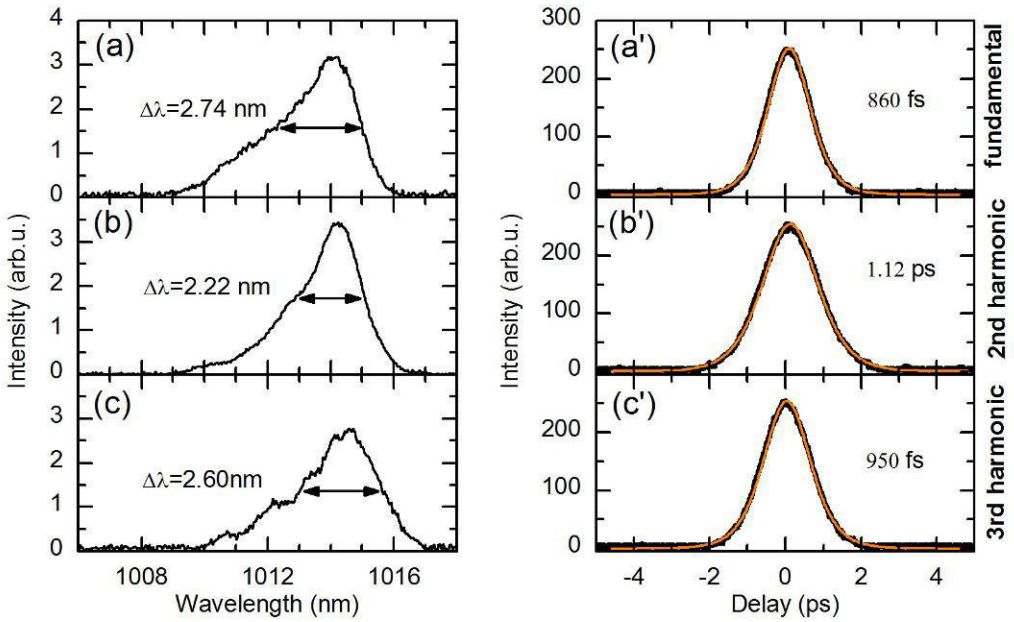

Figure 8. (a)–(c) Optical spectra for the SML VECSEL in the regimes of fundamental, second-harmonic and third-harmonic mode-locking, respectively. (a′)–(c′) Autocorrelation traces (black) with sech² fits (orange) corresponding to signal shown in (a)–(c), respectively.

4.3 Quantum dot VECSEL chip

In this section, we present the first passively-self-mode-locked optically-pumped QD-VECSEL. The measurements indicated sub-picosecond duration of the laser pulses in the mode-locked regime with 750mW average output power at 1.5 GHz repetition rate. The RF spectrum which was measured over a span of 6.5 GHz using a 100 kHz resolution bandwidth (RBW), is shown in Fig. 9(a). Moreover, Fig. 9(b) shows an RF spectrum of the fundamental repetition rate measured over a span of 1 MHz using a RBW of 10 kHz. Here, a clear peak at 1.5 GHz with a signal to noise ratio of about 45 dB is observed.

Fig. 10(a) presents the corresponding optical spectrum of the SML QD-VECSEL at room temperature centered at 1038 nm. The mode-locked pulse duration is yielded assuming sech² shaped pulses in the autocorrelation trace representatively shown in Fig. 10 (b). In a temperature dependence study, pulse durations varied between approximately 0.8 and 1.0 ps.

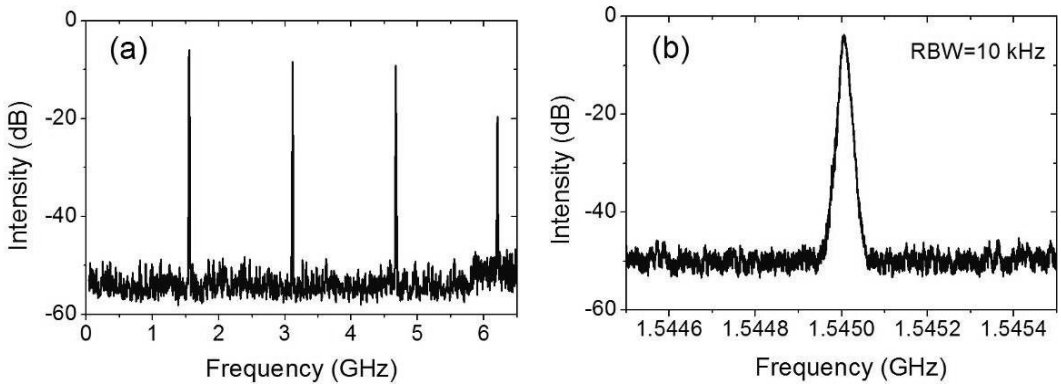

Figure 9. RF spectra measured over (a) a span of 6.5 GHz and a RBW of 100 kHz, showing the first 4 harmonics, and (b) a span of 1 MHz and a RBW of 10 kHz, with the RF signal centered around 1.545 GHz.

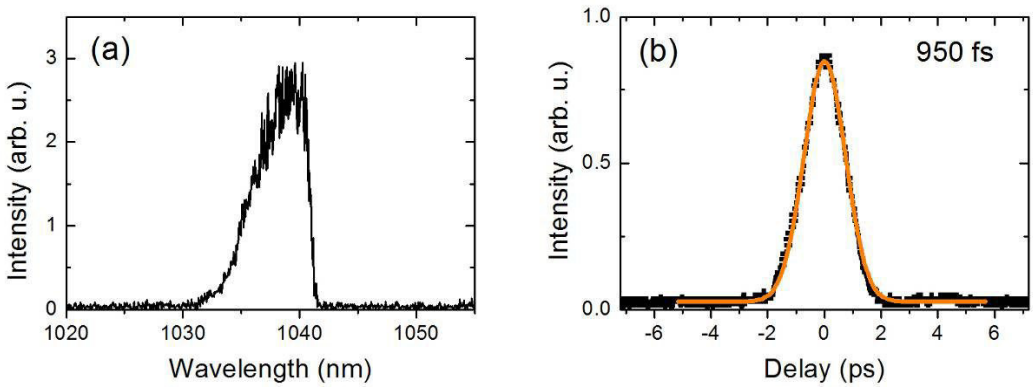

Figure 10. (a) Optical spectrum of the SML QD-VECSEL. (b) Corresponding autocorrelation trace. Black dotted: experimental data. Orange line: fit curve assuming a $sech^2$ pulse.

5. CONCLUSIONS

In summary, we presented recent developments in the field of semiconductor disk lasers, well known as VECSELs, which provide access to various operation modes and features for a broad wavelength range. In addition to high-power operation, frequency stabilization and frequency conversion techniques, the field of mode-locking of VECSELs gained much attraction in recent years, with the efforts of the community leading towards an alternative source for pulsed lasers. In this context, we highlight the demonstration of self-mode-locking VECSELs as a variation of mode-locked VECSELs which do not require a saturable absorber mirror for pulsed operation, and thus circumvent some limitations set by saturable absorbers. Results are presented for a quantum well and a quantum dot device to emphasize that this quite young technique, even though the mechanism behind the effect has yet not been well understood, is capable of enabling mode-locked operation for different gain media as well as cavity configurations.

ACKNOWLEDGEMENTS

The authors acknowledge financial support by the DFG (GRK 1782 and SFB 1083) and EU FP7 program through FAST-DOT project (contract No. 224338). M. Gaafar acknowledges support from the Yousef Jameel scholarship funds. The authors would like to thank Innolume GmbH for the fabrication of the QD structures and Prof. O.G. Okhotnikov from Tampere University of Technology for the preparation of the QD-VECSELs.

REFERENCES

[1] Kuznetsov, M., Hakimi, F., Sprague, R. and Mooradian, A., "High-power (>0.5-W CW) diode-pumped vertical-external-cavity surface-emitting semiconductor lasers with circular TEM00 beams," IEEE Photonics Technol. Lett. 9, 1063-1065 (1997).

[2] Wang, T.-L., Heinen, B., Hader, J., Dineen, C., Sparenberg, M., Weber, A., Kunert, B., Koch, S. W., Moloney, J. V., Koch, M., and Stolz, W., "Quantum design strategy pushes high-power vertical-external-cavity surface-emitting lasers beyond 100 W," Laser Photonic Rev., 6(5), L12–L14 (2012)

[3] Hader, J., Wang, T.-L., Moloney, J. V., Heinen, B., Koch, M., Koch, S. W., Kunert, B., and Stolz, W., "On the measurement of the thermal impedance in vertical-external-cavity surface-emitting lasers," J. Appl. Phys., 113(15), 153102 (2013).

[4] Heinen, B., Zhang, F., Sparenberg, M., Kunert, B., Koch, M., and Stolz, W., "On the Measurement of the Thermal Resistance of Vertical-External-Cavity Surface-Emitting Lasers (VECSELs)," IEEE J. Quantum Electron., 48(7), 934–940 (2012).

[5] Heinen, B., Wang, T. L., Sparenberg, M., Weber, A., Kunert, B., Hader, J., Koch, S. W., Moloney, J. V., Koch, M. and Stolz, W., "106 W continuous-wave output power from vertical-external-cavity surface-emitting laser," Electron. Lett. 48 (9), 516-517 (2012).
[6] Al Nakdali, D., Shakfa, M. K., Gaafar, M., Butkus, M., Fedorova, K. A., Zulonas, M., Wichmann, M., Zhang, F., Heinen, B., Rahimi-Iman, A., Stolz, W., Rafailov, E. U., and Koch M., "High-Power Quantum-Dot Vertical-External-Cavity Surface-Emitting Laser Exceeding 8 W," IEEE Photonics Technol. Lett. 26(15), 1561 (2014)
[7] Zhang, F., Heinen, B., Wichmann, W., Möller, C., Kunert, B., Rahimi-Iman, A., Stolz, W. and Koch, M., "A 23-watt single-frequency vertical-external-cavity surface-emitting laser," Opt. Express 22, 12817-12822 (2014).
[8] Wichmann, M., Shakfa, M. K., Zhang, F., Heinen, B., Scheller, M., Rahimi-Iman, A., Stolz, W., Moloney, J. V., Koch, S. W. and Koch, M., "Evolution of multi-mode operation in vertical-external-cavity surface-emitting lasers," Opt. Express 21(26) 31940 (2013).
[9] Keller, U. and Tropper, A. C., "Passively modelocked surface-emitting semiconductor lasers," Physics Reports 429, 67–120 (2006).
[10] Moloney, J.V., Kilen, I., Bäumner, A., Scheller, M., and Koch, S.W., "Nonequilibrium and thermal effects in mode-locked VECSELS," Opt. Express 22(6), 6422–6427 (2014).
[11] Chen, Y. F., Lee, Y. C., Liang, H. C., Lin, K. Y., Su, K. W. and Huang, K. F., "Femtosecond high-power spontaneous mode-locked operation in vertical-external cavity surface-emitting laser with gigahertz oscillation," Opt. Lett. 36(23), 4581–4583 (2011).
[12] Scheller, M., Yarborough, J. M., Moloney, J. V., Fallahi, M., Koch, M., and Koch, S. W., "Room temperature continuous wave milliwatt terahertz source," Opt. Express 18(26), 27112–27117 (2010).
[13] Wichmann, M., Stein, M., Rahimi-Iman, A., Koch, S. W., and Koch, M., "Interferometric Characterization of a Semiconductor Disk Laser driven Terahertz Source," J. Infrared Milli. Terahz. Waves 35(6-7), 503–508 (2014).
[14] Hoogland, S., Dhanjal, S., Tropper, A. C., Roberts, S. J., Häring, R., Paschotta, R., and Keller, U., "Passively mode-locked diode-pumped surface-emitting semiconductor laser," IEEE Photon. Technol. Lett. 12(9), 1135–1137 (2000).
[15] Wilcox, K.G., Tropper, A.C., Beere, H.E., Ritchie, D.A., Kunert, B., Heinen, B., Stolz, W., "4.35 kW peak power femtosecond pulse mode-locked VECSEL for supercontinuum generation," Opt. Express 21(2), 1599–1605 (2013)
[16] Mangold, M., Wittwer, V. J., Zaugg, C. A., Link, S. M., Golling, M., Tilma, B. W., and Keller, U., "Femtosecond pulses from a modelocked integrated external-cavity surface emitting laser (MIXSEL)," Opt. Express 21(21), 24904–24911 (2013).
[17] Zaugg, C. A., Sun, Z., Wittwer, V. J., Popa, D., Milana, S., Kulmala, T. S., Sundaram, R. S., Mangold, M., Sieber, O. D., Golling, M., Lee, Y., Ahn, J. H., Ferrari, A. C., and Keller, U., "Ultrafast and widely tuneable vertical-external-cavity surface-emitting laser, mode-locked by a graphene-integrated distributed Bragg reflector," Opt. Express 21(25), 31548–31559 (2013).
[18] Husaini, S., and Bedford, R. G., "Graphene saturable absorber for high power semiconductor disk laser mode-locking," Appl. Phys. Lett. 104(16), 161107 (2014).
[19] Seger, K., Meiser, N., Choi, S. Y., Jung, B. H., Yeom, D.-I., Rotermund, F., Okhotnikov, O., Laurell, F., and Pasiskevicius, V., "Carbon nanotube mode-locked optically-pumped semiconductor disk laser," Opt. Express 21(15), 17806–17813 (2013).
[20] Kornaszewski, L., Maker, G., Malcolm, G. P. A., Butkus, M., Rafailov, E. U. and Hamilton, C. J., "SESAM-free mode-locked semiconductor disk laser," Laser Photonics Rev. 6(6), L20–L23 (2012).
[21] Albrecht, A. R., Wang, Y., Ghasemkhani, M., Seletskiy, D. V., Cederberg, J. G. and Sheik-Bahae, M., "Exploring ultrafast negative Kerr effect for mode-locking vertical external-cavity surface-emitting lasers," Opt. Express 21(23), 28801–28808 (2013).
[22] Gaafar, M., Möller, C., Wichmann, M., Heinen, B., Kunert, B., Rahimi-Iman, A., Stolz, W. and Koch, M., "Harmonic self-mode-locking of optically pumped semiconductor disc laser," Electron. Lett. 50(7), 542–543 (2014).
[23] Gaafar, M., Al Nakdali, D., Möller, C., Fedorova, K. A., Wichmann, M., Shakfa, M. K., Zhang, F., Rahimi-Iman, A., Rafailov, E. U. and Koch, M., "Self-mode-locked quantum-dot vertical-external-cavity surface-emitting laser," Opt. Lett. 39(15), 4623–4626 (2014).
[24] Liang, H. C., Tsou, C. H., Lee, Y. C., Huang, K. F. and Chen, Y. F., "Observation of self-mode-locking assisted by high-order transverse modes in optically pumped semiconductor lasers," Laser Phys. Lett. 11, 105803 (2014).
[25] Gaafar, M., Richter, P., Keskin, H., Möller, C., Wichmann, M., Stolz, W., Rahimi-Iman, A. and Koch, M., "Self-mode-locking semiconductor disk laser," Opt. Express 22(23), 28390–28399 (2014).

Bibliography

[1] N. G. Basov, O. N. Kroklin, and Y. M. Popov,"Production of negative temperature states in p-n junctions of degenerate semiconductors," *Pis'ma Zh. Eksp. Theor. Fiz*, vol. 40, p1879. Also, *Sov. phys. JETP*, vol. 13, 1961.

[2] E. Wintner, *Handbook of the Eurolaser Academy*. Springer-Verlag US, 1998.

[3] W. W. Chow, S. W. Koch, *Semiconductor-Laser Fundamentals*. Springer-Verlag, Berlin, Heidelberg, Germany, 1999.

[4] M. Kuznetsov, F. Hakimi, R. Sprague, and A. Mooradian, "Design and Characteristics of High-Power (0.5-W CW) Diode-Pumped Vertical-External-Cavity Surface-Emitting Semiconductor Lasers with Circular TEM_{00} Beams," *IEEE Journal of Photonics Technolgy Letters*, vol. 5, no. 3, 1999.

[5] S. Ranta, M. Tavast, T. Leinonen, N. Van Lieu, G. Fetzer and M. Guina,"1180 nm VECSEL with output power beyond 20 W," *Electronics Letters*, vol.49, no. 1, 2013.

[6] S. Calvez, J. E. Hastie, M. Guin, O. G. Okhotnikov, and M. D. Dawson,"Semiconductor disk lasers for the generation of visible and ultraviolet radiation," *Laser Photon*, vol. 3, no. 5, 2009.

[7] L. Fan, M. Fallahi, J. Hader, A. R. Zakharian, M. Kolesik, J. V. Moloney, T. Qiu, A. Schulzgen, N. Peyghambarian, S. W. Koch, W. Stolz, and J. T. Murray, "Over 3 W high-efficiency vertical-external-cavity surfaceemitting lasers

and application as efficient fiber laser pump sources," *Appl.Phys. Lett*, vol. 86, no. 21, 2005.

[8] L. Fan, T. Hsu, M. Fallahi, J. T. Murray, R. Bedford, Y. Kaneda, J. Hader, A. R. Zakharian, J. V. Moloney, S. W. Koch, and W. Stolz, "Tunable high-power high-brightness linearly polarized vertical-external-cavity surfaceemitting lasers," *Appl.Phys. Lett*, vol. 88, no. 2, 2006.

[9] F. Zhang, B. Heinen, M. Wichmann, C. Möller, B. Kunert, A. Rahimi-Iman, W. Stolz, and M. Koch,"23-watt single-frequency vertical-external-cavity surface-emitting laser," *Opt. Express*, vol. 22, no. 11, 2014.

[10] J. A. Lott, A. R. Kovsh, N. N. Ledentsov, and D. Bimberg, "GaAs-Based InAs/InGaAs quantum dot vertical cavity and vertical external cavity surface emitting lasers emitting near 1300 nm," *Pacific Rim Conference on Lasers and Electro-Optics*, pp. 160 – 161, Tokyo, Japan, 2005.

[11] D. Al Nakdali, M. K. Shakfa, M. Gaafar, M.Butukus, K. A. Fedorova, M. Zulonas, M. Wichmann, F. Zhang, B. Heinen, A. Rahimi-Iman, W. Stolz, E. U. Rafailov, and M. Koch, "High-Power Quantum-Dot Vertical-External-Cavity Surface-Emitting Laser Exceeding 8 W," *IEEE Photonics Technol. Lett*, vol. 26, no. 15, 2014.

[12] D. Al Nakdali, M. Gaafar, M. K. Shakfa, F. Zhang, M. Vaupel, K. A. Fedorova, A. Rahimi-Iman, E. U. Rafailov, and M. Koch, "High-Power Operation of Quantum-Dot Semiconductor Disk Laser at 1180 nm," *IEEE Photonics Technol. Lett*, vol. 27, no. 10, 2015.

[13] N. Schulz, J. M. Hopkins, M. Rattunde, D. Burns , and J. Wagner ,"High-brightness long-wavelength semiconductor disk lasers," *Laser & Photon*, no. 3, 2008.

[14] C. Wilmsen, H. Temkin, and L. A. Coldren, *Vertical-Cavity Surface-Emitting Lasers -Design, Fabrication, Characterization, and Applications*. Cambridge Studies in Modern Optics, 1999.

[15] D.I. Babic, and S.W. Corzine, "Analytic expressions for the reflection delay, penetration depth, and absorptance of quarter-wave dielectric mirrors," *IEEE Quantum Electron*, vol. 28, 1992.

[16] J. Rautiainen, I. Krestnikov, M. Butkus, E. U. Rafailov, and O. G. Okhotnikov, "Optically pumped semiconductor quantum dot disk laser operating at 1180 nm," *Optics Letters*, vol. 35, no. 5, 2010.

[17] T. D. Germann, A. Strittmatter, J. Pohl, U. W. Pohl, D. Bimberg, J. Rautiainen, M. Guina, and O. G. Okhotnikov,"Temperature-stable operation of a quantum dot semiconductor disk laser," *Applied Physics Letters*, vol. 93, no. 5, 2008.

[18] A. R. Albrecht, C. P. Hains, T. J. Rotter, A. Stintz, K. J. Malloy, G. Balakrishnan, and J. V. Moloney,"High power 1.25 μm InAs quantum dot vertical external-cavity surface-emitting laser," *Journal of Vacuum Science and Technology B*, vol. 29, no. 3, 2011.

[19] M. Butkus, K. G. Wilcox, J. Rautiainen, O. G. Okhotnikov, S. S. Mikhrin, I. L. Krestnikov, A. R. Kovsh, M. Hoffmann, T. Südmeyer, U. Keller, and E. U. Rafailov,"High-power quantum-dot-based semiconductor disk laser," *Optics Letters*, vol. 34, no. 11, 2009.

[20] O. G. Okhotnikov, *Semiconductor Disk Lasers*. Wiley-VCH Verlag GmbH and Co, 2010

[21] A. C. Troppera, and S. Hoogland,"Design of Extended cavity surface-emitting semiconductor lasers," *Prog. Quantum Electron*, vol. 30, no. 1, 2006.

[22] J. Hader, J. V. Moloney, and S. Koch,"Microscopic evaluation of spontaneous emission- and Auger-processes in semiconductor lasers," *IEEE Journal of Quantum Electronics*, vol. 41, no. 5, 2005.

[23] M. Kuznetsov, F. Hakimi, R. Sprague, and A. Mooradian, "High-Power (0.5-W CW) Diode-Pumped Vertical-External-Cavity Surface-Emitting Semiconductor Lasers with Circular TEM_{00} Beams," *IEEE Journal of Photonics Technolgy Letters*, vol. 9, no. 8, 1999.

[24] J. Rautiainen, M. Butkus, I. Krestnikov, E. U. Rafailov, and O. Okhotnikov, "High-power quantum dot semiconductor disk lasers," *Proc. of SPIE*, vol. 8242, 2012.

[25] M. Butkus, J. Rautiainen, O. G. Okhotnikov, C. J. Hamilton, G. P. A. Malcolm, S. S. Mikhrin, I. L. Krestnikov, D. A. Livshits, and E. U. Rafailov,"Quantum dot based semiconductor disk lasers for 1-1.3 μm," *IEEE J. Sel. Top. Quantum Electron*, vol. 17, no. 6, 2011.

[26] B. Heinen, T.-L. Wang, M. Sparenberg, A. Weber, B. Kunert, J. Hader, S. W. Koch, J. V. Moloney, M. Koch, and W. Stolz,"106 W continuouswave output power from vertical-external-cavity surface-emitting laser," *Electron. Lett*, vol. 48, no. 9, 2012.

[27] A. R. Albrecht, T. J. Rotter, C. P. Hains, A. Stintz, J. V. Moloney, K. J. Malloy, and G. Balakrishnan,"Multi-watt 1.25 μm quantum dot VECSEL," *Electron. Lett*, vol. 46, no. 12, 2010.

[28] A. Laurain, C. Mart, J. Hader, J. V. Moloney, B. Kunert, and W. Stolz,"15 W single frequency optically pumped semiconductor laser with submegahertz linewidth," *IEEE Photonics Technol. Lett*, vol. 26, no. 2, 2014.

[29] U. Keller and A. C. Tropper,"Passively modelocked surface-emitting semiconductor lasers," *Phys. Rep*, vol. 429, no. 2, 2006.

[30] M Scheller, T.-L. Wang, B Kunert, W. Stolz, S. W. Koch, and J. V. Moloney,"85.7 MHz repetition rate modelocked semiconductor disk laser: fundamental and soliton bound states," *Electron. Lett*, vol. 48, no. 10, 2012.

[31] M. Butkus, E. A. Viktorov, T. Erneux, C. J. Hamilton, G. Maker, G. P. A. Malcolm, and E. U. Rafailov,"Passively modelocked VECSEL emitting 682 fs pulses with 5.1 W of average output power," *Opt. Express*, vol. 21, no. 21, 2013.

[32] J. Rautiainen, I. Krestnikov, J. Nikkinen, and O. G. Okhotnikov,"2.5 W orange power by frequency conversion from a dual-gain quantum-dot disk laser," *Opt. Lett*, vol. 35, no. 12, 2010.

[33] M. Gaafar, P. Richter, H. Keskin, C. Möller, M. Wichmann, W. Stolz, A. Rahimi-Iman, and M. Koch,"Self-mode-locking semiconductor disk laser," *Opt. Express*, vol. 22, no. 23, 2014.

[34] A Rantamäki, A Sirbu, A Mereuta, E Kapon, and O. G. Okhotnikov,"3 W of 650 nm red emission by frequency doubling of wafer-fused semiconductor disk laser," *Opt. Express*, vol. 18, no. 21, 2010.

[35] M. Butkus, C. J. Hamilton, J. Rautiainen, O. G. Okhotnikov, S. S. Mikhrin, I. L. Krestnikov, and E. U. Rafailov,"Broadly tunable 1250 nm quantum dot-based semiconductor disk laser," *IET Optoelectron*, vol. 5, 2011.

[36] A. Garnache, A. Ouvrard, L. Cerutti, D. Barat, A. Vicet, F. Genty, Y. Rouillard, D. Romanini, and E. Cerda-Mendez,"2–2.7 μm single frequency tunable Sbbased lasers operating in CW at RT: Microcavity and external-cavity VCSELs, DFB," *Proc. SPIE*, vol. 6184, 2006.

[37] F-Q Li, K. Liu, N. Zong, B.-H. Feng, J.-Y. Zhang, Q.-J. Peng, D.-F. Cui, and Z.-Y. Xu,"Compact 7.8-W 1-GHz-repetition-rate passively mode-locked TEM_{00} Nd:YVO_4 laser under 880 nm diode direct-in-band pumping," *Opt. Commun*, vol. 284, no. 19, 2011.

[38] T. Schwarzbäck, R. Bek, F. Hargart, C. A. Kessler, H. Kahle, E. Koroknay, M. Jetter, and P. Michler,"High-power InP quantum dot based semiconductor disk laser exceeding 1.3 W," *Appl. Phys. Lett*, vol. 102, no. 9, 2013.

[39] P. J. Schlosser, J. E. Hastie, S. Calvez, A. B. Krysa, and M. D. Dawson,"InP/AlGaInP quantum dot semiconductor disk lasers for CW TEM00 emission at 716–755 nm," *Opt. Express*, vol. 17, no. 24, 2009.

[40] T. D. Germann, A. Strittmatter, U. W. Pohl, D. Bimberg, J. Rautiainen, M. Guina, and O. G. Okhotnikov,"Quantum-dot semiconductor disk lasers," *J. Cryst. Growth*, vol. 310, no. 23, 2008.

[41] T. A. Rantamäki, J. Rautiainen, L. Toikkanen, I. Krestnikov, M. Butkus, E. U. Rafailov, and O. Okhotnikov,"Flip chip quantum-dot semiconductor disk laser at 1200 nm," *IEEE Photonics Technol. Lett*, vol. 24, no. 15, 2012.

[42] M. Butkus, J. Rautiainen, O. G. Okhotnikov, S. S. Mikhrin, I. L. Krestnikov, and E. U. Rafailov,"Flip 1270 nm quantum dot based semiconductor disk lasers," *22nd IEEE international semiconductor laser conference (ISLC)*, 2010.

[43] C. Bückers, E. Kühn, C. Schlichenmaier, S. Imhof, A. Thränhardt, J. Hader, J. V. Moloney, O. Rubel, W. Zhang, T. Ackemann, and S. W. Koch,"Quantum modeling of semiconductor gain materials and vertical-externalcavity surface-emitting laser systems," *Phys. Status Solidi B*, vol. 247, no. 4, 2010.

[44] J. Hader, T.-L. Wang, J. V. Moloney, B. Heinen, M. Koch, S. W. Koch, B. Kunert, W. Stolz,"On the measurement of the thermal impedance in vertical-external-cavity surface-emitting lasers," *J. Appl. Phys*, vol. 113, 2013.

[45] R. G. Bedforda, M. Kolesikb, J. L. A. Chillac, M. K. Reedc, T. R. Nelsona, and J. V. Moloneyb,"Power-limiting mechanisms in VECSELs," *Proc. of SPIE*, vol. 5814, 2005.

[46] J. Singh, *Electronic and Optoelectronic Properties of Semiconductor Structures*. Cambridge University Press, New York, United States of America, 2003.

[47] E. Kühn, A. Thränhardt, C. Bückers, S. W. Koch, J. Hader,"Numerical study of the influence of an antireflection coating on the operating properties of vertical-external-cavity surface-emitting lasers," *Journal of Applied Physics*, vol. 106, 2009.

[48] T. Numai, *Fundamentals of Semiconductor Lasers*. Springer-Verlag, Berlin, Heidelberg, Germany, 2003.

[49] Y. Yu. Peter, M. Cardona, *Fundamentals of Semiconductors*. Springer-Verlag, Berlin, Heidelberg, Germany, 2001.

[50] J. V. Moloney, J. Hader, and S. W. Koch,"Numerical study of the influence of an antireflection Quantum design of semiconductor active materials: laser and amplifier applications," *Laser & Photon*, no. 1, 2007.

[51] A. J. Kemp, A. J. Maclean, J. E. Hastie, S. A. Smith, J. M. Hopkins, S. Calvez, and G. J. Valentine, M. D. Dawson, and D. Burns,"Thermal lensing, thermal

management and transverse mode control in microchip VECSELs," *Appl. Phys. B*, vol. 83, 2006.

[52] A. Chernikov, J. Herrmann, M. Scheller, M. Koch, B. Kunert, W. Stolz, S. Chatterjee, S. W. Koch, T. L. Wang, Y. Kaneda, J. M. Yarborough, J. Hader, and J. V. Moloney,"Influence of the spatial pump distribution on the performance of high power vertical-external-cavity surface-emitting lasers," *Appl. Phys. Lett.*, vol. 97, 2010.

[53] M. I. Mishchenko,L. D. Travis, and A. A. Lacis, *Scattering, Absorption, and Emission of Light by Small Particles*. Cabridge University Press, New York, UK, 2004.

[54] A. Chernikov, J. Herrmann, M. Koch, B. Kunert, W. Stolz, S. Chatterjee, S. W. Koch, T. Wang, Y. Kaneda, J. M. Yarborough, J. Hader, and J. V. Moloney,"Heat Management in High-Power Vertical-External-Cavity Surface-Emitting Lasers," *IEEE Journal Of Selected Topics In Quantum Electronicsv*, vol. 17, no. 6, 2011.

[55] B. Heinen, F. Zhang, M. Sparenberg, B. Kunert, M. Koch, and W. Stolz,"On the Measurement of the Thermal Resistance of Vertical-External-Cavity Surface-Emitting Lasers (VECSELs)," *IEEE Journal Of Quantum Electronicsv*, vol. 48, no. 7, 2012.

[56] D. Al Nakdali, M. K. Shakfa, B. Heinen, B. Kunert, W. Stolz, S. W. Koch, J. Hader, J. V. Moloney, A. Rahimi-Iman, and M. Koch,"Analysis of optical scattering losses in vertical external-cavity-surface-emitting-lasers," *Appl. Phys. B*, 2015.

Wissenschaftlicher Werdegang von

Persönliche Daten:

Name : Al Nakdali
Vorname : Dalia
Geburtsdatum : 02.04.1982
Geburtsort : Homs - Syrien

Werdegang:

11/2010 - 09/2015 : Doktorandin am Fachbereich Physik der Philipps-Universität Marburg; in der Arbeitsgruppe Experimentelle Halbleiterphysik von Prof. Dr. Martin Koch.

09/2007 - 04/2010 : Hochschule für Laserforschung und -Anwendung, Damaskus Universität; postgradualen Studium.
Abschluss: Master der Laserwissenschaft und -anwendungen

09/2004 - 09/2005 : Abteilung Physik, Fakultät für Naturwissenschaften, Al-Baath Universität; postgradualen Studium.
Abschluss: Diplom des postgradualen Studiums auf dem Gebiet Physik des Festkörpers "Solid State Physics"

09/2000 - 07/2004 : Abteilung Physik, Fakultät für Naturwissenschaften, Al-Baath Universität (Homs - Syrien); Studium der Physik.
Abschluss: Bachelor in physikalische Wissenschaften

07/2000 : Abitur (Wissenschaftlicher Abschnitt) am Gymnasium "Asmaa-Gymnasium" (Homs - Syrien).